STUDY OF SURFACE FUNCTIONALIZED CARBON QUANTUM DOT - NUCLEIC ACID CONJUGATE FOR BIOIMAGING APPLICATIONS

A thesis submitted to

D. Y. PATIL EDUCATION SOCIETY,

(DEEMED TO BE UNIVERSITY), KOLHAPUR

FOR THE DEGREE OF

DOCTOR OF PHILOSOPHY

IN

STEM CELL AND REGENERATIVE MEDICINE

UNDER THE FACULTY OF

INTERDISCIPLINARY STUDIES

BY

Ms. ANUJA ARVIND VIBHUTE

M.Sc.

UNDER THE GUIDANCE OF

Dr. ARPITA PANDEY-TIWARI

M. Sc., Ph.D.

DEPARTMENT OF MEDICAL BIOTECHNOLOGY AND

STEM CELL AND REGENERATIVE MEDICINE

CENTRE FOR INTERDISCIPLINARY RESEARCH,

D. Y. PATIL EDUCATION SOCIETY,

(DEEMED TO BE UNIVERSITY), KOLHAPUR- 416 006.

(2024)

DECLARATION

I hereby declare that the thesis entitled **"Study of Surface Functionalized Carbon Quantum Dot-Nucleic Acid Conjugate for Bioimaging Applications"** submitted for the degree of **Doctor of Philosophy (Ph.D.)** in **Stem Cell and Regenerative Medicine** under the faculty of **Centre for Interdisciplinary Research (CIR)**, **D. Y. Patil Education Society (Deemed to be University), Kolhapur** is completed and written by me, has not previously formed the basis for the Degree or Diploma or other similar titles of the this or other University or examining body.

Date:

Place: Kolhapur

Research Student

Ms. Anuja Arvind Vibhute
Centre for Interdisciplinary Research,
D. Y. Patil Education Society,
(Deemed to be University),
Kolhapur – 416 006

CERTIFICATE

This is to certify that the thesis entitled ***"Study of surface functionalized carbon quantum dots-nucleic acid conjugate for bioimaging applications"*** which is being submitted herewith for the award of the Degree of ***Doctor of Philosophy (Ph.D.)*** in ***Stem Cell and Regenerative Medicine*** of ***D. Y. Patil Education Society (Deemed to be University), Kolhapur***, is the result of the original research work completed by ***Ms. Anuja Arvind Vibhute*** under my supervision and guidance and to the best of my knowledge and belief the work embodied in this thesis has not formed earlier the basis for the award of any degree or similar title of this or any other University or examining body.

Date:

Place: **Kolhapur**

Research Guide

Dr. Arpita Pandey-Tiwari
Associate Professor
Department of Medical Biotechnology and
Stem Cell and Regenerative Medicine,
Centre for Interdisciplinary Research,
D. Y. Patil Education Society,
(Deemed to be University),
Kolhapur – 416 006

Dr. Meghnad Joshi
HOD,
Department of Medical Biotechnology
and Stem cell & Regenerative Medicine,
Centre for Interdisciplinary Research,
D. Y. Patil Education Society,
(Deemed to be University),
Kolhapur – 416 006

Prof. C. D. Lokhande
Dean and Research Director,
Centre for Interdisciplinary Research,
D. Y. Patil Education Society,
(Deemed to be University),
Kolhapur – 416 006

ACKNOWLEDGEMENTS

This was a wonderful journey—one that pushed your knowledge, let you identify your strengths and shortcomings, and strengthened your mind and emotions. The people I met along my journey made it more fascinating and wonderful. I would like to take this opportunity to acknowledge those fascinating people.

It is my immense pleasure to express my gratitude and thanks to my mentor and supervisor **Dr. Arpita Pandey-Tiwari**, Associate Professor, Stem Cell and Regenerative Medicine and Medical Biotechnology, Centre for Interdisciplinary Research, D. Y. Patil Education Society (Deemed to be University), Kolhapur for giving a resourceful platform to work in 'Nanobiotechnology Lab'. Her propitious advice, scientific approach, and scrupulous scrutinizes have inspired me to accomplish my goals. She has been and will continue to be my greatest source of motivation to aim high and accomplish great things in life by working hard and never giving up.

I would like to sincerely thank Vice-Chancellor **Prof. R. K. Mudgal** and the Registrar **Dr. V. V. Bhosale** for their inspiration and support. I thank **Prof. C. D. Lokhande,** Dean and Research Director, Center for Interdisciplinary Research who helped me with all their insightful guidance and valuable suggestions. I am also thankful to all **teaching and non-teaching staff** of the Centre for Interdisciplinary Research for their cooperation. I would like to thank **Dr. Sonali Rohiwal,** Institute of Animal Physiology and Genetics Czech Republic for the collaboration. I am also thankful to my collaborators in **Shivaji University**, Kolhapur who have contributed to the successful completion of this work, one way or the other.

I am very grateful to my colleagues **Ms. Tejaswini Patil, Ms. Rutuja Gambhir, Mrs. Sargun Basrani, Ms. Sayali Chougule, Ms. Tanjila Gavandi, Ms. Shivani Patil** for being there for me in any situation and supporting and helping me. Of course, the company rendered by them in the department will

ever be remembered. I am thankful to my juniors **Ms. Pranoti Kamble, and Ms. Vishakha Parkhe**. I express my gratitude to **Mr. Omkar Nille**, Research Scholar at Shivaji University, for his valuable assistance with the research and fluorescence spectroscopy analysis.

In addition, I acknowledge the funding support from Mahatma Jyotiba Phule Research and Training Institute (MAHAJYOTI) of the Government of Maharashtra state for **Mahatma Jyotiba Phule Research Fellowship (MJPRF)** sanctioned to me.

Last but not least I would like to thank the special people who supported me throughout my journey both in academics and life, my family. I am deeply grateful to my mother **Mrs. Anita Vibhute** and father **Mr. Arvind Vibhute** for their love and care. I am thankful to my late grandmother **Mrs. Shantabai Vibhute** who is the source of my motivation. I must acknowledge my stress buster, my son **Viraj**.

The list remains incomplete without acknowledging the support from my dear husband, **Mr. Shekhar Sutar** who is always with me in any situation and equally with me towards the completion of this thesis. I owe my extended family members as well for believing in me.

~Anuja Vibhute

Place: Kolhapur

SUMMARY OF RESEARCH WORK

Papers Published in International Journals [7]

1) **Vibhute A**, Nille O, Kolekar G, Rohiwal S, Patil S, Lee S, Tiwari AP. Fluorescent carbon quantum dots functionalized by poly l-lysine: efficient material for antibacterial, bioimaging, and anti-angiogenesis applications. Journal of Fluorescence. 32(5) (2022) 1789-800, **https://doi.org/10.1007/s10895-022-02977-4. (I.F- 2.6).**
2) **Vibhute A**, Patil T, Gambhir R, Tiwari AP. Fluorescent carbon quantum dots: Synthesis methods, functionalization, and biomedical applications. Applied Surface Science Advances. 11(2022) 10031-10047, **https://doi.org/10.1016/j.apsadv.2022.100311. (I.F- 6.04).**
3) **Vibhute A**, Patil T, Malavekar D, Patil S, Lee S, Tiwari AP. Green synthesis of fluorescent carbon dots from Annona squamosa leaves: optical and structural properties with bactericidal, anti-inflammatory, anti-angiogenesis applications. Journal of Fluorescence. 33(4) (2023) 1619-1629, **https://doi.org/10.1007/s10895-023-03159-6. (I.F- 2.6).**
4) **Vibhute A,** Patil T, Pandey-Tiwari A. Bio-Conjugated Carbon Quantum Dots for Intracellular Uptake and Bioimaging Applications. Journal of Fluorescence. 1(1) (2025) 1-11, **https://doi.org/10.1007/s10895-024-04103-y. (I.F-2.6)**
5) Patil TP, **Vibhute AA**, Patil SL, Dongale TD, Tiwari AP. Green synthesis of gold nanoparticles via Capsicum annum fruit extract: Characterization, antiangiogenic, antioxidant and anti-inflammatory activities. Applied Surface Science Advances. 13 (2023) 100372-100382, **https://doi.org/10.1016/j.apsadv.2023.100372. (I.F-6.04).**
6) Patil T, Gambhir R, **Vibhute A**, Tiwari AP. Gold nanoparticles: Synthesis methods, functionalization, and biological applications. Journal of Cluster Science. 34(2) (2023) 705-725, **https://doi.org/10.1007/s10876-022-02287-6. (I.F- 3.447).**
7) Nille OS, Patil AS, **Vibhute AA,** Shendage SS, Tiwari AP, Anbhule PV, Sohn D, Gore AH, Kolekar GB. Route-dependent tailoring of carbon dot release in alginate hydrogel beads (HB-Alg@ WTR-CDs): A versatile platform for biomedical applications. International Journal of Biological Macromolecules. 257(1) (2024) 128126-128140, **https://doi.org/10.1016/j.ijbiomac.2023.128126. (I.F-8.2).**

Published Book Chapter [1]

1) Gambhir RP, **Vibhute AA**, Patil TP, Tiwari AP. Surface-Functionalized Iron Oxide (Fe_3O_4) Nanoparticles for Biomedical Applications. In Chemically Deposited Metal Chalcogenide-based Carbon Composites for Versatile Applications. Cham: Springer International Publishing. (2023) 411-432, **https://doi.org/10.1007/978-3-031-23401-9_15.**

Granted Indian Patent [1]

1) A method for detection of folic acid from serum/ urine samples using surface functionalized carbon quantum dots, **Ms. Anuja Vibhute,** Dr. Arpita Pandey-Tiwari, Prof. C. D. Lokhande (Patent No. 538842).

Granted (Indian) Copyright [1]

2) Practical Handbook of Immunology, **Ms. Anuja Vibhute,** Dr. Arpita Pandey Tiwari, (Registration No.- L-133612/2023).

Conferences/ Workshops Attended/ Poster/ Papers Presented

1) **International Conference** on "Stem cells and regenerative medicine–academic and industrial outlooks" (SCRM-AIO-2021), held on 19th-20th March 2021
2) **One-day workshop** on "Development of Scientific Instrumentation" organized by Stem Cell and Regenerative Medicine (SCRM), D. Y. Patil Education Society, Kolhapur on 17th December 2021.
3) **Participated in hands-on training programme** on "Bio Atomic Force Microscopy (Bio-AFM) organised by Shivaji University, Kolhapur on 4-5th January 2022
4) **Poster presentation** in "DYANSHODH 2022" organised by Centre for Interdisciplinary Research (CIR), D. Y. Patil Education Society, Kolhapur on 28th February 2022.
5) **Participated in International conference** on "Emerging and Re-emerging Infections (ICERI) 2022" organised by Stem Cell and Regenerative Medicine (SCRM), D. Y. Patil Education Society, Kolhapur on 8th April 2022.
6) **Participated in workshop** on "Protein Purification Techniques and Polyclonal Antibody Development" organised by Stem Cell and Regenerative Medicine

(SCRM), D. Y. Patil Education Society, Kolhapur and iSERA, Shirala on 21-22nd April 2022.

7) **Presented poster at International Workshop** on Recent Trends in Functional Nanomaterials for Technological Applications held on 3rd August 2022 organized by Amity University, Mumbai.

8) **Participated in Maharashtra Start-up Yatra** 2022 organized by Maharashtra State Innovation Society on 14th October 2022.

9) **Presented poster at International Conference** on Emerging Trends in Applied Microbiology and Food Science (ETAMFS) organized by the Department of Microbiology and Food Processing and Packaging, Y. C. Institute of Science, Satara held on 2nd-3rd December 2022.

10) **Presented poster** in "DYANSHODH-2023" organized by Centre for Interdisciplinary Research (CIR), D. Y. Patil Education Society, Kolhapur held on 9th March 2023.

11) **Participated in the hands-on workshop** entitled "MOLECULAR DOCKING" conducted jointly by Global Biomedical Research Foundation, Chennai and Kairos Kinetic (OPC) Private Limited, Chennai on 9th September 2023.

12) **Participated in "One day International Conference** on Advanced Materials and Applications (ICAMA-2023)" jointly organized by Department of Chemistry and IQAC of M. H. Shinde Mahavidyalaya, Tisangi, Tal-Gaganbavda, Dist-Kolhapur held on Saturday, 1st July 2023.

13) **Oral presentation at International Conference** on "Nanotechnology Addressing the Convergence of Materials Science, Biotechnology and Medical Science" (IC-NACMBM-2024), organized by Centre for Interdisciplinary Research (CIR), D. Y. Patil Education Society, Kolhapur held on 12th-14th February 2024.

14) **Presented poster** in "DYANSHODH-2024" organized by Centre for Interdisciplinary Research (CIR), D. Y. Patil Education Society, Kolhapur held on 28th February 2024.

ABBREVIATIONS

AE-HPLC	Anion-Exchange high-performance liquid chromatography
AFM	Atomic force microscopy
CCD	Charged coupled device
CdS	Cadmium sulphide
CdSe	Cadmium selenide
CNP	Carbon nanoparticles
CQDs	Carbon quantum dots
Ct-DNA	Calf thymus DNA
CT	Computerized tomography
CZE	Capillary Zone Electrophoresis
DC	Direct current
DFT	Density functional theory
DLS	Dynamic light scattering
DNA	Deoxyribonucleic acid
dsDNA	Double-stranded DNA
EDA	Ethylenediamine
EDC	1-ethyl-3-(3-dimethyl aminopropyl)-carbodiimide
EDTA	Ethylenediaminetetraacetic acid
EtOH	Ethanol
FTIR	Fourier transform infrared spectroscopy
GE	Gel electrophoresis
HDA	1-hexadecyl amine
HPLC	High-performance liquid chromatography
HRTEM	High-resolution transmission electron microscopy
KDa	Kilodalton
mL	Millilitre
MRI	Magnetic resonance imaging
NaCl	Sodium chloride
NaOH	Sodium Hydroxide
$NaNH_2$	Sodium amide

N-CQD	Nitrogen carbon quantum dots
NHS	N-hydroxysuccinimide
NIR	Near-infrared
nm	Nanometer
OPD	o-phenylenediamine
PAGE	Polyacrylamide gel electrophoresis
PEG	Polyethylene glycol
pH	Potential of Hydrogen
PEI	Polyethyleneimine
PL	Photoluminescence
PLL	Poly L lysine
PLLCQD	Poly L lysine carbon quantum dots
PET	Positron Emission Tomography
QY	Quantum yield
RB	Rose Bengal
RNA	Ribonucleic acid
RNAi	RNA interference
rpm	Rotation per minute
SAED	Selected area electron diffraction
SEC	Size exclusion chromatography
SEM	Standard error of measurement
SF	Silk fibroin
ssDNA	Single-stranded DNA
TAE	Tris-acetate-EDTA buffer
TEM	Transmission electron microscopy
UHPLC	Ultra-high-performance liquid chromatography
μm	Micrometre
UV	Ultraviolet
XPS	X-ray photoelectron spectroscopy
XRD	X-ray diffraction
ZnO	Zinc oxide
ZnS	Zinc sulphite
ZnSe	Zinc selenide
ζ potential	Zeta potential

INDEX

Chapter I: Introduction to Carbon quantum dots and literature survey

Chapter II: Purification and Characterization Techniques for Carbon Quantum Dots

Chapter III: Synthesis and characterization of surface functionalized carbon quantum dots

Chapter IV: Optimization parameters for nucleic acid binding on surface functionalized carbon quantum dots

Chapter V: Surface functionalized carbon quantum dot-nucleic acid conjugate for in-vitro bioimaging applications

LIST OF FIGURES

Chapter I: Introduction to Carbon quantum dots and literature survey

Chapter II: Purification and Characterization Techniques for Carbon Quantum Dots

Chapter III: Synthesis and characterization of surface functionalized carbon quantum dots

Chapter IV: Optimization parameters for nucleic acid binding on surface functionalized carbon quantum dots

Chapter V: Surface functionalized carbon quantum dot-nucleic acid conjugate for in-vitro bioimaging applications

LIST OF TABLES

Chapter I: Introduction to Carbon quantum dots and literature survey

Chapter V: Surface functionalized carbon quantum dots-nucleic acid conjugates for in-vitro bioimaging applications

CHAPTER I

INTRODUCTION TO CARBON QUANTUM DOTS AND LITERATURE REVIEW

1.1 Introduction:

The combination of carbon quantum dots (CQDs) with nucleic acids is a major advancement in bioimaging within the field of biomedical research. By combining the unique features of CQDs with the customizable abilities of nucleic acids, scientists are opening up new possibilities for accurate diagnosis and specialized treatments. This convergence of nanotechnology and biomedicine holds the promise of revolutionizing the understanding and treatment of complex diseases. With the growing need for better imaging techniques, studying CQD-nucleic acid combinations has become crucial, offering significant potential for personalized medicine and precise healthcare solutions. This chapter delves into the synergistic relationship between CQDs and nucleic acid, highlighting their collaborative impact on enhancing bioimaging techniques.

1.2 History of CQDs:

CQDs are a class of carbon-based nanomaterials that have garnered significant attention in recent years due to their unique properties and diverse potential applications, including optoelectronics, sensing, bioimaging, and photocatalysis.

The history of CQDs is relatively short compared to other carbon-based materials like carbon nanotubes and graphene. In 2004, Xu and his team [1] accidentally discovered fluorescent carbon nanoparticles while working on single-walled carbon nanotubes. This unexpected finding revealed the unique optical properties of these nanoparticles and sparked interest in their potential applications.

Two years later, in 2006, Sun and his colleagues [2] synthesized non-toxic carbon nanoparticles of various sizes and termed them CQDs. These CQDs, a type of quantum dot, measure less than 10 nanometers in size. These pioneering studies played a crucial role in the early understanding and characterization of CQDs, paving the way for subsequent research efforts focused on their synthesis through various methods and the exploration of their properties and applications across diverse fields.

The discoveries by Xu et al. [1] and Sun et al. [2] were significant milestones in the development of CQDs. Since then, research in this field has continued to evolve,

with contributions from numerous scientists and research groups worldwide, leading to deeper insights into the synthesis, properties, and applications of CQDs.

1.3 Size and Structure:

CQDs can exhibit various structures, ranging from sp^2-hybridized graphitic carbon to amorphous carbon domains. Their precise structure often depends on the synthesis route and the conditions employed during fabrication. The size of CQDs can be tuned by adjusting parameters such as temperature, pressure, synthesis precursors, and reaction time.

In its bulk form, carbon generally has low solubility in water and exhibits weak fluorescence. These limitations reduce its suitability for applications requiring strong optical properties and compatibility with aqueous environments. However, CQDs, a specialized form of carbon nanoparticles, possess unique characteristics that set them apart.

CQDs are exceptionally small, typically less than 10 nm in size, which enhances their quantum confinement effects—a phenomenon in which the electronic and optical properties of materials change significantly at the nanoscale. This quantum confinement contributes to their strong luminescence, enabling CQDs to emit bright fluorescence under UV or visible light excitation.

A key feature of CQDs is their water solubility, which arises from the presence of functional groups, particularly carboxylic acid (-COOH) groups, on their surface. Carboxylic groups are commonly found in CQDs due to the use of carboxyl-rich precursors (e.g., citric acid) during synthesis, as well as surface oxidation processes. These groups enhance water solubility and biocompatibility while also providing active sites for functionalization.

The carboxylic groups not only improve solubility by facilitating interactions with water molecules but also enhance the surface reactivity of CQDs, making them suitable for conjugation with biomolecules or other functional agents. As a result, CQDs combine the advantages of small size, high fluorescence, and water solubility—attributes largely influenced by their surface chemistry and structural features—making them highly versatile for applications in bioimaging, sensing, and drug delivery.

Typically, CQDs are carbon-based nanomaterials with sizes below 10 nm, and all nanoscale carbon materials fall under this classification. They possess a spatial structure comprising sp^2/sp^3 hybridization, with fluorescent emission being an intrinsic property [2].

1.4 Properties of CQDs:

Over the past few years, CQDs have attracted significant interest from chemists due to their distinct properties, including their natural abundance, high surface area, adaptable functionalization, non-cytotoxicity, and excellent water solubility. These unique characteristics make CQDs highly attractive for various applications. CQDs exhibit exceptional optical properties, such as strong photoluminescence, which can be tuned by controlling their size, surface chemistry, and composition. Figure 1.1 illustrates the key properties of CQDs and their potential attributes. These properties are discussed in detail in the following sections.

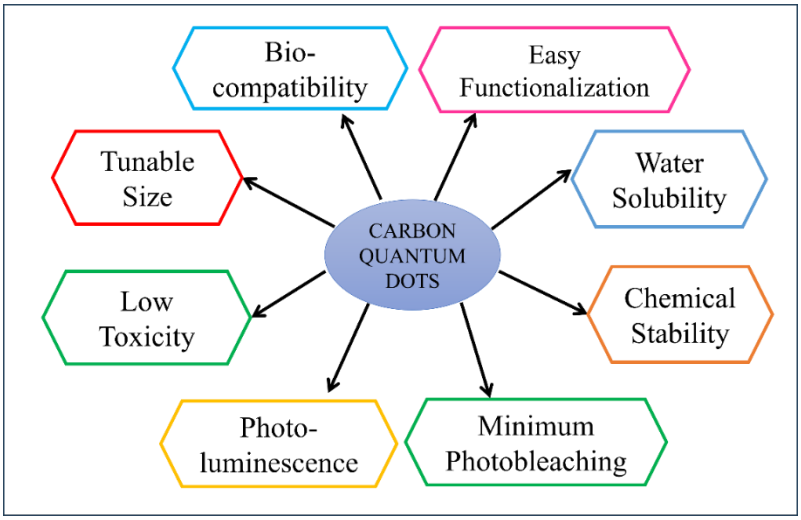

Figure 1.1: Properties of CQDs.

1.4.1 Photoluminescence (PL):

Photoluminescence (PL) is a phenomenon in which a material emits light after absorbing photons. In the case of CQDs, this process occurs due to the recombination of electron-hole pairs. When CQDs are excited by photons, typically through UV or visible light irradiation, electrons absorb energy and transition to higher energy levels, leaving behind holes in the lower energy levels. As these excited electrons return to their ground state, they emit photons, resulting in the characteristic light emission of

CQDs. For instance, smaller CQDs tend to emit light at shorter wavelengths (blue or green), whereas larger CQDs emit light at longer wavelengths (red or near-infrared).

To date, no researchers have identified a definitive PL mechanism for CQDs. However, two primary light-emission mechanisms have been proposed: one based on band gap transitions in the conjugated π domain and the other on surface defects of CQDs [3].

Some studies attribute the red-shift in the emission of CQDs to quantum size effects, based on the first explanation. Specifically, CQDs exhibit particle size-dependent PL behavior when their size is smaller than their exciton radius [4]. The surface state is the primary factor influencing fluorescence variation in CQDs. This refers to the relationship between the luminescence properties of CQDs and their surface functional groups [5]. These functional groups can create various energy potential traps, with both sp^2- and sp^3-hybridized regions contributing to surface energy traps [6]. The fluorescence of CQDs derived from surface state defects is attributed to the localized π-electron structure of electron-hole pairs in the sp^2 state. In doped CQDs, the luminescence mechanism is primarily governed by surface state luminescence. Additionally, doping can significantly enhance the fluorescence quantum yield of CQDs [7].

In addition, some CQDs exhibit up-conversion photoluminescence (UCPL) [8], a phenomenon in which light of a shorter wavelength is emitted after the sequential absorption of two or more photons with a longer wavelength. CQDs with UCPL properties are highly advantageous for in vivo imaging due to their unique ability to emit light when excited by longer-wavelength radiation, such as near-infrared (NIR).

1.4.2 Tunable emission:

The emission spectrum of CQDs can be precisely controlled by adjusting synthesis parameters such as reaction temperature, precursor composition, and surface functionalization. This tunability allows researchers to modify the emission properties of CQDs to suit specific application requirements.

One fascinating property of CQDs is their ability to modify their optical and electrical properties based on particle size. As illustrated in Figure 1.2, this feature

enables the achievement of a wide range of wavelengths and conductive behaviors. To analyze the optical and structural properties of synthesized CQDs and optimize their performance, advanced characterization techniques such as spectroscopy, microscopy, and electrochemical methods are employed [9].

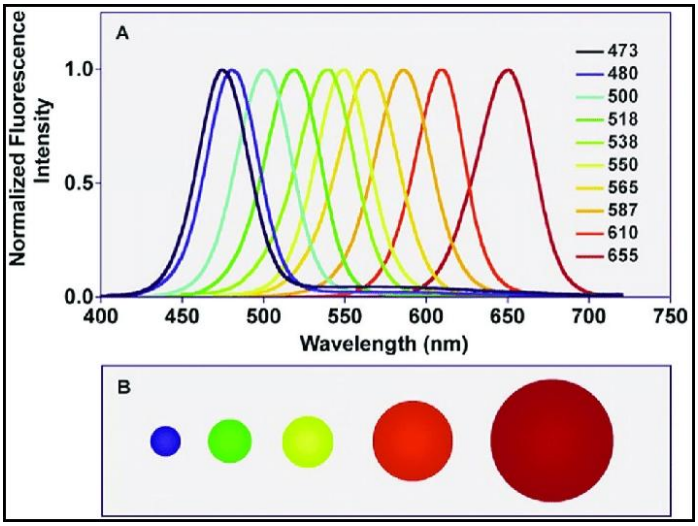

Figure 1.2: A) Size-dependent fluorescence emission spectra of QDs and (B) different relative particle sizes with diameters between 2.1-7.5 nm [9].

For instance, in bioimaging applications, CQDs with emission wavelengths in the near-infrared (NIR) region are preferred due to their deeper tissue penetration and reduced autofluorescence. Similarly, in applications such as sensors, optoelectronics, and photocatalysis, CQDs can be tailored to exhibit specific emission characteristics that align with the desired functionality.

1.4.3 Quantum yield (QY):

QY is the ratio of emitted number of photons to number of photons absorbed. It quantifies the ability of particle to release absorbed electromagnetic radiation as photons. The QY of CQDs are proportional to its fluorescence property. Surface functionalization of CQD also affects QY. High QY of CQD is generally attributed to presence of varied organic fluorescence on the surface of CQDs.

1.4.4 Surface functionalization:

The surface of CQDs plays a crucial role in determining their optical properties and stability. Surface passivation and functionalization with various organic ligands or

polymers can enhance the PL quantum yield, improve colloidal stability, and impart biocompatibility to CQDs. Additionally, surface functionalization enables the conjugation of biomolecules such as nucleic acids, peptides, antibodies, and small molecules, expanding the applications of CQDs in biosensing and targeted imaging.

Surface passivation is particularly important for enhancing the PL properties of CQDs and facilitating the adsorption of biomolecules onto their surface. CQDs consist of both sp^2 and sp^3 carbon domains, which contain numerous defects that create energy gaps, leading to variations in their PL behavior [10].

Various polymers, such as polyethylene glycol (PEG) and polyethyleneimine (PEI), have been employed for surface functionalization. This highlights the crucial role of functionalization agents in enhancing PL properties. Utilizing this approach, nitrogen, oxygen, sulfur, and phosphorus groups have also been doped into CQDs [11].

Overall, surface functionalization with organic molecules and polymers is an effective strategy for enhancing the fluorescence intensity of CQDs. Optimizing functionalization conditions and selecting appropriate functionalization agents can lead to CQDs with enhanced fluorescence properties.

In summary, the exceptional optical properties of CQDs, particularly their strong PL and tunable emission, make them promising materials for a wide range of applications in bioimaging, sensing, and optoelectronics.

1.4.5 Minimum photobleaching:

CQDs exhibit remarkable resistance to photobleaching, making them highly desirable for long-term imaging and sensing applications. Photobleaching refers to the irreversible loss of fluorescence intensity when fluorophores are exposed to prolonged light irradiation. Unlike traditional organic dyes or fluorescent proteins, CQDs demonstrate exceptional photostability due to their robust carbon-based structure and resistance to photo-induced degradation.

This characteristic allows CQDs to retain their fluorescence even under prolonged or intense light exposure, ensuring consistent and reliable performance in applications like bioimaging, optoelectronics, and photodynamic therapy. Their

minimal photobleaching not only enhances their suitability for dynamic and time-lapse studies but also reduces signal loss, thereby improving the accuracy and efficiency of fluorescence-based techniques [12].

1.4.6 Biocompatibility:

CQDs are highly valued for their excellent biocompatibility, making them ideal for a wide range of biomedical applications. As carbon-based nanomaterials, CQDs exhibit minimal toxicity and negligible immunogenicity, ensuring safe interactions with living cells and tissues. Their surface can be easily functionalized with biocompatible molecules, enabling targeted delivery for therapeutic or diagnostic purposes.

Due to their ability to interact with biological environments without causing adverse effects, CQDs have been extensively used in bioimaging, drug delivery, and biosensing. Additionally, their water solubility and chemical stability make them well-suited for both *in vivo* and *in vitro* applications, highlighting their potential as a safe and effective tool in regenerative medicine and nanomedicine [13].

1.5 Synthesis of CQDs:

Over the past decade, researchers have developed numerous methods for synthesizing CQDs, which can be broadly classified into top-down and bottom-up approaches. This chapter provides a detailed overview of the synthesis methods for CQDs. Figure 1.3 illustrates the different techniques used.

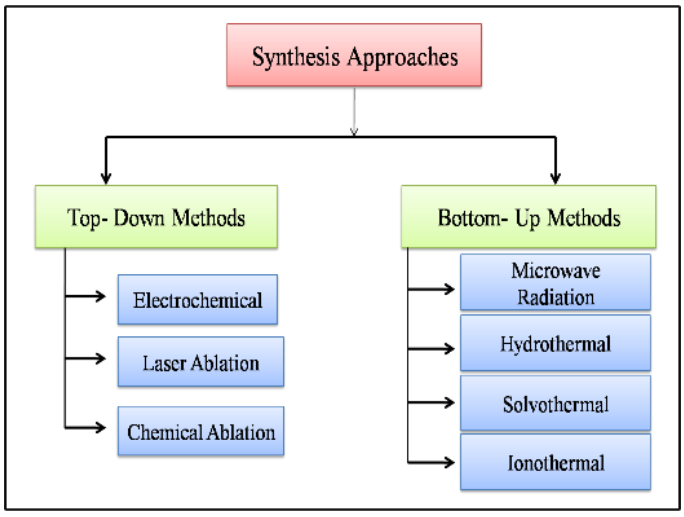

Figure 1.3: Synthesis methods of CQDs.

However, several challenges arise during CQD synthesis. One major issue is carbonaceous accumulation during carbonization, which can be addressed using methods such as electrochemical synthesis, confined pyrolysis, or solution chemistry techniques. Another challenge is maintaining size control and uniformity, as achieving consistent CQD size is crucial for ensuring reproducibility in manufacturing and applications. Additionally, the surface properties of CQDs play a significant role in their solubility and overall functionality, making it essential to carefully optimize surface chemistry both during and after synthesis to enhance their suitability for specific applications.

1.5.1 Electrochemical method:

The electrochemical approach is a top-down method for synthesizing CQDs through the nonselective chemical cutting of carbon materials such as graphite, carbon nanotubes, or carbon fiber electrodes. However, CQDs produced using this method often exhibit uneven sizes and distributions, necessitating additional purification steps like filtration or chromatography to obtain monodispersed CQDs.

In a reported method, CQDs are synthesized from o-phenylenediamine (OPD) through a series of steps, including polymerization, carbonization, and passivation at an anode. Initially, OPD molecules undergo oxidation at the anode, where electrons are removed from the nitrogen atom, leading to the formation of free radicals. These radicals subsequently react with other OPD molecules, forming dimers, trimers, and polymers. Due to the negligible protonation of the amino group in OPD, the resulting polymers predominantly adopt ladder-like structures.

To obtain CQDs, the polymers are further subjected to carbonization and passivation. Notably, during electrolysis, the formation of NaCl, H_2, and Cl_2 occurs at the cathode and anode, which also plays a role in CQD formation [14].

A modified one-pot electrochemical synthesis of CQDs was reported by Deng et al. [15]. In their study, CQDs were fabricated using alcohol as a precursor within a three-electrode system. This system comprised platinum sheets as the working and counter electrodes, while calomel electrodes served as reference electrodes. The electrode distance was controlled using rubber plugs.

During the electrochemical process, alcohol undergoes carbonization, resulting in the formation of extremely small carbon particles, or CQDs. This method provides a simple and efficient approach for synthesizing high-quality CQDs. Figure 1.4 illustrates this electrochemical carbonization process.

For the electrochemical synthesis of green CQDs, graphite rods were used as electrodes in an alcoholic NaOH solution, with a constant current of 50 mA applied via a DC power supply. The electrolyte solution (0.1M NaOH and EtOH) facilitated the formation of $C_2H_5ONa^+$ and OH^- ions. The negatively charged OH^- ions migrated toward the anode, initiating the electrochemical cutting of graphite and the production of CQDs. This mechanism effectively generates green CQDs [16].

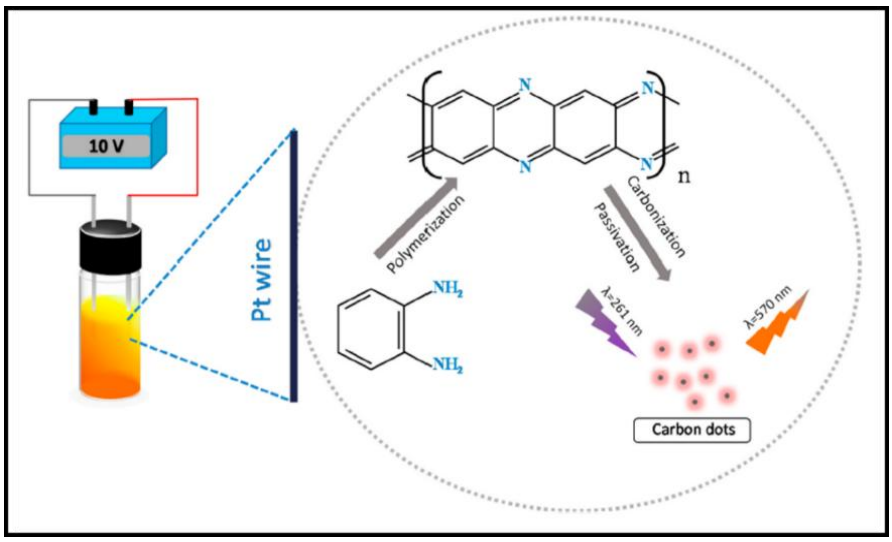

Figure 1.4: Schematic representation of CQD fabrication process using the electrochemical method with OPD as the carbon source [15].

1.5.2 Laser ablation:

The laser ablation method is widely used to obtain colloidal nanoparticle solutions in various solvents. This technique offers several advantages, including high fabrication rates, fine particle sizes, and excellent monodispersity. In this process, a laser beam is directed onto a target material, rapidly heating and vaporizing it. The vaporized material then condenses in the surrounding liquid medium, forming nanoparticles. By adjusting laser parameters such as energy and pulse duration, the size and shape of the nanoparticles can be precisely controlled.

Additionally, using multi-target precursors enables the synthesis of nanoparticles with diverse compositions. By selecting different target materials and fine-tuning laser settings, researchers can engineer nanoparticles with tailored material properties for specific applications, including catalysis, energy storage, and sensing. Overall, laser ablation is a versatile and efficient method for producing colloidal nanoparticles with controlled size, composition, and properties for a wide range of applications. In a study conducted by Y. Hou et al. [17], N-heptane was selected as the solvent for the laser ablation process. Activated carbon (5 mg) was dispersed in 10 mL of N-heptane using ultrasonication for 20 minutes. Following dispersion, laser irradiation was performed for 130 minutes, during which the suspension changed to a yellowish hue, confirming the formation of CQDs (as illustrated in Figure 1.5).

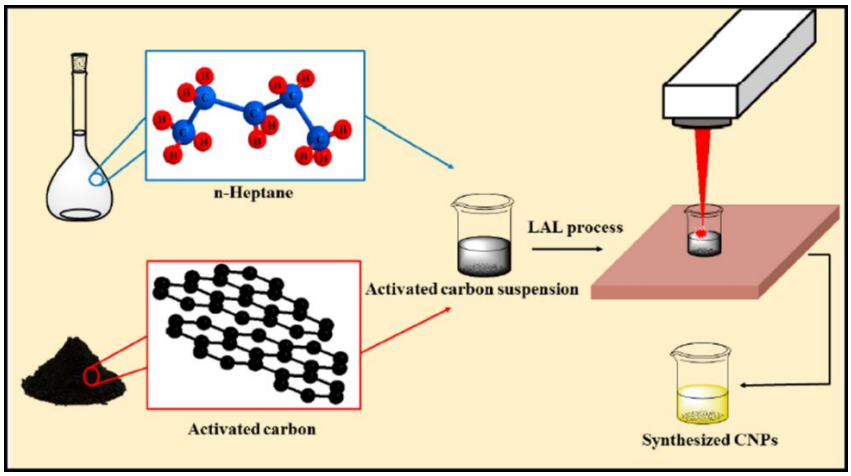

Figure 1.5: Schematic representation of laser ablation method for synthesis of carbon nanoparticles [17].

This method employs laser ablation to disperse powders, producing nanomaterials with a homogeneous surface structure and a narrow size distribution. Additionally, during laser ablation, complex functionalization of nanoparticles can be achieved by incorporating specific ligands into various liquid media, enabling active species to interact with molecules in solution [18].

In another study, hexagonal boron nitride (hBN) was used as a precursor for CQD synthesis via laser ablation. The femtosecond laser ablation technique successfully tuned the PL of boron nitride quantum dots (BNQDs) from the ultraviolet (UV) to the green region. The synthesized CQDs exhibited three distinct luminescence wavelengths: UV, blue, and green. Various liquids, including ethanol, diethylamine,

and ethylenediamine, were used as dispersion media for hBN powder, leading to the formation of BNCQDs, which hold potential as fluorescence probes for bioimaging. Additionally, polyethyleneimine (PEI) and graphite were utilized in laser ablation to synthesize fluorescent carbon dots, further demonstrating the versatility of this technique [19].

Kaczmarek et al. [20] proposed the use of nanoparticles or quasi-molecular fluorophores synthesized by combining PEI and ethylenediamine (EDA). Their study revealed that the QY—a measure of photon emission efficiency—was five times higher in the dialysate (the liquid that passes through a dialysis membrane) than in the retentate (the remaining liquid after dialysis). This suggests the presence of free fluorescent molecules, which significantly contribute to the observed luminescence.

1.5.3 Microwave radiation:

Numerous synthesis methods have been developed for preparing carbon nanoparticles, offering a diverse range of approaches. However, many of these methods are time-consuming, complex, and economically unfeasible. Unlike traditional microwave-assisted synthesis, reverse microwave-assisted synthesis accelerates chemical reactions at low temperatures, operating within a power range of 100W–200W.

This method was used to rapidly synthesize nitrogen-doped carbon quantum dots (N-CQDs) by mixing a 10% glucose solution with a 25% ammonium hydroxide solution in a 5:1 ratio. The mixture was subjected to microwave irradiation at 100°C for 1 minute, yielding N-CQDs with a high nitrogen content, primarily in the form of pyridinic/NH_2 groups.

Additionally, these N-CQDs demonstrated photocatalytic activity in degrading Rose Bengal (RB), a highly toxic organic dye classified as genotoxic, mutagenic, and cytotoxic [21]. An alternative synthesis approach utilized silk fibroin (SF), a biomedical waste material, making it a sustainable option for applications in bioimaging, biosensing, and drug delivery.

Ko N. R et al. [22] proposed alternative methods for synthesizing nitrogen-doped CQDs using cocoon silk through an autoclave process. However, the microwave

assisted method is considered more advantageous due to its shorter synthesis time and the production of larger, more uniform CQDs. The literature highlights several mechanisms for enhancing reactions via microwave-assisted techniques, including thermal effects, specific microwave effects, and non-thermal effects.

In this study, lemon and onion biomass were used for the microwave-assisted synthesis of CQDs, as illustrate in Figure 1.6. This developed analytical approach analyzed various commercial vitamin and mineral supplements, with a particular focus on riboflavin quantification. This method has been evaluated against established techniques, demonstrating its potential for accurate riboflavin determination [23].

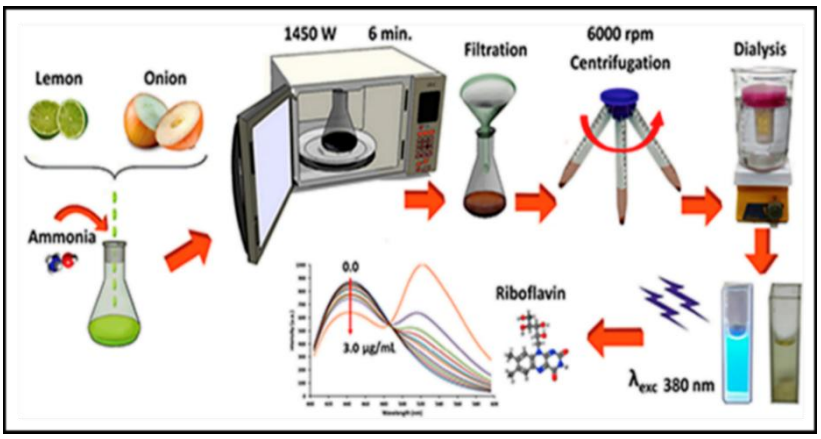

Figure 1.6: Schematic representation of microwave-assisted CQDs from lemon and onion [23].

1.5.4 Hydrothermal/ solvothermal method:

Hydrothermal synthesis is a bottom-up approach for preparing nanomaterials, based on a solution-phase reaction process. In this method, a Teflon-lined autoclave is used, where high temperatures and pressures are applied to the reaction materials. Pressure is generated by tightly sealing the autoclave valves.

CQDs can be synthesized via single-step pyrolysis using citric acid and branched PEI at temperatures above 200°C. The PEI-functionalized CQDs, exhibiting a QY of 42.5%, have been utilized for chemical sensing [24].

CQDs synthesized from carrot juice via the hydrothermal method demonstrated maximum photoluminescence excitation at 360 nm, emitting at 442 nm, revealing a

Stokes shift of 82 nm [25]. The emission peak wavelength varies with excitation due to the broad size distribution of CQDs.

A facile one-step approach has been employed to synthesize nitrogen and sulfur-doped CQDs from L-lysine and thiourea. These CQDs exhibit a high QY of 53.19%, emit strong blue fluorescence under UV light, and have been applied for picric acid detection [26].

Several studies have explored small organic molecules as carbon sources for CQD synthesis. For instance, Chen et al. [27] utilized carbon tetrachloride as a carbon source and $NaNH_2$ as a nitrogen dopant via the hydrothermal method, yielding nitrogen-doped CQDs with a graphite-like structure (~3.3 nm lateral size and 0.5–5 nm height).

In hydrothermal-assisted pyrolysis, Kundu et al. [28] adopted a green synthesis route using citric acid, passivated with branched PEI, to enhance surface functionality. The resulting nitrogen-doped CQDs exhibited multicolor emission, making them suitable for cellular imaging.

Xie et al. [29] synthesized green-emitting CQDs from highland barley (carbon source) and ethylenediamine (nitrogen source) using the hydrothermal method. These CQDs demonstrated selective and sensitive Hg^{2+} detection via fluorescence quenching, exhibiting excitation-dependent fluorescence with a size range of 4.5–7 nm and strong blue emission. Figure 1.7 illustrates the hydrothermal synthesis of CQDs using 1,5-diaminonaphthalene (DAN) and citric acid, along with the resulting CQD structure.

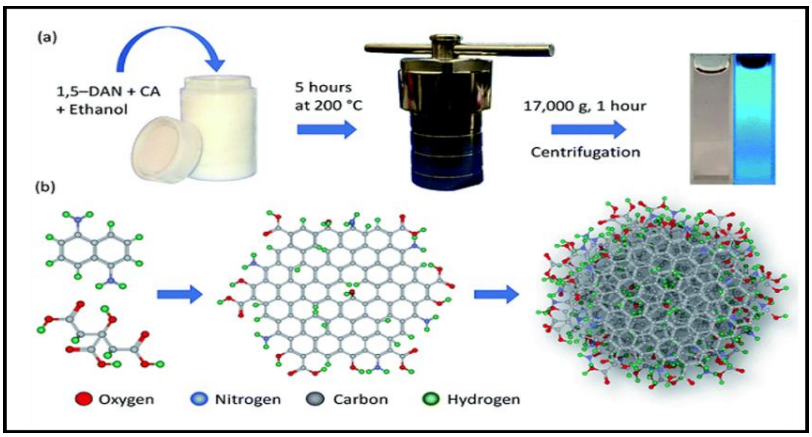

Figure 1.7: (a) Schematic representation of CQD by hydrothermal method using 1,5-diaminonaphthalene (1,5-DAN) and citric acid, and (b) Reaction pathway and particle structure [29].

1.5.5 Pyrolysis method:

The field of CQDs was revolutionized by Emmanuel P. Giannelis and his research team [30], who pioneered a novel synthesis method involving the controlled carbonization and pyrolysis of organic small molecules. This breakthrough led to the creation of highly luminescent CQDs, opening new frontiers in materials science. Their research revealed that ammonium citrate salts play a crucial role in CQD synthesis, where the organic ammonium component acts as a surface modifier, and citrate serves as the primary carbon source. This synergistic interaction results in brightly fluorescent CQDs with diverse applications across various fields.

By carefully selecting surface modifiers, researchers have fine-tuned CQD properties, yielding both organic and hydrophilic variants. Notably, they discovered that amide functionalization in CQDs, essential for modulating reactive oxygen species (ROS) generation, originates from surface proteins of bacterial origin. Beyond citrate-based precursors, a variety of small organic molecules have been successfully employed in pyrolytic CQD synthesis, including: EDTA-derived polymers, Epoxy-enriched polystyrene, Natural precursors such as hair, tea leaves, konjac flour, and red pepper.

The diversity of these precursor materials highlights the versatility of CQD synthesis, paving the way for cutting-edge applications in biomedicine, optoelectronics, and beyond.

Figure 1.8: Schematic representation of fennel seeds CQD synthesis by pyrolysis technique [31].

Mono-dispersed CQDs were successfully synthesized from *Foeniculum vulgare* (fennel seeds) through a one-step thermal decomposition approach (Figure 1.8) [31]. These CQDs exhibited: (a) High photostability with resistance to photodegradation, (b) Superior colloidal stability, (c) pH stability without the need for additional surface passivation, and (d) Strong excitation-independent photoluminescence.

The reaction time and temperature during pyrolysis significantly impact CQD formation, influencing size, structure, and optical properties. However, a major limitation of the carbonization-pyrolysis method is the difficulty in achieving precise size and structural control due to carbon aggregation during synthesis. Consequently, purification and sonication are critical steps to ensure monodispersed, high-quality CQDs.

1.6 CQDs-Nucleic acid conjugate:

1.6.1 Introduction to nucleic acid and its significance:

DNA serves as the blueprint for the genetic information of an organism. It contains instructions necessary for the development, growth, and functioning of living organisms. RNA acts as an intermediary molecule that translates the genetic information encoded in DNA into functional proteins through the process of transcription and translation. Understanding the structure and function of nucleic acids is unraveling the complexities of genetic diseases, cancer, and developmental disorders.

Nucleic acid plays pivotal roles in diagnostic techniques such as polymerase chain reaction (PCR), DNA sequencing, and gene expression profiling. These methods enable the detection of genetic mutations, infectious agents, and gene expression patterns associated with diseases. In biomedicine, nucleic acids serve as therapeutic agents in gene therapy, RNA interference (RNAi), and antisense therapy. These approaches leverage the ability of nucleic acids to modulate gene expression, target specific molecular pathways, and treat genetic disorders and viral infections.

Nucleic acid can be conjugated with various nanoparticles, quantum dots, and fluorophores to enhance their imaging properties, target specificity, and biocompatibility. Their multifaceted roles underscore their significance in biomedical research and their potential to revolutionize healthcare in the future.

1.6.2 Methods for conjugation of nucleic acids with CQDs:

The conjugation of nucleic acids with CQDs has potential uses in biosensing, bioimaging, drug delivery, and therapies. Here are some methods commonly used for conjugating nucleic acids with CQDs:

1.6.2.1 Covalent conjugation:

Covalent conjugation involves the formation of strong, stable chemical bonds between CQDs and nucleic acids. For covalent conjugation, CQDs can be functionalized with amine groups and carboxyl groups. In amine group functionalization CQDs conjugated with nucleic acids via amide bond formation. Amine functionalization involves introducing amino ($-NH_2$) groups onto the surface of CQDs. This can be accomplished by using amine-reactive cross-linkers like NHS (N-hydroxysuccinimide) esters. Nucleic acids can be conjugated with carboxyl functionalized CQDs through carboxyl functionalization. Carboxyl functionalization involves introducing carboxyl (-COOH) groups onto the surface of CQDs. This can be achieved through various methods as oxidation of hydroxyl groups and surface modification with carboxyl groups. The oxidizing agents such as nitric acid and potassium permanganate were used to oxidize hydroxyl groups. For surface functionalization with carboxyl groups citric acid and succinic anhydride were used.

These covalent conjugation methods offer advantages such as increased stability and control over the conjugation process. However, careful optimization of reaction conditions is required to ensure efficient conjugation while maintaining the integrity and functionality of both CQDs and nucleic acids. Additionally, the choice between amine and carboxyl functionalization depends on factors such as the desired orientation of the conjugated molecules and compatibility with downstream applications.

1.6.2.2 Non-covalent conjugation:

Non-covalent conjugation refers to the association or binding of molecules through noncovalent interactions, such as hydrogen bonding, van der Waals forces, π-π interactions, electrostatic interactions, and hydrophobic interactions, rather than forming strong chemical bonds. π-π stacking interactions between the aromatic rings of nucleic acids and the surface of CQDs can facilitate non-covalent conjugation. In

electrostatic interactions, functionalized CQDs with charged groups can interact electrostatically with nucleic acids, which are negatively charged under physiological conditions. This type of conjugation is common in various biological processes and the design of functional materials.

Each of these methods offers advantages and limitations depending on the specific application requirements, such as conjugation efficiency, stability, and biocompatibility. The choice of method depends on factors such as the desired stability of the conjugate, the specificity of the interaction, and the compatibility with downstream applications.

Recent studies have focused on the interaction between CQDs and different types of DNA, including double-stranded DNA (dsDNA) and single-stranded DNA (ssDNA). These interactions have shown distinct fluorescence behavior [32]. For instance, Loo et al. [33] developed a sensing platform that utilized CQDs and a fluorescently labeled ssDNA probe called the FAM L-probe. This platform was designed to detect a specific DNA strand. The fluorescence of the FAM L-probe (ssDNA) was effectively quenched by CQDs when it was in the presence of single-stranded DNA unless it formed a double-stranded DNA complex with the target DNA.

In summary, the interaction between CQDs and different types of DNA, such as dsDNA and ssDNA, has demonstrated unique fluorescence behavior, leading to the development of sensitive sensing platforms for DNA detection. The findings suggest that the interaction between positively charged CQDs can have significant effects on the structure and conformation of DNA [34]. The ability of CQDs to induce the transition of B-DNA to Z-DNA highlights their potential role in modulating important biological processes [35]. The binding of CQDs to the major groove of DNA further supports their strong interactions with nucleic acids. This understanding of the interaction between CQDs and DNA can have implications not only in sensing applications but also in the development of novel strategies for DNA manipulation and control in biotechnology and nanomedicine [36].

1.7 Characterization techniques to confirm CQD-nucleic acid conjugates:

To confirm the successful conjugation of nucleic acids with CQDs, comprehensive characterization using various analytical techniques are essential. Spectroscopic

methods, such as UV-Vis absorption spectroscopy and fluorescence spectroscopy, evaluate changes in the optical properties of CQD-nucleic acid conjugates compared to bare CQDs. Dynamic light scattering (DLS) and zeta potential measurements provide valuable insights into the size distribution and surface charge of the conjugates, which are critical for their stability and colloidal behavior. Additionally, transmission electron microscopy (TEM) and atomic force microscopy (AFM) offer morphological analysis, revealing details about particle size, shape, and surface structure.

1.8 Need for Bioimaging:

The phrase "bioimaging" especially refers to fundamental imaging techniques that entail the non-invasive observation and real-time detection of biological activity. Today, bioimaging has become a significant, dependable medical technique for identifying and treating a variety of illnesses that affect the human body while barely interfering with normal biological functions. Bioimaging facilitates the measurement of ions and metabolite levels, as well as the observation of subcellular organelles, cells, tissues, and even multicellular organisms. Light, electrons, ultrasound, X-rays, magnetic resonance, and positrons have all been used up to this point [37].

1.9 Bioimaging techniques:

Modern imaging technologies focus on structural and anatomical imaging at the organ or tissue level. Each imaging modality has its own advantages and limitations in terms of specificity, sensitivity, cost-effectiveness, and spatial and temporal resolution [38].

For example, radioisotope imaging enables simultaneous visualization of multiple target tissues in a single scan, supported by computerized analytics. However, this technique has significant drawbacks, including non-specificity in disease detection, making it difficult to distinguish between benign and malignant tumors. It also struggles with precise localization of the emission source and exposes patients to high radiation levels, increasing health risks such as gene mutation.

Similarly, conventional X-ray imaging is a widely used and practical diagnostic tool with relatively low radiation exposure. However, it has several limitations, including the extensive use of ionizing radiation, which can be harmful to the human

body, a time-consuming film development process, and low accuracy in detecting physical abnormalities. In contrast, digital X-ray imaging addresses many of these limitations by significantly reducing radiation exposure, allowing for easy image processing with higher resolution, and being more cost-effective and environmentally friendly.

Computed Tomography (CT) scanning provides high-resolution, cross-sectional images and enables rapid image acquisition. However, its high radiation dose makes it unsuitable for frequent use, and some patients may experience adverse reactions to the procedure.

Ultrasound imaging is a non-invasive and cost-effective alternative to radioisotope imaging, X-rays, and CT scans. It provides clear visualization of soft tissues without radiation exposure, making it a safer option. However, ultrasound has limitations, such as lower resolution compared to other imaging techniques and limited penetration through bone, which restricts its application in skeletal imaging [39].

Positron Emission Tomography (PET) imaging offers high sensitivity, making it valuable for detecting metabolic and functional changes. However, it relies on radioactive tracers, which increase radiation exposure, and its high operational costs require expensive cyclotrons for radionuclide production.

Magnetic Resonance Imaging (MRI) provides high spatial resolution, particularly for soft tissue and neurological imaging. However, it has drawbacks, including lower sensitivity compared to other imaging techniques and limited ability to provide precise chemical or dynamic data [40].

Each imaging technique has its strengths and weaknesses. While MRI and PET offer superior resolution and sensitivity, they come with high costs and operational challenges. Ultrasound remains a safer and more economical choice, although it has some resolution limitations. Digital X-ray and CT scanning provide detailed imaging, but concerns about radiation exposure remain significant. The choice of imaging modality depends on clinical requirements, safety considerations, and cost-effectiveness.

Due to their specific drawbacks, conventional imaging technologies have been found unsuitable for biophotonics applications, often leading to ineffective diagnosis. Enhancing imaging techniques for better cellular visualization has become a critical area of focus, aiming to enable faster and more accurate detection, screening, diagnosis, and image-assisted treatment of life-threatening diseases, including cancer.

In this context, fluorescence imaging, when combined with appropriate contrast agents, presents a highly effective approach for both fundamental research and clinical diagnosis. Unlike traditional imaging methods, fluorescence imaging utilizes lower excitation energy within the visible spectrum, making it a safer alternative. Additionally, it offers several significant advantages, including a safer optical regime, enhanced sensitivity and selectivity for molecular-level imaging, a higher signal-to-noise ratio, multidimensional imaging capabilities, and seamless integration with conventional imaging techniques.

1.10 Literature survey

1.10.1 Review of CQD synthesis strategies:

Semiconductor QDs have garnered significant attention over the past two decades due to their numerous applications in electronics, electrochemistry, biotechnology, sensors, and catalysis. While ZnS, ZnSe, CdS, CdSe, and silicon QDs have been extensively used as fluorescent probes for cell labeling, their cytotoxicity renders them unsuitable for *in vivo* biological applications [41].

Recently, CQDs have emerged as promising alternative fluorescent nanoprobes due to their availability, thermal stability, and relatively non-cytotoxic nature [42]. CQDs have demonstrated versatile applications, including bioimaging [43], catalysis [44], and the photoreduction of metals [45], owing to their high electron donor-acceptor ability. Additionally, CQDs have shown potential in biosensing [46], particularly due to their peroxidase-like activity [47].

CQDs or carbon nanoparticles (CNPs) can be synthesized through various techniques, including microwave irradiation of sucrose [48] or polyethylene glycol, combustion of carbon soot [49], activated carbon [50] or carbon xerogels [51] using

nitric acid, proton beam irradiation of nanodiamonds [52], solvothermal degradation of graphene oxide [53], and electrochemical oxidation of graphite [54].

One of the most intriguing features of CQDs is their PL properties, which exhibit excitation-dependent emission intensity [55], similar to that of semiconductor QDs. However, the origin of this fascinating property remains a subject of debate. It is speculated that quantum effects, emissive traps [56], and primarily the radiative recombination of excitons contribute to the PL characteristics of CQDs.

Yang et al. [57] proposed that introducing different functional groups onto the surface of CQDs can create surface defects, potentially leading to PL properties. However, the exact mechanism underlying this phenomenon requires further clarification. Proper surface passivation is essential to enhance the PL intensity of carbon nanomaterials with inherently low QY. Various amine-terminated organic molecules have been employed to achieve this enhancement.

Post-passivated CQDs exhibit a significant increase in PL intensity, often surpassing their original fluorescence levels. Sun and co-workers [58] demonstrated that doping CQDs with ZnO and ZnS, followed by surface passivation with PEG-1500N, resulted in a substantial enhancement of PL intensity. Additionally, Baker et al. [59] reported a rapid single-step laser passivation method for CDs in organic solvents.

More recently, Wang et al. [47] introduced a simple method for synthesizing fluorescent carbon nanoparticles from carbohydrates without surface passivation. Their study explored the enhancement of PL properties in CQDs through the influence of various cations and anions. While surface passivation remains the most effective technique for improving QY, the precise impact of metal ions and organic substances on PL intensity remains unclear in many cases.

The introduction of divalent metal ions such as Sn^{2+}, Cd^{2+}, and Zn^{2+} effectively enhances PL intensity of carbonaceous nanodots synthesized from starch. Among these, Sn^{2+} exhibits the highest enhancement effect, while Cd^{2+} has the lowest. However, a particularly intriguing phenomenon was observed upon the addition of a small amount of Cu^{2+}, which caused a drastic quenching of the PL.

Systematic fluorescence enhancement and quenching were also noted in the presence of organic solvents for all QDs synthesized from chitosan, alginic acid, and starch. Extensive studies on PL intensity variations with changes in pH and excitation wavelength have been conducted, leading to plausible speculations regarding the mechanisms behind fluorescence enhancement and quenching.

The highest fluorescent metal-doped QDs were further utilized as bioimaging agents against *Staphylococcus aureus* as a model organism. The influence of anions and cations on PL properties was previously reported by Wang et al. [47], demonstrating that an increase in the valency of cations, anions, or both resulted in a gradual enhancement of PL intensity. Table 1.1 provides a summary of the precursors, synthesis routes, and applications of these CQDs.

Table 1.1: Different synthesis routes with precursor and applications of CQDs

Sr No.	Precursors	Synthesis route	Application	Ref.
1.	Graphite rods	Electrochemical method, hydrothermal treatment	Water splitting	[60]
2.	Graphite rods, NH_3, and urea	Electrochemical method, Hydrothermal treatment, Pyrolysis	Water splitting	[61]
4.	Graphite rods	Electrochemical method	Acid catalysis	[62]
7.	Adenosine triphosphate	Hydrothermal	Fe^{3+} Sensing	[63]
8.	Juju bees	Hydrothermal	Sensing	[64]
9.	Sweet potatoes	Hydrothermal	Sensing	[65]
10.	Jinhua bergamot	Hydrothermal	Sensing	[66]
11.	N-Methyl pyrrolidone,	Pyrolysis	Bioimaging, electrocatalysts	[67]

	dimethyl-imidazolidinone			
12.	Diammonium hydrogen citrate, urea	Solid state reaction	Sensor, bioimaging,	[68]
13.	Citric acid, diethylenetriamine, gadolinium chloride	Hydrothermal	Bioimaging	[69]
14.	Hair	Carbonization-microwave	Bioimaging	[70]
15.	Gelatin	Hydrothermal	Bioimaging, fluorescent Ink	[71]
16.	Citric acid, cysteamine	Hydrothermal	Composites, bioimaging	[72]
17.	Alanine, ethylenediamine	Hydrothermal	Biosensing, bioimaging	[73]
18.	Amino acids	Electrochemical/electroanalytical	Bioimaging	[74]
19.	Orange juice	Hydrothermal treatment at 120°C	Bioimaging	[75]
20.	Citric acid	Hydrothermal	Drug Delivery	[76]
21.	Branched PEI, ammonium persulfate	Hydrothermal	Gene Delivery	[77]
22.	Arginine and glucose	Microwave-assisted pyrolysis	Non-viral gene delivery	[78]

The concept of doping in CQDs was first introduced in 2012, with nitrogen doping gaining prominence following the pioneering work of Zhu et al. [79]. In the same year, Li's group [80] explored co-doping strategies, incorporating magnesium and nitrogen atoms. More recently, a strategy capable of doping up to three different atoms onto the pristine surface has been developed, significantly improving QY through the synergistic effect of the doped atoms [81].

In 2013, Anilkumar et al. [82] investigated the crosslinking of surface-passivated CQDs to enhance their optical performance. Beyond improving QY, recent modifications have focused on developing synthetic strategies to obtain well-defined CQDs with high scalability and reproducibility. These experimental advancements in CQD research have been continuously supported by theoretical interpretations, particularly from density functional theory (DFT) and time-dependent DFT (TD-DFT) studies, which provide insights into doping, functionalization, and passivation processes [83].

1.10.2 Literature survey on surface functionalized CQDs-based bioimaging applications:

Table 1.2 illustrates the various bioimaging applications utilizing functionalized CQDs. It includes details about the carbon source, the functionalizing agent used, and the specific imaging targets.

Table 1.2: Bioimaging applications based on functionalized CQDs with a carbon source, functionalizing agent, and target of imaging.

Sr. No	Carbon Source	Functionalization agent, Nanoprobe size	Imaging probe	Ref
1.	Glycerol and a silane molecule	Nitrogen doping, ~6.1 nm	Fe^{3+}	[84]
2.	(3-aminopropyl) triethoxysilane (APTES)	3.5 ± 0.5 nm	Mitochondria	[85]
3.	*p*-phenylenediamine	4-formylbenzeneboronic acid, ~1.73 nm	Cell nucleus	[86]
4.	Citric acid	Polyethylene glycol,	Cell nucleus	[87]
5.	Citric acid	N, N-dimethylaniline, 2~0.4 nm	Lysosome	[88]

6.	Konjac flour	magnetic mesoporous silica nanoparticles,	Mitochondria	[89]
7.	o-phenylenediamine	(3-Carboxyprop-1-yl) (triphenyl) phosphonium bromide, 3–8 nm	Peroxynitrite in mitochondria	[90]
8.	2,4-dihydroxy benzaldehyde, 2,3-dimethyl benzothiazole iodide	--, 6.78 ± 0.3 nm	RNA	[91]
9.	m-phenylenediamine, 1,2,3-propane tricarboxylic acid	--, 4.34 ± 1.13 nm	ClO^- in cell nucleus	[92]
10.	L-tryptophan, L-phenylalanine	DNA, 4.8 nm	MFC-7, HepG 2 cells	[93]
11.	lotus root	Glutathione, 1−3.8 nm	Human bladder cancer T24 cells	[94]
12.	$CdSO_4$, *C. sinensis* plant leaves	--, 2−5 nm	A549 lung cancer cell	[95]
13.	Sucrose, oil acid	--, ~1.84 nm	16 HBE cells	[96]
14.	Polyolefin waste	--, 1.5-3.5 nm	MDA-MB 468 cell	[97]
15.	Citric acid-urea/neutral red-triethyl amine	MnO_2 nanosheet/MnO_2 nanoflower, ~5 nm	Glutathione	[98]
16.	2-azidoimidazole	--, 5.0 nm	Cysteine	[99]
17.	Gram shells	--, 3–5 nm	Escherichia coli	[100]
18.	Aconitic acid	--, 1.6 nm	Targeted imaging of folate receptor over expressed cancer cells	[101]
19.	Tartaric acid, urea	--, 3 nm	Multicolor cell imaging	[102]
20.	Folic acid	Stearic acid-g-polyethyleneimine, --	Triple Negative Breast Cancer	[103]

1.10.3 Literature survey on surface functionalized CQDs-nucleic acid conjugation-based bioimaging applications:

Surface functionalization of CQDs plays a crucial role in their conjugation with nucleic acids and subsequent bioimaging applications. Functional groups such as amine ($-NH_2$), carboxyl (-COOH), and hydroxyl (-OH) are introduced onto CQD surfaces to facilitate covalent or non-covalent interactions with nucleic acids. Yan C et al. [104] developed amino-functionalized CQDs that were conjugated with DNA probes via carbodiimide chemistry for fluorescence imaging of specific mRNA sequences in live cells. Similarly, Fu Z et al. [105] reported carboxyl-functionalized CQDs conjugated with aptamers for selective imaging of cancer biomarkers. These studies demonstrated that functionalization enhances stability, target specificity, and biocompatibility.

The ability of CQD-nucleic acid conjugates to selectively bind target biomolecules makes them highly effective for bioimaging applications. In fluorescence imaging, Prakash A et al. [106] synthesized nitrogen-doped CQDs conjugated with microRNA probes for fluorescence imaging of cancer cells, achieving high sensitivity and low background interference. Multiplexed imaging is another advantage, where surface-engineered CQDs with diverse functional groups enable the emission of different fluorescence wavelengths. Das et al. [107] introduced dual-emission CQDs conjugated with distinct nucleic acid sequences for the simultaneous detection of multiple intracellular targets, facilitating advanced disease diagnostics. Additionally, CQD-nucleic acid conjugates have been utilized for real-time live-cell imaging.

The stability and non-toxicity of CQD-nucleic acid conjugates are crucial for *in vivo* applications. Researchers have developed passivation strategies using PEG and zwitterionic coatings to improve biocompatibility.

Despite significant advancements, challenges such as photobleaching, potential cytotoxicity at higher concentrations, and limited *in vivo* penetration remain. Future research should focus on optimizing functionalization techniques to enhance target specificity and developing hybrid CQDs with superior optical properties for high-resolution bioimaging.

Nucleic acids, especially DNA, are one of the most stable classes of biomolecules. DNA is not only a carrier of genetic information but also a versatile

structural tool for the engineering and self-assembling of nanostructures. The natural selection of DNA as the hereditary material during evolution is due to its remarkable tolerance to chemical reactivity. DNA has several interesting characteristics, which are: (i) polyanionic nature, (ii) hybridizability, and (iii) persistence length. In this regard, the DNA template has dramatically enhanced the scalability, programmability, and functionality of the self-assembled DNA nanostructures. These capabilities provide opportunities for a wide range of biomedical applications in biosensing, bioimaging, drug delivery, and disease therapy.

Deoxyribonucleic acid (DNA) is a biomolecule made up of nucleobases that are strung together in a sequence to form a chain of polynucleotides. There are four basic nucleobases in DNA, namely adenine (A), thymine (T), cytosine (C), and guanine (G). The number and sequence of these basic nucleobases in the polynucleotide chain determine the encoding information and structural function of the DNA. Based on the Watson-Crick pairing interactions, helical duplexes or more complex structures can be formed from the basic nucleobases. This pairing interaction allows for the easy holding together of multiple building units such as colloid nanoparticles. The binding mode of small molecules to the DNA double helical structure features three major modes of non-covalent interactions, including electrostatic interactions, groove binding, and intercalation [108].

Calf thymus DNA (DNA from calf thymus) is high-quality double-stranded template DNA isolated from the thymus of male and female calves. Calf thymus DNA (Ct-DNA) is used for research into the interaction between DNA and other agents. It is also used in the preparation of prehybridization and hybridization solutions and DNA polymerase assays. Ct-DNA is also used to study the binding parameters and binding specificity of proteins, nucleotides, and chemical reagents. It is frequently used in pull-down assays and chromatographic procedures. There are many reports available on Ct-DNA interaction with pesticides, insecticides, antiviral, and anticancer drugs [109-112]. The Ct-DNA with nanoparticles such as silver [113], TiO_2 [114], iron oxide [115], zinc oxide [116], selenium nanoparticles [117], and nickel oxide [118] were studied for binding interaction. The common binding patterns were seen as groove binding and intercalation.

Chun-Yan Liang et al. [119] reported the interaction binding mechanism of CQDs with Ct-DNA using ascorbic acid as a carbon precursor. UV-vis absorbance, fluorescence spectroscopy, circular dichroism spectroscopy, and electrochemical approaches were employed to study the binding mechanism between CQDs and Ct-DNA. The binding mode observed between CQDs and Ct-DNA was intercalation.

In another study, Yang et al. [120] synthesized CQDs with PEI and folic acid, which were used to deliver plasmids encoding the enhanced green fluorescent protein into HEK 293T cells. These CQDs can be applied in biological systems for the selective imaging of folate receptor-positive cancer cells, distinguishing them from normal cells.

Pentaethylenehexamine CQDs (PCDs) synthesized by Wei Zhang et al. [121] showed lower cytotoxicity and high transfection efficiency at its plasmid composite in comparison to PEI (widely used gene delivery vector for transfection).

Currently, there are no existing reports on the synthesis of poly L lysine (PLL) surface functionalized CQDs using the bottom-up pyrolysis method, based on the literature study conducted. So, we aim to prepare PLL surface functionalized CQDs nucleic acid conjugate for bioimaging applications.

1.11 Orientation and purpose of the thesis:

The thesis consists of six chapters. **Chapter 1** provides a brief introduction to bioimaging and its necessity in medical diagnostics. It discusses the evolution of major bioimaging techniques from plain radiography to fluorescence imaging, commonly used nanoprobes for bioimaging along with their associated challenges, and the potential of CQDs as alternative nanoprobes. The advantages of CQDs over traditional nanoprobes, various synthetic routes for CQD preparation, and their limitations are comprehensively reviewed. Furthermore, this chapter delves into the synthesis of surface-functionalized CQDs and their bioimaging applications, including CQD-nucleic acid conjugates.

Chapter 2 focuses on the purification methods for CQDs and provides an in-depth exploration of the working principles and theoretical background of various spectroscopic and microscopic techniques. The purification methods discussed in this chapter are crucial for obtaining CQDs of desirable size. A thorough understanding of

these techniques is crucial for precisely analyzing data and gaining valuable insights into the size, morphology, optical properties, and surface chemistry of CQDs. This chapter provides a detailed overview of CQD purification methods and characterization techniques.

Chapter 3 explores the synthesis of surface-functionalized CQDs (PLLCQDs) through pyrolysis, utilizing glucose as a precursor. The influence of temperature, pH, and concentration is systematically examined to optimize PLLCQD synthesis. Various spectroscopic techniques, including UV-vis spectroscopy, fluorescence spectroscopy, Fourier transform infrared spectroscopy (FTIR), X-ray diffraction (XRD), and X-ray photoelectron spectroscopy (XPS), are employed to investigate the optical, structural, and surface chemical properties of the synthesized PLLCQDs. Additionally, microscopic techniques such as TEM and AFM are used to assess their size, shape, and morphology. This chapter presents a comprehensive study on the synthesis and characterization of PLLCQDs, emphasizing their imaging potential.

Chapter 4 focuses on the conjugation of PLLCQDs with nucleic acids, highlighting the optimization of the conjugation process. Key parameters, including Ct-DNA concentration, incubation time, and pH, are systematically adjusted and analyzed using various analytical techniques. The success of the conjugation is validated through a gel retardation assay and zeta potential measurements. Additionally, the chapter discusses the significance of Ct-DNA binding to PLLCQDs and its role in bioimaging applications. The attachment of Ct-DNA to PLLCQDs enhances imaging capabilities, enabling researchers to gain deeper insights into cellular functions. Overall, this chapter highlights optimization PLLCQD-Ct-DNA conjugate and underscores the potential of Ct-DNA conjugation for advanced bioimaging applications.

Chapter 5 investigates the *in-vitro* bioimaging applications of surface-functionalized PLLCQD-nucleic acid conjugates. It begins with a brief overview of the experimental setup for preparing and characterizing these conjugates, followed by a cell viability assay conducted on human embryonic kidney (HEK-293) cells. The in-vitro bioimaging study evaluates cell viability and DNA transfection using PLLCQDs alone, PLLCQD-nucleic acid conjugates, and DNA. The MTT assay is employed to assess cell viability, while confocal microscopy is used for *in-vitro* bioimaging analysis.

Chapter 6 provides a summary of the key findings and conclusions from each chapter, highlighting the importance of PLLCQDs and PLLCQD-Ct-DNA conjugates in bioimaging applications. These conjugates have shown significant potential as alternative tools for bioimaging techniques. The surface functionalization of PLLCQDs enhances their stability and compatibility with biological systems, while nucleic acid conjugation further broadens their application in targeted imaging and intracellular DNA delivery. The *in-vitro* bioimaging potential of these conjugates was assessed through cell viability assays and Ct-DNA uptake studies, confirming their biocompatibility and efficiency in imaging. Overall, this chapter underscores the crucial role of PLLCQD and PLLCQD-Ct-DNA conjugates as promising nanoprobes for advanced bioimaging applications.

1.12 References:

1. Xu X., Ray R., Gu Y., Ploehn H. J., Gearheart L., Raker K., Scrivens W. A., Electrophoretic analysis and purification of fluorescent single-walled carbon nanotube fragments, Journal of the American Chemical Society. 126 (40) (2004) 12736-12737, DOI-10.1021/ja040082h.
2. Sun Y. P., Zhou B., Lin Y., Wang W., Fernando K. S., Pathak P., Meziani M. J., Harruff B. A., Wang X., Wang H., Luo P. G., Quantum-sized carbon dots for bright and colorful photoluminescence, Journal of the American Chemical Society. 128 (24) (2006) 7756-7757, DOI-10.1021/ja062677d.
3. Zhao S., Wu S., Jia Q., Huang L., Lan M., Wang P., Zhang W., Lysosome targetable carbon dots for highly efficient photothermal/photodynamic synergistic cancer therapy and photoacoustic/two-photon exited fluorescence imaging, chemical Engineering Journal. 388 (1) (2020) 124212-124225, DOI-10.1016/j.cej.2020.124212.
4. Zhu S., Song Y., Zhao X., Shao J., Zhang J., Yang B., The photoluminescence mechanism in carbon dots (graphene quantum dots, carbon nanodots, and polymer dots): current state and future perspective, Nano Research. 8 (1) (2015) 355-381, DOI-10.1007/s12274-014-0644-3.
5. Xia C., Zhu S., Feng T., Yang M., Yang B., Evolution and synthesis of carbon dots: from carbon dots to carbonized polymer dots, Advanced Science. 6 (1) (2019) 1-23, DOI-10.1002/advs.201901316.
6. Xu X., Mo L., Li Y., Pan X., Hu G., Lei B., Zhang X., Zheng M., Zhuang J., Liu Y., Hu C., Construction of carbon dots with color-tunable aggregation-induced emission by nitrogen-induced intramolecular charge transfer, Advanced Materials. 33 (1) (2021) 2104872, DOI-10.1002/adma.202104872.
7. Chan K. K., Yap S. H., Yong K.T., Biogreen synthesis of carbon dots for Biotechnology and nanomedicine applications, Nano-Micro Letters. 10 (1) (2018) 1-42. DOI-10.1007/s40820-018-0223-3
8. Xu Q., Gao J., Wang S., Wang Y., Liu D., Wang J., Quantum dots in cell imaging and their safety issues, Journal of Material Chemistry B. 9 (2021) 5765-5779, DOI-10.1039/D1TB00729G.
9. Girma W. M., Fahmi M. Z., Permadi A., Abate M. A., Chang J. Y., Synthetic strategies and biomedical applications of I–III–VI ternary quantum dots, Journal of Materials Chemistry B. 5 (31) (2017) 6193-6216, DOI-10.1039/C7TB01156C.

10. Miao P., Han K., Tang Y., Wang B., Lin T., Cheng W., Recent advances in carbon nanodots: synthesis, properties and biomedical applications. Nanoscale. 7 (5) (2015) 1586-1595, DOI-10.1039/C4NR05712K.

11. Xu Y., Wu M., Liu Y., Feng X. Z., Yin X. B., He X.W., Zhang Y. K., Nitrogen-doped carbon dots: a facile and general preparation method, photoluminescence investigation, and imaging applications. Chemistry–A European Journal. 19 (7) (2013) 2276-2283, DOI-10.1002/chem.201203641.

12. Zhang L., Yang X., Yin Z., Sun L., A review on carbon quantum dots: Synthesis, photoluminescence mechanisms and applications. Luminescence. 37(10) (2022) 1612-1638, DOI-10.1002/bio.4351.

13. Tian X., Zeng A., Liu Z., Zheng C., Wei Y., Yang P., Zhang M., Yang F., Xie F., Carbon quantum dots: In vitro and in vivo studies on biocompatibility and biointeractions for optical imaging. International journal of nanomedicine. 28(1) (2020) 6519-6529, DOI-10.2147/IJN.S257645.

14. Sayyah S. M., El-Deeb M. M., Kamal S. M., Azooz R. E., Electropolymerization of Ophenylenediamine on Pt-electrode from aqueous acidic solution: kinetic, mechanism, electrochemical studies and characterization of the polymer obtained, Journal of Applied Polymer Science. 112 (6) (2009) 3695-3706, DOI-10.1002/ app.29802.

15. Deng J., Lu Q., Mi N., Li H., Liu M., Xu M., Tan L., Xie Q., Zhang Y., Yao S., Electrochemical synthesis of carbon nanodots directly from alcohols, Chemistry: A European Journal. 20 (17) (2014) 4993-4999, DOI-10.1002/ chem.201304869.

16. Devi N. R., Kumar T. V., Sundramoorthy A. K., Electrochemically exfoliated carbon quantum dots modified electrodes for detection of dopamine neurotransmitter, Journal of Electrochemical Society. 165 (12) (2018) G3112, DOI-10.1149/2.0191812jes.

17. Hou Y., Lu Q., Deng J., Li H., Zhang Y., One-pot electrochemical synthesis of functionalized fluorescent carbon dots and their selective sensing for mercury ion, Analytica Chimica Acta. 866 (1) (2015) 69–74, DOI-10.1016/j.aca.2015.01.039.

18. Zhang D., Gokce B., Barcikowski S., Laser synthesis and processing of colloids: fundamentals and applications, Chemical Reviews. 117 (5) (2017) 3990–4103, DOI-10.1021/acs.chemrev.6b00468.

19. Nguyen V., Yan L., Zhao N., Van Canh N., Hang N. T., Le P. H., Tuning photoluminescence of boron nitride quantum dots via surface functionalization by

femtosecond laser ablation, Journal of Molecular Structure. 1244 (1) (2021) 1-7, DOI-10.1016/j.molstruc.2021.130922.

20. Kaczmarek A., Hoffman J., Morgiel J., Mościcki T., Stobiński L., Szymański Z., Małolepszy A., Luminescent carbon dots synthesized by the laser ablation of graphite in polyethylenimine and ethylenediamine, Materials. 14 (4) (2021) 1–13, DOI-10.3390/ma14040729.

21. Feng J., Wang W. J., Hai X., Yu Y. L., Wang J. H., Green preparation of nitrogen doped carbon dots derived from silkworm chrysalis for cell imaging, Journal of Material Chemistry: B. 4 (3) (2016) 387–393, DOI-10.1039/c5tb01999k.

22. Ko N. R, Nafiujjaman M, Cherukula K, Lee SJ, Hong SJ, Lim HN, Park CH, Park IK, Lee YK, Kwon IK. Microwave-assisted synthesis of biocompatible silk fibroin-based carbon quantum dots. Particle & Particle Systems Characterization. 35 (3) (2018) 1700300-1700334, DOI-10.1002/ppsc.201700300.

23. Monte-Filho S. S., Andrade S. I., Lima M. B., Araujo M. C., Synthesis of highly fluorescent carbon dots from lemon and onion juices for determination of riboflavin in multivitamin/mineral supplements, Journal of Pharmaceutical Analysis. 9 (3) (2019) 209–216, DOI-10.1016/j.jpha.2019.02.003.

24. Wang H., Ma Q., Wang Y., Wang C., Qin D., Shan D., Chen J., Lu X., Resonance energy transfer based electrochemiluminescence and fluorescence sensing of riboflavin using graphitic carbon nitride quantum dots, Analytical Chimica Acta. 973 (1) (2017) 34–42, DOI-10.1016/j.aca.2017.03.041.

25. Dinç S., A simple and green extraction of carbon dots from sugar beet molasses: biosensor applications, Sugar Industry. 141 (9) (2016) 560–564, DOI-10.36961/ si17741.

26. Dong Y., Wang R., Li H., Shao J., Chi Y., Lin X., Chen G., Polyamine-functionalized carbon quantum dots for chemical sensing, Carbon 50 (8) (2012) 2810–2815, DOI-10.1016/j. carbon.2012.02.046.

27. Chen X., Gong F., Cao Z., Zou W., Gu T., Highly cysteine-selective fluorescent nanoprobes based on ultrabright and directly synthesized carbon quantum dots, Analytical and Bioanalytical Chemistry. 410 (12) (2018) 2961–2970, DOI-10.1007/ s00216-018-0980-3.

28. Kundu A., Lee J., Park B., Ray C., Sankar K. V., Kim W. S., Lee S. H., Cho I. J., Jun S. C., Facile approach to synthesize highly fluorescent multicolor emissive

carbon dots via surface functionalization for cellular imaging, Journal of Colloid Interface Science. 513 (1) (2018) 505–514, DOI-10.1016/j.jcis.2017.10.095.

29. Xie Y., Cheng D., Liu X., Han A., Green hydrothermal synthesis of N-doped carbon dots from biomass highland barley for the detection of Hg^{2+}, Sensors. 19 (14) (2019) 1-18, DOI-10.3390/s19143169.

30. Bourlinos A. B., Karakassides M. A., Kouloumpis A., Gournis D., Bakandritsos A., Papagiannouli I., Aloukos P., Couris S., Hola K., Zboril R., Krysmann M., Synthesis, characterization and non-linear optical response of organophilic carbon dots, Carbon. 61 (1) (2013) 640-643, DOI-10.1016/j.carbon.2013.05.017.

31. Dager A., Uchida T., Maekawa T., Tachibana M., Synthesis and characterization of mono-disperse carbon quantum dots from fennel seeds: photoluminescence analysis using machine learning. Scientific reports. 9 (1) (2019) 14004, DOI-10.1038/s41598-019-50397-5.

32. Ouyang X., Liu J., Li J., Yang R., A carbon nanoparticle-based low-background biosensing platform for sensitive and label-free fluorescent assay of DNA methylation. Chemical Communications. 48 (1) (2012) 88-90, DOI-10.1039/C1CC15511C.

33. Loo A. H., Sofer Z., Bouša D., Ulbrich P., Bonanni A., Pumera M., Carboxylic carbon quantum dots as a fluorescent sensing platform for DNA detection. ACS applied materials & interfaces. 8 (3) (2016) 1951-1957, DOI-10.1021/acsami.5b10160.

34. Wang C. I., Wu W. C., Periasamy A. P., Chang H.T., Sensitive and selective DNA probe based on “turn-on” photoluminescence of C-dots@ RGO. Analytical and bioanalytical chemistry. 406 (1) (2014) 6917-6923, DOI-10.1007/s00216-014-7658-2.

35. Sun H., Ren J., Qu X., Carbon nanomaterials and DNA: From molecular recognition to applications. Accounts of Chemical Research. 49 (3) (2016) 461-470, DOI-10.1021/acs.accounts.5b00515.

36. Feng L., Zhao A., Ren J., Qu X., Lighting up left-handed Z-DNA: photoluminescent carbon dots induce DNA B to Z transition and perform DNA logic operations. Nucleic acids research. 41 (16) (2013) 7987-7996, DOI-10.1093/nar/gkt575.

37. Rich A., Zhang S., Z-DNA: the long road to biological function. Nature Reviews Genetics. 4 (7) (2003) 566-572, DOI-10.1038/nrg1115.

38. Cer R. Z., Bruce K. H., Mudunuri U. S., Yi M., Volfovsky N., Luke B. T., Bacolla A., Collins J. R., Stephens R. M., Non-B DB: a database of predicted non-B DNA-forming motifs in mammalian genomes. Nucleic acids research. 39 (suppl_1) (2010) 383-391, DOI-10.1093/nar/gkq1170.

39. http://cab.ku.dk/what_is_bioimaging.

40. Zhang K. Y., Yu Q., Wei H., Liu S., Zhao Q., Huang W., Long-lived emissive probes for time-resolved photoluminescence bioimaging and biosensing. Chemical reviews. 118 (4) (2018) 1770-1839, DOI-10.1021/acs.chemrev.7b00425.

41. Mahmoudi M., Hosseinkhani H., Hosseinkhani M., Boutry S., Simchi A., Journeay W. S., Subramani K., Laurent S., Magnetic resonance imaging tracking of stem cells in vivo using iron oxide nanoparticles as a tool for advancing clinical regenerative medicine. Chemical reviews. 111 (2) (2011) 253-280, DOI-10.1021/cr1001832.

42. Hardman R., A toxicologic review of quantum dots: toxicity depends on physicochemical and environmental factors. Environmental health perspectives. 114 (2) (2006) 165-172, DOI-10.1289/ehp.8284.

43. Yang S. T., Wang X., Wang H., Lu F., Luo P.G., Cao L., Meziani M. J., Liu J. H., Liu Y., Chen M., Huang Y., Carbon dots as nontoxic and high-performance fluorescence imaging agents. The Journal of Physical Chemistry C. 113 (42) (2009) 18110-18114, DOI-10.1021/jp9085969.

44. Ray S. C., Saha A., Jana N. R., Sarkar R., Fluorescent carbon nanoparticles: synthesis, characterization, and bioimaging application. The Journal of Physical Chemistry C. 113 (43) (2009) 18546-18551, DOI-10.1021/jp905912n.

45. Liu C., Zhang P., Tian F., Li W., Li F., Liu W., One-step synthesis of surface passivated carbon nanodots by microwave assisted pyrolysis for enhanced multicolor photoluminescence and bioimaging. Journal of Materials Chemistry. 21 (35) (2011) 13163-13167, DOI-10.1039/C1JM12744F.

46. Yadav P. K., Chandra S., Kumar V., Kumar D., Hasan S. H., Carbon quantum dots: synthesis, structure, properties, and catalytic applications for organic synthesis. Catalysts. 13 (2) (2023) 1-22, DOI-10.3390/catal13020422.

47. Wang X., Qu K., Xu B., Ren J., Qu X., Multicolor luminescent carbon nanoparticles: synthesis, supramolecular assembly with porphyrin, intrinsic peroxidase-like catalytic activity and applications. Nano Research. 2011 (4) (2011) 908-920, DOI-10.1007/s12274-011-0147-4.

48. Zhou L., Lin Y., Huang Z., Ren J., Qu X., Carbon nanodots as fluorescence probes for rapid, sensitive, and label-free detection of Hg^{2+} and thiols in complex matrices. Chemical communications. 48 (8) (2012) 1147-1149, DOI-10.1039/C2CC16791C.

49. Liu H., Ye T., Mao C., Fluorescent carbon nanoparticles derived from candle soot. Angewandte Chemie. 119 (34) (2007) 6593-6595, DOI-10.1002/ange.200701271.

50. Dong Y., Zhou N., Lin X., Lin J., Chi Y., Chen G., Extraction of electrochemiluminescent oxidized carbon quantum dots from activated carbon. Chemistry of Materials. 22 (21) (2010) 5895-5899, DOI-10.1021/cm1018844.

51. Chandra S., Mitra S., Laha D., Bag S., Das P., Goswami A., Pramanik P., Fabrication of multi-structure nanocarbons from carbon xerogel: a unique scaffold towards bio-imaging. Chemical Communications. 47 (30) (2011) 8587-8589, DOI-10.1039/C1CC11848J.

52. Yu S. J., Kang M. W., Chang H. C., Chen K. M., Yu Y. C., Bright fluorescent nanodiamonds: no photobleaching and low cytotoxicity. Journal of the American Chemical Society. 127 (50) (2005) 17604-17605, DOI-10.1021/ja0567081.

53. Wei W., Xu C., Ren J., Xu B., Qu X., Sensing metal ions with ion selectivity of a crown ether and fluorescence resonance energy transfer between carbon dots and graphene. Chemical communications. 48 (9) (2012) 1284-1286, DOI-10.1039/C2CC16481G.

54. Chandra S., Das P., Bag S., Laha D., Pramanik P., Synthesis, functionalization and bioimaging applications of highly fluorescent carbon nanoparticles. Nanoscale. 3 (4) (2011) 1533-1540, DOI-10.1039/C0NR00735H.

55. Zhu S., Zhang J., Qiao C., Tang S., Li Y., Yuan W., Li B., Tian L., Liu F., Hu R., Gao H., Strongly green-photoluminescent graphene quantum dots for bioimaging applications. Chemical communications. 47 (24) (2011) 6858-6860, DOI-10.1039/C1CC11122A.

56. Kim T. W., Chung P. W., Slowing I. I., Tsunoda M., Yeung E. S., Lin V. S., Structurally ordered mesoporous carbon nanoparticles as a transmembrane delivery vehicle in human cancer cells. Nano letters. 8 (11) (2008) 3724-3727, DOI-10.1021/nl801976m.

57. Yang Y., Cui J., Zheng M., Hu C., Tan S., Xiao Y., Yang Q., Liu Y., One-step synthesis of amino-functionalized fluorescent carbon nanoparticles by hydrothermal carbonization of chitosan. Chemical Communications. 48 (3) (2012) 380-382, DOI-10.1039/C1CC15678K.

58. Sun Y. P., Zhou B., Lin Y., Wang W., Fernando K. S., Pathak P., Meziani M. J., Harruff B. A., Wang X., Wang H., Luo P. G., Quantum-sized carbon dots for bright and colorful photoluminescence. Journal of the American Chemical Society. 128 (24) (2006) 7756-7757, DOI-10.1021/ja062677d.

59. Baker S. N., Baker G.A., Luminescent carbon nanodots: emergent nanolights. Angewandte Chemie International Edition. 49 (38) (2010) 6726-6744, DOI-10.1002/anie.200906623.

60. Wu X., Zhao J., Guo S., Wang L., Shi W., Huang H., Liu Y., Kang Z., Carbon dot and $BiVO_4$ quantum dot composites for overall water splitting via a two-electron pathway. Nanoscale. 8 (39) (2016) 17314-17321, DOI-10.1039/c6nr05864g.

61. Amiralian N., Annamalai P. K., Memmott P., Taran E., Schmidt S., Martin D. J., Easily deconstructed, high aspect ratio cellulose nanofibres from Triodia pungens; an abundant grass of Australia's arid zone, RSC Adv. 5 (1) (2015) 32124–32132, DOI-10.1039/C5RA02936H.

62. Li H., Liu R., Kong W., Liu J., Liu Y., Zhou L., Zhang X., Lee S.T., Kang Z., Carbon quantum dots with photo-generated proton property as efficient visible light-controlled acid catalyst. Nanoscale. 6 (2) (2014) 867-873, DOI-10.1039/C3NR03996J.

63. Shangguan J., Huang J., He D., He X., Wang K., Ye R., Yang X., Qing T., Tang J., Highly Fe^{3+} selective fluorescent nanoprobe based on ultrabright N/P codoped carbon dots and its application in biological samples. Analytical chemistry. 89 (14) (2017) 7477-7484, DOI- 10.1021/acs.analchem.7b01053.

64. Kim K., Kim J., Synthesis of carbon quantum dots from jujubes for detection of iron (III) ions, Journal of Nanoscience and Nanotechnology. 18 (2) (2017) 1320–1322, DOI-10.1166/jnn.2018.14901.

65. Shen J., Shang S., Chen X., Wang D., Cai Y., Facile synthesis of fluorescence carbon dots from sweet potato for Fe^{3+} sensing and cell imaging, Material Science Engineering: C. 76 (1) (2017) 856–864, DOI-10.1016/j.msec.2017.03.178.

66. Yu J., Song N., Zhang Y. K., Zhong S. X., Wang A. J., Chen J., Green preparation of carbon dots by Jinhua bergamot for sensitive and selective fluorescent detection of Hg^{2+} and Fe^{3+}, Sensors Actuators: B Chemical. 214 (1) (2015) 29–35, DOI-10.1016/j.snb.2015.03.006.

67. Lei Z., Xu S., Wan J., Wu P., Facile synthesis of N-rich carbon quantum dots by spontaneous polymerization and incision of solvents as efficient bioimaging probes

and advanced electrocatalysts for oxygen reduction reaction, Nanoscale. 8 (4) (2016) 2219–2226, DOI-10.1039/c5nr07335a.

68. Khan W. U., Wang D., Zhang W., Tang Z., Ma X., Ding X., Du S., Wang Y., High quantum yield green-emitting carbon dots for Fe (III) detection, biocompatible fluorescent ink and cellular imaging, Scientific Reports. 7 (1) (2017), DOI-10.1038/s41598-017-15054-9.

69. Yu C., Xuan T., Chen Y., Zhao Z., Liu X., Lian G., Li H., Gadolinium-doped carbon dots with high quantum yield as an effective fluorescence and magnetic resonance bimodal imaging probe, Journal of Alloys Compounds. 688 (1) (2016) 611–619, DOI-10.1016/j.jallcom.2016.07.226.

70. Zhang J. H., Niu A., Li J., Fu J. W., Xu Q., Pei D. S., In vivo characterization of hair and skin derived carbon quantum dots with high quantum yield as long-term bioprobes in zebrafish, Scientific Reports. 6 (1) (2016) 1-12, DOI-10.1038/srep37860.

71. Liang Q., Ma W., Shi Y., Li Z., Yang X., Easy synthesis of highly fluorescent carbon quantum dots from gelatin and their luminescent properties and applications, Carbon. 60 (1) (2013) 421–428, DOI-10.1016/j.carbon.2013.04.055.

72. Yang M., Meng X., Li B., Ge S., Lu Y., N, S co-doped carbon dots with high quantum yield: tunable fluorescence in liquid/solid and extensible applications, Journal of Nanoparticle Research. 19 (6) (2017), DOI-10.1007/s11051-017-3914-7.

73. Niu W. J., Li Y., Zhu R. H., Shan D., Fan Y. R., Zhang X. J., Ethylenediamine-assisted hydrothermal synthesis of nitrogen-doped carbon quantum dots as fluorescent probes for sensitive biosensing and bioimaging, Sensors Actuators: B Chemistry. 218 (1) (2015) 229–236, DOI-10.1016/j.snb.2015.05.006.

74. Niu F., Xu Y., Liu J., Song Z., Liu M., Liu J., Controllable electrochemical/ electroanalytical approach to generate nitrogen-doped carbon quantum dots from varied amino acids: pinpointing the utmost quantum yield and the versatile photoluminescent and electrochemiluminescent applications, Electrochimica Acta. 236 (1) (2017) 239–251, DOI-10.1016/j.electacta.2017.03.085.

75. Sahu S., Behera B., Maiti T. K., Mohapatra S., Simple one-step synthesis of highly luminescent carbon dots from orange juice: application as excellent bio-imaging agents, Chemical Communication. 48 (70) (2012) 8835–8837, DOI-10.1039/ c2cc33796g.

76. Yang L., Wang Z., Wang J., Jiang W., Jiang X., Bai Z., He Y., Jiang J., Wang D., Yang L., Doxorubicin conjugated functionalizable carbon dots for nucleus targeted delivery and enhanced therapeutic efficacy, Nanoscale. 8 (12) (2016) 6801–6809, DOI-10.1039/c6nr00247a.

77. Hu L., Sun Y., Li S., Wang X., Hu K., Wang L., Liang X. J., Wu Y., Multifunctional carbon dots with high quantum yield for imaging and gene delivery, Carbon 67 (1) (2014) 508–513, DOI-10.1016/j. carbon.2013.10.023.

78. Cao X., Wang J., Deng W., Chen J., Wang Y., Zhou J., Du P., Xu W., Wang Q., Wang Q., Yu Q., Photoluminescent cationic carbon dots as efficient non-viral delivery of plasmid SOX9 and chondrogenesis of fibroblasts, Scientific Reports. 8 (1) (2018) 7057-7068, DOI-10.1038/s41598-018-25330-x.

79. Zhu S., Meng Q., Wang L., Zhang J., Song Y., Jin H., Zhang K., Sun H., Wang H., Yang B., Highly photoluminescent carbon dots for multicolor patterning, sensors, and bioimaging. Angewandte Chemie International Edition. 52 (14) (2013) 3953-3957, DOI-10.1002/ange.201300519.

80. Li F., Liu C., Yang J., Wang Z., Liu W., Tian F., Mg/N double doping strategy to fabricate extremely high luminescent carbon dots for bioimaging. RSC Advance. 4 (1) (2013) 3201–3205, DOI-10.1039/C3RA43826K.

81. Peng H., Travas-Sejdic J., Simple aqueous solution route to luminescent carbogenic dots from carbohydrates. Chemistry of Materials. 21 (23) (2009) 5563-5565, DOI-10.1021/cm901593y.

82. Anilkumar P., Cao L., Yu J.J., Tackett K.N., Wang P., Meziani M.J., Sun Y.P., Crosslinked carbon dots as ultra-bright fluorescence probes. Small. 9 (4) (2013) 545-551, DOI-10.1002/smll.201202000.

83. Wang C., Ding Y., Bi X., Luo J., Wang G., Lin Y., Carbon quantum dots-Ag nanoparticle complex as a highly sensitive “turn-on” fluorescent probe for hydrogen sulfide: a DFT/TD-DFT study of electronic transitions and mechanism of sensing. Sensors and Actuators B: Chemical. 1 (1) (2018) 404-409, DOI-10.1016/j.snb.2018.02.186.

84. Gao G., Jiang Y. W., Jia H. R., Yang J., Wu F. G., On-off-on fluorescent nanosensor for Fe^{3+} detection and cancer/normal cell differentiation via silicon-doped carbon quantum dots. Carbon. 134 (1) (2018) 232-243, DOI-10.1016/j.carbon.2018.02.063

85. Gao G., Jiang Y. W., Yang J., Wu F. G., Mitochondria-targetable carbon quantum dots for differentiating cancerous cells from normal cells. Nanoscale. 9 (46) (2017) 18368-18378, DOI-10.1039/C7NR06764J.

86. Phukan K., Sarma R. R., Dash S., Devi R., Chowdhury D., Carbon dot-based nucleus targeted fluorescence imaging and detection of nuclear hydrogen peroxide in living cells. Nanoscale Advances. 4 (1) (2022) 138-149, DOI-10.1039/D1NA00617G.

87. Yang L., Jiang W., Qiu L., Jiang X., Zuo D., Wang D., Yang L., One pot synthesis of highly luminescent polyethylene glycol anchored carbon dots functionalized with a nuclear localization signal peptide for cell nucleus imaging. Nanoscale. 7 (14) (2015) 6104-6113, DOI-10.1039/C5NR01080B.

88. Guo S., Sun Y., Geng X., Yang R., Xiao L., Qu L., Li Z., Intrinsic lysosomal targeting fluorescent carbon dots with ultrastability for long-term lysosome imaging. Journal of Materials Chemistry: B. 8 (4) (2020) 736-742, DOI- 10.1039/C9TB02043H.

89. Zhang Y., Shen Y., Teng X., Yan M., Bi H., Morais P. C., Mitochondria-targeting nano platform with fluorescent carbon dots for long time imaging and magnetic field-enhanced cellular uptake. ACS applied materials & interfaces. 7 (19) (2015) 10201-102012, DOI-10.1021/acsami.5b00405.

90. Wu X., Sun S., Wang Y., Zhu J., Jiang K., Leng Y., Shu Q., Lin H., A fluorescent carbon-dots-based mitochondria-targetable nanoprobe for peroxynitrite sensing in living cells. Biosensors and Bioelectronics. 90 (2017) 501-507, DOI-10.1016/j.bios.2016.10.060.

91. Yin X., Sun Y., Yang R., Qu L., Li Z., RNA-responsive fluorescent carbon dots for fast and wash-free nucleolus imaging. Spectrochimica Acta Part A: Molecular and Biomolecular Spectroscopy. 237 (1) (2020) 1-8, DOI-10.1016/j.saa.2020.118381.

92. Wu H., Pang L. F., Wei N., Guo X. F., Wang H., Nucleus-targeted N-doped carbon dots via DNA-binding for imaging of hypochlorous in cells and zebrafish. Sensors and Actuators B: Chemical. 333 (1) (2021) 129626-129638, DOI-10.1016/j.snb.2021.129626.

93. Wang Z., Fu B., Zou S., Duan B., Chang C., Yang B., Zhou X., Zhang L., Facile construction of carbon dots via acid catalytic hydrothermal method and their application for target imaging of cancer cells. Nano Research. 9 (1) (2016) 214-223, DOI-10.1007/s12274-016-0992-2.

94. Yu C., Jiang X., Qin D., Mo G., Zheng X., Deng B., Facile syntheses of s, n-co-doped carbon quantum dots and their applications to a novel off–on nanoprobe for detection of 6-thioguanine and its bioimaging. ACS Sustainable Chemistry & Engineering. 7(19) (2019) 16112-161120, DOI-10.1021/acssuschemeng.9b02886.

95. Shivaji K., Mani S., Ponmurugan P., De Castro C. S., Lloyd Davies M., Balasubramanian M. G., Pitchaimuthu S., Green-synthesis-derived CdS quantum dots using tea leaf extract: antimicrobial, bioimaging, and therapeutic applications in lung cancer cells. ACS Applied Nano Materials. 1 (4) (2018) 1683-1693, DOI-10.1021/acsanm.8b00147.

96. Chen B., Li F., Li S., Weng W., Guo H., Guo T., Zhang X., Chen Y., Huang T., Hong X., You S., Large scale synthesis of photoluminescent carbon nanodots and their application for bioimaging. Nanoscale. 5 (5) (2013) 1967-1971, DOI-10.1039/C2NR32675B.

97. Kumar S., Kumari A., Kumar A., Sahu S. K., Synthesis of green fluorescent carbon quantum dots using waste polyolefins residue for Cu^{2+} ion sensing and live cell imaging. Sensors and Actuators B: Chemical. 254 (1) (2018) 197-205, DOI-10.1016/j.snb.2017.07.075.

98. He D., Yang X., He X., Wang K., Yang X., He X., Zou Z., A sensitive turn-on fluorescent probe for intracellular imaging of glutathione using single-layer MnO_2 nanosheet-quenched fluorescent carbon quantum dots. Chemical communications. 51 (79) (2015) 14764-14767, DOI-10.1039/C5CC05416H.

99. Tang Z., Lin Z., Li G., Hu Y., Amino nitrogen quantum dots-based nanoprobe for fluorescence detection and imaging of cysteine in biological samples. Analytical chemistry. (2017) 89 (7) 4238-4245, DOI-10.1021/acs.analchem.7b00284.

100. Das P., Bose M., Ganguly S., Mondal S., Das A. K., Banerjee S., Das N. C., Green approach to photoluminescent carbon dots for imaging of gram-negative bacteria *Escherichia coli*. Nanotechnology. 28 (19) (2017) 1-13, DOI-10.1088/1361-6528/aa6714.

101. Qian J., Quan F., Zhao F., Wu C., Wang Z., Zhou L., Aconitic acid-derived carbon dots: Conjugated interaction for detecting folic acid and fluorescence targeted imaging of folate receptor overexpressed cancer cells. Sensors and Actuators B: Chemical. 262 (1) (2018) 444-451, DOI-10.1016/j.snb.2018.01.227.

102. Konar S, Kumar BP, Mahto MK, Samanta D, Shaik MA, Shaw M, Mandal M, Pathak A. N-doped carbon dot as fluorescent probe for detection of cysteamine and

multicolor cell imaging. Sensors and Actuators B: Chemical. 286 (2019) 77 85, DOI-10.1016/j.snb.2019.01.117.

103. Sarkar P, Ghosh S, Sarkar K. Folic acid based carbon dot functionalized stearic acid-g-polyethyleneimine amphiphilic nanomicelle: Targeted drug delivery and imaging for triple negative breast cancer. Colloids and Surfaces B: Biointerfaces. 197 (2021) 1-31, DOI-10.1016/j.colsurfb.2020.111382.

104. Yan C, Guo L, Shao X, Shu Q, Guan P, Wang J, Hu X, Wang C. Amino acid–functionalized carbon quantum dots for selective detection of Al^{3+} ions and fluorescence imaging in living cells. Analytical and Bioanalytical Chemistry. 413 (15) 3965-3974, DOI- 10.1007/s00216-021-03348-x.

105. Fu Z., Xiang J., Aptamer-functionalized nanoparticles in targeted delivery and cancer therapy. International Journal of Molecular Sciences. 21 (23) (2020) 9123-9138, DOI-10.3390/ijms21239123.

106. Prakash A., Yadav S., Yadav U., Saxena P.S., Srivastava A., Recent advances on nitrogen-doped carbon quantum dots and their applications in bioimaging: A review. Bulletin of Materials Science. 46 (1) (2023) 7-15, DOI- 10.1007/s12034-022-02846-7.

107. Das S., Mondal S, Ghosh D. Carbon quantum dots in bioimaging and biomedicines. Frontiers in Bioengineering and Biotechnology. 11 (1) (2024) 1333752-1333771, DOI- 10.3389/fbioe.2023.1333752.

108. Jang J. H., Schaffer D. V., Shea L. D., Engineering biomaterial systems to enhance viral vector gene delivery. Molecular therapy. 19 (8) (2011) 1407-1415, DOI-10.1038/mt.2011.111.

109. Pack D. W., Hoffman A. S., Pun S., Stayton P. S., Design and development of polymers for gene delivery. Nature reviews Drug discovery. 4 (7) (2005) 581-593, DOI-10.1038/nrd1775.

110. Putnam D., Polymers for gene delivery across length scales. Nature materials. 5 (6) (2006) 439-451, DOI-10.1038/nmat1645.

111. Li S. M., Rizzo M. A., Bhattacharya S., Huang L., Characterization of cationic lipid-protamine–DNA (LPD) complexes for intravenous gene delivery. Gene therapy. 5 (7) (1998) 930-937, DOI-10.1038/sj.gt.3300683.

112. Ding C., Zhu A., Tian Y., Functional surface engineering of C-dots for fluorescent biosensing and *in vivo* bioimaging. Accounts of chemical research. 47 (1) (2014) 20-30, DOI-10.1021/ar400023s.

113. Roy S., Sadhukhan R., Ghosh U., Das T. K., Interaction studies between biosynthesized silver nanoparticle with calf thymus DNA and cytotoxicity of silver nanoparticles. Spectrochimica Acta Part A: Molecular and Biomolecular Spectroscopy. 141 (1) (2015) 176-184, DOI-10.1016/j.saa.2015.01.041.

114. Kathiravan A., Renganathan R., Photoinduced interactions between colloidal TiO_2 nanoparticles and calf thymus-DNA. Polyhedron. 28 (7) (2009) 1374-1378, DOI-10.1016/j.poly.2009.02.040.

115. Sohrabijam Z., Saeidifar M., Zamanian A., Enhancement of magnetofection efficiency using chitosan coated superparamagnetic iron oxide nanoparticles and calf thymus DNA. Colloids and Surfaces B: Biointerfaces. 152 (1) (2017) 169-175, DOI-10.1016/j.colsurfb.2017.01.028.

116. Singh A., Kaushik M., Physicochemical investigations of zinc oxide nanoparticles synthesized from Azadirachta Indica (Neem) leaf extract and their interaction with Calf-Thymus DNA. Results in Physics. 13 (1) (2019) 1-9, DOI-10.1016/j.rinp.2019.102168.

117. Ezhuthupurakkal P. B., Polaki L. R., Suyavaran A., Subastri A., Sujatha V., Thirunavukkarasu C., Selenium nanoparticles synthesized in aqueous extract of Allium sativum perturb the structural integrity of Calf thymus DNA through intercalation and groove binding. Materials Science and Engineering: C. 74 (1) (2017) 597-608, DOI-10.1016/j.msec.2017.02.003.

118. Sarkar N., Sharma R. S., Kaushik M., Green synthesis and physiochemical characterization of nickel oxide nanoparticles: Interaction studies with Calf thymus DNA. Luminescence. 35 (2) (2020) 178-186, DOI-10.1002/bio.3709.

119. Liu C., Zhang P., Zhai X., Tian F., Li W., Yang J., Liu Y., Wang H., Wang W., Liu W., Nano-carrier for gene delivery and bioimaging based on carbon dots with PEI-passivation enhanced fluorescence. Biomaterials. 33 (13) (2012) 3604-3613, DOI-10.1016/j.biomaterials.2012.01.052.

120. Yang S. T., Cao L., Luo P. G., Lu F., Wang X., Wang H., Meziani M. J., Liu Y., Qi G., Sun Y.P., Carbon dots for optical imaging in vivo. Journal of the American Chemical Society. 131(32) (2009) 11308-11309, DOI-10.1021/ja904843x.

121. Zhang W., Chen J., Gu J., Bartoli M., Domena J. B., Zhou Y., Ferreira B. C., Cilingir E. K., McGee C. M., Sampson R., Arduino C., Nano-carrier for gene delivery and bioimaging based on pentaetheylenehexamine modified carbon dots.

Journal of colloid and interface science. 639 (1) (2023) 180-192, DOI-10.1016/j.jcis.2023.02.046.

CHAPTER II

PURIFICATION AND CHARACTERIZATION TECHNIQUES FOR CARBON QUANTUM DOTS

2.1 Introduction:

CQDs can be synthesized by various methods, as discussed earlier in Chapter I. They can be purified using a variety of techniques, depending on research objectives and requirements. The purification methods explained in detail include filtration, dialysis, solvent extraction, electrophoresis, and chromatography.

Additionally, this chapter describes the working principles of various spectroscopic and microscopic techniques for better interpretation of the electronic, optical, and structural properties of CQDs. UV-Vis spectroscopy, fluorescence spectroscopy, FTIR, XPS, and XRD are employed for a detailed analysis of the chemical composition, functional groups, and surface states of fluorescent CQDs. The surface morphology and crystallinity are analyzed using HRTEM with selected area electron diffraction (SAED) and AFM techniques.

2.2 Purification techniques:

Purification techniques for CQDs play a crucial role in controlling their size distribution, which directly influences their optical and physicochemical properties. Several methods are employed to achieve size-selective purification, including dialysis, centrifugation, chromatography, filtration, solvent extraction, and gel electrophoresis (figure 2.1) [1].

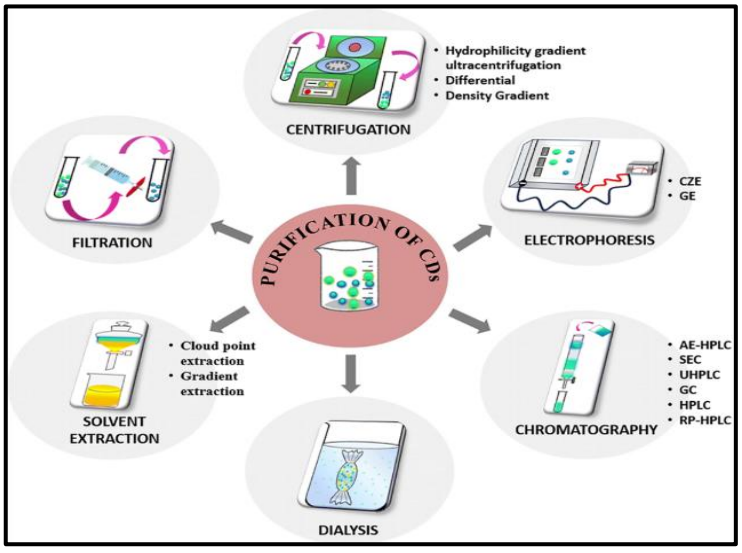

Figure 2.1: Schematic representation of different techniques reported for the purification and separation of CQDs [1].

The use of plant- or animal-based precursors introduces significant complexity due to their unknown chemical composition. During synthesis, fluorescent impurities may form, posing substantial challenges in analyzing the PL properties of CQDs. These impurities can alter or obscure the true optical characteristics of CQDs, leading to pronounced differences in fluorescence performance [2]. Bartolomei and Prato [3] emphasized the importance of purification and chemical characterization in identifying molecular fluorophores. Therefore, purification is essential for effectively separating CQDs from associated byproducts, ensuring accurate characterization and preventing errors caused by interference from these fluorophores.

However, during the synthesis process of CQDs, various impurities and byproducts may form, potentially affecting their performance and limiting their applications. Therefore, the purification of CQDs is crucial to remove these impurities and ensure the consistency and reliability of their properties.

2.2.1 Filtration:

Filtration is a simple process used to purify products that contain nanoparticles of various sizes. The product is allowed to pass through a filter with fixed pore diameters. The larger particles that cannot pass through the pore are retained on the filter surface, while the smaller ones are collected as filtrate. This method is typically used as an initial purification step to separate insoluble or suspended particles or agglomerates in CQD samples after they have been manufactured.

The filter's pore diameter should be optimized to prevent pore clogging, which tends to occur when the diameter ranges between 0.1-1 μm. Additionally, the concentrated sample must be diluted before filtration to avoid clogging. Previous reports on CQD purification suggest the use of filters with specific pore sizes or the use of syringe filters.

In the subsequent chapter of the thesis, the synthesis procedure is detailed, particularly focusing on the post-synthesis steps, including filtration. Following the successful synthesis of CQDs, the resultant solution was subjected to filtration to ensure the removal of impurities and unreacted materials. This critical step was performed using a 0.22 μm syringe filter, which effectively separates any particulate matter or larger aggregates from the solution. The use of a syringe filter with such a fine pore

size ensures that the CQDs obtained are of high purity, uniform size, and suitable for subsequent characterization and applications. This meticulous filtration process plays a pivotal role in enhancing the quality and consistency of the CQDs.

2.2.2 Dialysis:

Dialysis is a widely used technique to purify CQDs by removing low molecular weight residual precursors and polymers. It works by allowing small fluorescent molecules to diffuse from an area of higher concentration to an area of lower concentration through a semipermeable membrane. This process is particularly effective for water-soluble CQD samples, which can be easily filtered and dialyzed. The process involves dissolving CQDs in water and dialyzing them through a semi-permeable membrane to remove low molecular weight impurities while retaining high molecular weight species in the retentate.

The composition of dialysate depends on various factors such as sample concentration, time, and bag molecular weight cutoff. To keep the dialysate diluted, it is necessary to regularly recharge the buffer solution with fresh deionized water to maintain the pH of the sample at an optimal level [4]. It is crucial to optimize the molecular weight cutoff of the dialysis membrane, the dialysis time, and the frequency of water replacement steps to achieve optimal purification results. While dialysis may not be effective in separating hydrophobic samples, it is often used as a purification procedure in research studies. Optimizing the dialysis membrane's molecular weight cutoff, water replacement steps, and dialysis time is crucial for optimal purification results. Although dialysis cannot separate hydrophobic samples, it is often used as a purification procedure in research studies [5].

In the following chapter of the thesis, CQDs were purified using dialysis with a 3.5 kDa MWCO dialysis membrane. This process was undertaken to enhance purity by removing smaller impurities, including unreacted precursors, by-products, and low-molecular-weight salts, which were not effectively eliminated during the filtration step.

2.2.3 Electrophoresis:

Electrophoresis relies on the movement of charged molecules in an electric field through a gel matrix, typically agarose or polyacrylamide. DNA is inherently negatively charged due to its phosphate backbone, and its mobility in the gel is influenced by its

size and charge. When DNA is conjugated to CQDs, the size, charge, or both are altered, leading to changes in the migration pattern during electrophoresis.

The separation of CQD samples in gel electrophoresis (GE) is crucial and is achieved through various migration properties that arise from sieve effects caused by an electric field. In a recent study, Xu et al. [6] demonstrated the separation of CQDs while purifying single-walled carbon nanotubes derived from arc discharge soot, using polyacrylamide gel electrophoresis (PAGE). It is possible to determine the relationship between the color of luminous CDs and their mobility by using PAGE. However, the gel's pore size, which is around 3-5 nm, causes it to have low separation effectiveness. This limitation makes it difficult to separate CQDs with a broad size range.

Capillary Zone Electrophoresis (CZE) is a technique used to separate different components with varying electrophoretic mobilities through an electrolyte solution inside a fused silica capillary. The separation is based on the charge-to-size ratio of these components. Baker and Colón [7] utilized CZE along with a diode array detector to distinguish between different Cyclodextrins (CQDs) produced when soot from an oil lamp flame oxidized. Their research focused on understanding how the buffer composition affects the electrophoretic pattern of a combination of negatively charged CQDs.

In the subsequent chapter, electrophoresis was employed to confirm the conjugation of CQDs with DNA. This analytical technique is widely used for assessing molecular interactions and is particularly effective for confirming the binding of biomolecules such as DNA to nanoparticles like CQDs. The results from electrophoresis provide visual and quantitative evidence of successful conjugation.

2.3 Characterization Techniques

2.3.1 Ultraviolet-Visible (UV-Vis) Spectroscopy:

UV-Vis Spectroscopy is the simplest analytical technique used to measure the absorption of light by substance for the elementary study of optical and electronic properties. Generally, the wavelength range of 190 nm to 400 nm and 400 nm to 800 nm are called ultraviolet range and visible light range respectively that are used for the analysis. Therefore, the absorption of ultraviolet light by the molecules causes the electrons to be promoted from the ground state to the excited state. The absorbed energy

is equal to the difference between higher and lower energy states. As a result, the molecules undergo various types of electronic transitions including σ–σ* (saturated C–C), π–π* (unsaturated C=C), n– σ* (C–O or C–N or C–X) and n-π* (C=O).

The UV-Vis spectroscopy system is composed of key components that facilitate the efficient operation of the UV-Vis spectrophotometer. The system directs electromagnetic radiation from a light source onto the sample under analysis. Depending on the setup, the light either passes through the sample or is reflected from its surface. The transmitted or reflected light is then collected and analyzed to generate the desired measurements.

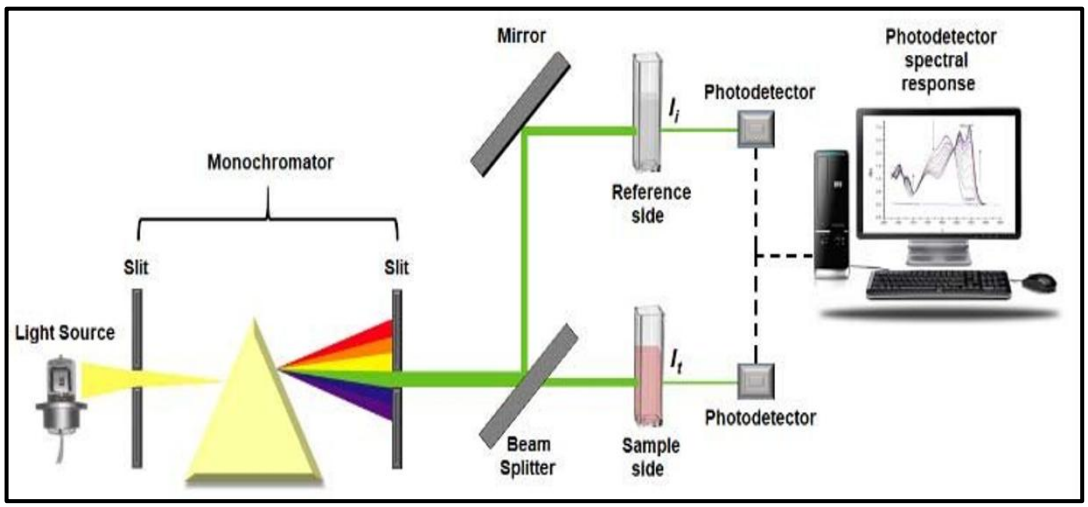

Figure 2.2: Schematic representation of working principle of UV-Vis Spectroscopy.

In Figure 2.2, the UV-Vis spectroscopy working principle is depicted. Initially, light is focused on the monochromator through the entrance slit from the light source. The monochromator utilizes an optical grating as a dispersing element to separate the light according to its wavelength. The dispersed light is then directed towards a charged coupled device (CCD), which is composed of individual tiny detectors. Each detector measures the intensity of light at a specific wavelength. The CCD is connected to a computer, where the readings from each detector are recorded and analyzed. The result obtained is a spectrum, which displays the intensity of light at each wavelength. Spectrophotometers are capable of measuring electromagnetic radiation across a wide range, from ultraviolet to infrared. The spectrum obtained from the measurements shows the relationship between the intensity of light and its corresponding wavelength.

The principle of UV-Vis spectrum is based on Beer–Lambert's law which states that the absorbance of a solution is directly proportional to the concentration of the absorbing species in the solution and the path length. The mathematical relationship between concentration and path length (or the length of the sample cell) is represented in equation 2.1 [8].

$$A = \log_{10} (I_0/I) = \varepsilon\, c\, l \ldots\ldots\ldots\ldots\ldots \text{(eq. 2.1)}$$

Where, A is the absorbance or optical density, I_0 and I are the intensity of incident light and transmitted light, ε is a constant known as the molar absorptivity or extinction coefficient, c is the concentration of solution and l is the path length.

This technique is widely used in qualitative and quantitative analysis, enabling the identification of compounds, determination of concentrations, and study of reaction kinetics. A linear relationship between absorbance and concentration allows for the accurate quantification of analytes, provided the system adheres to Beer–Lambert's law. However, deviations may occur due to factors such as high analyte concentration, instrumental limitations, or chemical interactions.

The UV–Vis spectra of the synthesized CQDs were recorded using an Agilent Cary 60 UV–Vis spectrophotometer (Instrument Version 2.00). For the measurements, 3 mL of the sample was placed in a quartz cuvette. The absorbance spectrum was scanned over a wavelength range of 190 to 800 nm with a step size of 1 nm.

2.3.2 Fluorescence Spectroscopy:

Fluorescence spectroscopy is a simple, contactless, and non-destructive technique used to analyze the electronic structure of nanomaterials. It helps in understanding defect states, bandgaps, surface functional groups, fluorescence properties, and the recombination mechanisms of nanomaterials.

When a substance absorbs a photon, electrons in the ground state become excited to a higher energy level, leaving behind a hole in the ground state. As these excited electrons return to the ground state through a radiative process, PL occurs. The energy of the emitted light corresponds to the difference in energy levels between the excited and ground states.

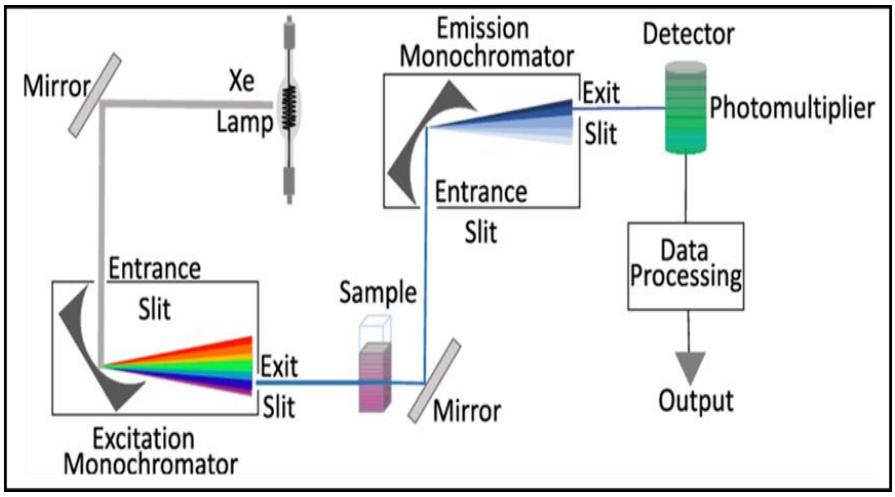

Figure 2.3: Schematic diagram of working principle of fluorescence spectroscopy.

A schematic representation of fluorescence spectroscopy is shown in Figure 2.3. In this process, light of a specific wavelength passes through a monochromator and excites the sample, causing electron transitions. The emitted light, resulting from electron-hole recombination, then passes through another monochromator before reaching the detector [9].

In the subsequent chapters, fluorescence spectroscopy was utilized for the characterization of an aqueous solution of CQDs. The measurements were performed using an FP-8300 Spectrofluorometer from JASCO, equipped with a 70 W xenon lamp as the excitation source. The fluorescence spectra were recorded at various excitation wavelengths to analyze the optical properties of the CQDs.

2.3.3 UV-Transilluminator:

An ultra-violet (UV) transilluminator (Figure 2.4) is a standard piece of equipment used in life science laboratories for the visualization of target DNA and proteins. The key application for a UV transilluminator is for visualization of DNA and protein agarose and polyacrylamide gels after electrophoresis. Gels can be directly placed onto the UV transilluminator; wavelength will vary on your particular application. Also, the CQDs change color after contact with UV-transilluminator.

The principle of a UV transilluminator is:

1. The agarose gel is stained with a fluorescent dye that binds to nucleic acid.
2. The stained gel is exposed to a UV light source, causing the dye to fluoresce.
3. The DNA fluoresces and becomes visible.

Figure 2.4: UV-transilluminator instrument.

At the time of electrophoresis, a fluorescent dye is used to stained agarose gel which binds with nucleic acids exposing the stained gel to a UVB light source which causes DNA segments to become visible and fluoresce. A UV transilluminator works by emitting high levels of UV radiation through a viewing surface. Depending on the type of sample, the UV transilluminator is operated in any of the three wavelength bands. 254, 312, and 365 nm are typical wavelengths. 312 nm are used for standard gel documentation in the gel doc system [10].

A UV-Transilluminator was employed to visually detect synthesized CQDs and to analyze CQD, CQD-DNA conjugate processed using agarose gel electrophoresis. The instrument used was a Vilber Lourmat ECX-F20.M UV-Transilluminator with a power rating of 90 W, providing reliable visualization for the characterization and verification processes.

2.3.4 Fourier Transform Infrared (FTIR) Spectroscopy:

FTIR spectroscopy is the most common analytical technique used to study virtually any sample in any state like liquids, pastes, powders, films, and fibers. The most significant advance of infrared spectroscopy is the introduction of the Fourier transform phenomenon. It works as an interferometer and exploits the well-established scientific process of fourier transformation. The fourier transform has meaningfully improved the quality of the infrared spectrum and minimized the time required to obtain data.

The principle of FTIR spectroscopy is based on the vibration of the atom in the molecule by passing infrared radiation through the sample. Some of the infrared radiation is absorbed by the sample, and some other portion is passed through (transmitted) the sample. The resultant spectrum is obtained through the molecular absorption and transmittance processes that provide detailed information about the molecular structure, functional groups, and atom connectivity.

In general, infrared spectroscopy deals with the interaction of the molecule with the IR radiation ranging between 4000 cm^{-1} and 400 cm^{-1}. This region is further split into two possible regions, first the range of region between 4000 cm-1 to 1000 cm^{-1}, this region is usually called the functional group's region, where the functional groups present within the molecules are identified. The region below 1000 cm^{-1}, known as the fingerprint region, is complex and challenging to assign every peak. However, it is highly useful for determining the molecular and compound structure. Each type of chemical bond produces a unique spectral fingerprint, ensuring that no two molecules generate identical IR spectra, which aids in identifying different functional groups in the sample. Figure 2.5 [11] presents a schematic illustration of the FTIR setup.

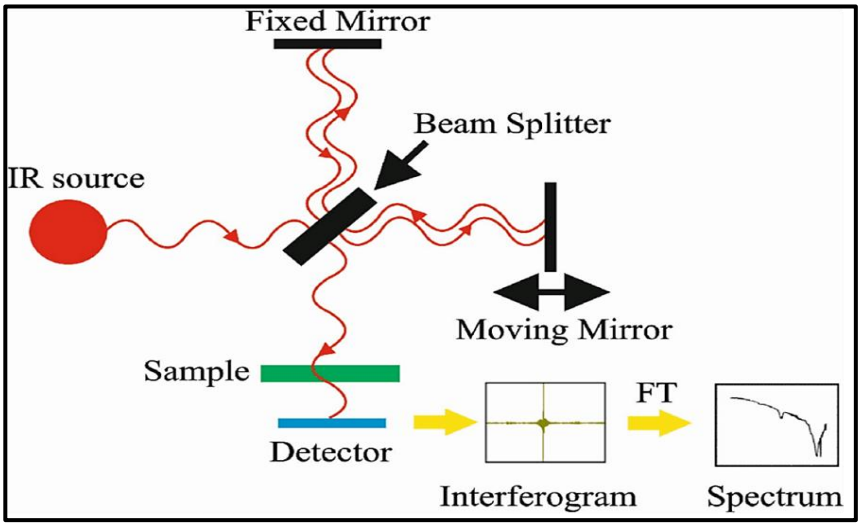

Figure 2.5: Schematic representation of FTIR.

FT-IR analysis was conducted for synthesized CQD samples using a 4600 Type-A FT-IR spectrometer equipped with a diamond Attenuated Total Reflectance (ATR) accessory. The ATR technique was employed for the analysis, utilizing the CQD liquid solution as the sample. The spectral data were collected over a wavenumber

range of 600–4000 cm^{-1}, which effectively captures the characteristic vibrational modes of functional groups present in the CQDs.

A total of 32 scans were averaged for each measurement to enhance the signal-to-noise ratio and ensure reliable results. The resolution was set at 8 cm^{-1}, allowing for sufficient differentiation of closely spaced spectral features while maintaining a balance between resolution and measurement time. This setup enabled precise characterization of the surface functionalities and chemical composition of the CQDs.

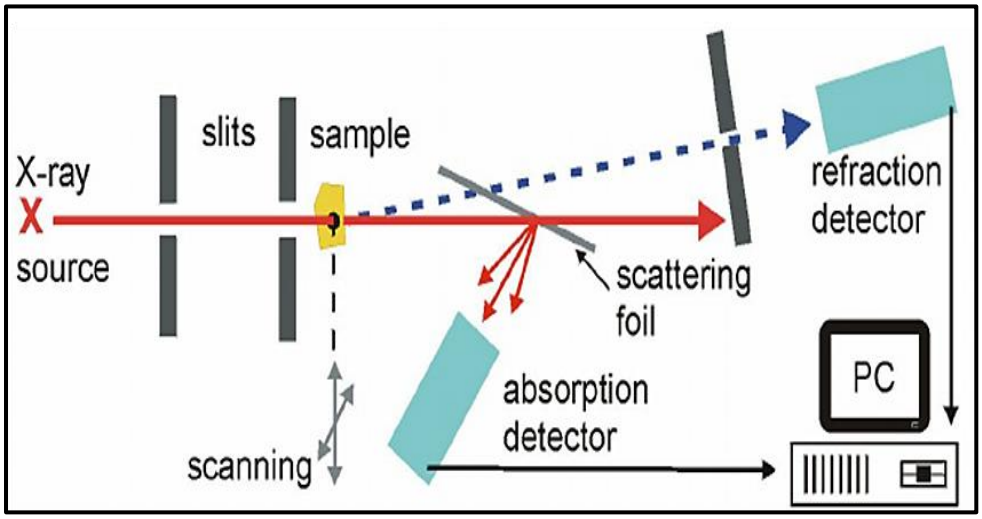

Figure 2.6: Diagram showing the working mechanism of XRD.

2.3.5 X-Ray Diffraction (XRD) Spectroscopy:

XRD is a non-destructive analytical technique mainly used for the phase identification of a crystalline material and gives information about unit cell dimensions. Also, we can find the size and internal stress of small crystalline regions. X-ray diffraction is depending on the crystalline structure of materials.

The working principle of the XRD method involves the scattering of X-rays due to the revolution of electrons in the atom's nucleus when the rays strike the nanoparticles. The scattered X-rays are reflected in various directions, which cause interference patterns. These patterns are either destructive or constructive (Fultz & Howe, 2013) but only the scattered X-rays that undergo constructive interaction result in diffraction.

The monochromatic X-ray gives constructive interference and destructive interferences. Generally, X-rays are created from a cathode ray tube. The

monochromatic radiation of X-rays is produced by filtering off in X-rays. According to Bragg`s law, contractive interference is produced when the monochromatic radiation is illuminated on the sample surface.

While the illumination of a monochromatic X-ray beam of wavelength (λ) strikes on the crystalline lattice plane with an angle, θ results in the successive planes (with distance 'd') are diffracted (Figure 2.6). Then the 'd' spacing value of the materials is analyzed by using Bragg's equation 2.2 [12].

$$n\lambda = 2d\sin\theta \quad \text{..... (eq. 2.2)}$$

Where n is an integer, λ is the wavelength of X-rays in angstroms, d is the interatomic spacing in angstroms and θ is the diffraction angle in degrees. The wavelength of the X-ray used for the analysis is 1.54 Å. This law relates the wavelength of electromagnetic radiation to the diffraction angle and the lattice spacing in a crystalline sample. By scanning the sample through a range of 2θ angles, all possible diffraction directions of the lattice should be identified due to the random orientation of the powdered material [12].

In the subsequent chapters, XRD analysis was employed to study the crystalline structure of the synthesized PLLCQDs. The analysis was performed using a Rigaku powder X-ray diffractometer (Miniflex 600, India), utilizing Al Kα radiation as the excitation source.

To prepare the sample for XRD, a glass coverslip was coated layer by layer with the PLLCQD solution to ensure a uniform and sufficient sample thickness for accurate diffraction measurements. Once prepared, the coated sample was subjected to XRD analysis. This technique allowed for the identification of the crystalline or amorphous nature of the PLLCQDs and provided insights into their structural properties, which are critical for understanding their functionality in various applications.

2.3.6 X-ray Photoelectron Spectroscopy (XPS):

XPS also called electron spectroscopy for chemical analysis (ESCA) is a meaningful device to investigate the chemical composition, element state, chemical state, electronic state, binding energy, and heteroatom functionalized or doped on carbon-based quantum dots.

The basic principle of XPS is based on the photoelectric effect. Each atom has a core electron, and the ionization energy of a core electron is theoretically equal to the binding energy when an X-ray beam is illuminated on the sample surface. As a result, the core electron in the atom absorbs X-ray energy (if the energy of the photon (hυ) is higher than the energy of the core electron). The core electron will be ejected from the atom and thrown out from the surface (kinetic energy EK) as shown in Figure 2.7 The binding energy of the core electron is related to the Einstein relationship.

The kinetic energy of an ejected photoelectron is measured by the instrument and the binding energy of these emitted electrons can be determined using the following equation 2.3 [13].

$$E_{binding} = E_{photon} - (E_{kinetic} + \varphi) \ldots\ldots\ldots\ldots \text{(eq. 2.3)}$$

Where $E_{binding}$ is the binding energy of an electron in materials, E_{photon} is the energy of the X-ray photons, $E_{kinetic}$ is the kinetic energy of ejected electron from the surface of materials and φ is the work function and it is adjustable instrumental correction factor [13].

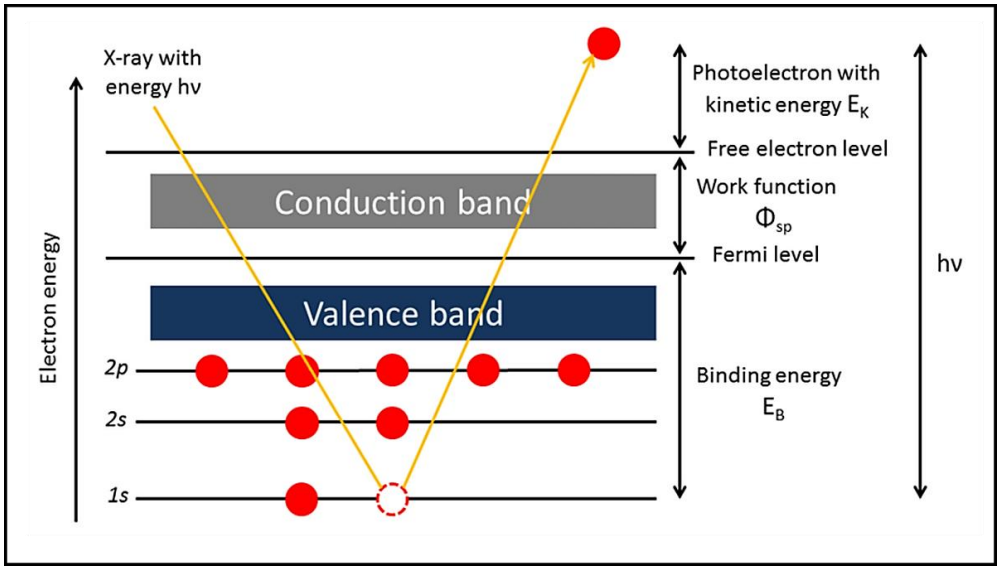

Figure 2.7: Schematic representation of working principle of XPS.

In the subsequent chapters, XPS was utilized for a detailed analysis of the elemental composition of the CQDs. The measurements were carried out using a K-Alpha XPS system equipped with an 8025-BesTec dual anode XR3E2 X-ray source. This advanced analytical technique enabled the identification of the elements present

in the CQDs and their corresponding oxidation states. The information obtained provided critical insights into the surface chemistry and functional groups, aiding in the characterization of the CQDs and their potential applications in biomedical and other fields.

2.3.7 Zeta Potential:

Zeta potential (ζ) measurement is one of the essential techniques that indicate the stability of colloidal dispersion of the samples. Zeta potential is the potential difference between the dispersion medium and the stationary layer of dispersed particles. Zeta potential measurement is a simple technique to understand the surface nature and stability of nanoparticles or colloidal particles.

When an electric field is applied to a nanoparticle-dispersed solution, particles move due to the interaction between the charged particle and the applied field. Under this condition when particles are illuminated with laser light, their scattered light and Particle velocity are then measured by observing the Doppler shift in electrophoretic light scattering. Particle mobility can be determined from measured particle velocity and known applied electric field. Thus, zeta potential can be calculated from particle mobility by using the Smoluchowski model equation 2.4 [14].

$$\zeta = U\eta\,(ka)\ \ldots\ldots\ldots \quad \text{(eq. 2.4)}$$

Where ζ is the zeta potential, U is the electrical mobility, η is the viscosity of the solvent, ε is the dielectric constant of the solvent, and f(ka) is the Henry constant. A schematic diagram of the zeta potential measurement technique is shown in Figure 2.8 [14].

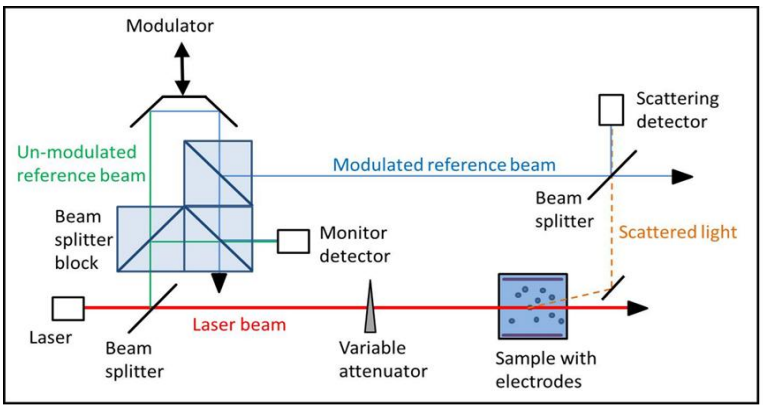

Figure 2.8: Working principle of Zetasizer.

The zeta potential of the CQDs was measured using a Malvern Zetasizer nanosystem (Litesizer 500). This instrument is specifically designed to assess the surface charge of nanoparticles dispersed in a liquid medium. Zeta potential is a critical parameter that indicates the stability of colloidal systems; it reflects the electrostatic potential at the slipping plane of particles.

2.3.8 High Resolution-Transmission Electron Microscopy (HRTEM):

TEM is a microscopy technique to understand the morphology and crystallography details (crystal structure, crystal phase, crystal defect) of ultrathin substances. In this technique, an image is formed after the interaction of the beam electron with the ultrathin specimen. The image is then magnified and focuses on the imagining device. The specimen is taken as less than 100 nm thickness pellet or specimen coated Cu-grid. TEM has greater resolving power compared to the light microscope because the de-Broglie wavelength of an electron is smaller than visible light.

The principle of HRTEM is similar to that of the optical microscope, but the source of HRTEM is the electron gun instead of light because the wavelength of an electron is much smaller than that of light. Principally, the electron beam is produced from the electron gun consisting of tungsten filament and passing through a thin copper grid specimen which contains the material to be analyzed. In this process, the electrons are diffracted, and the diffracted electrons travel through the high vacuum column to avoid the collision with air molecules which hinder the electron travel. The diffracted electrons are focused on the electromagnetic condenser lenses along with the column. Finally, the electron beams are passed through the specimen and diffracted based on the internal structure (Figure 2.9).

The HRTEM technique is used for the two-dimensional projection of crystals with defects. The HRTEM provides a high-resolution image at an atomic level because of the use of both transmitted and diffracted electrons which create the interference image, that is the phase contrast images which can be as small as the unit cell of a crystal. Therefore, all the electrons emerging from the specimen are combined at the point on the image plane. The phase-contrast images are formed by removing the objective aperture entirely or by using a large objective aperture. The phase contrast ensures that not only the transmitted beam but also the diffracted ones are allowed to

contribute to the image. The selected area electron diffraction pattern was also obtained by this method using SAED aperture and removal of objective aperture. It is formed by back focal planes derived by adjusting the objective lens [15].

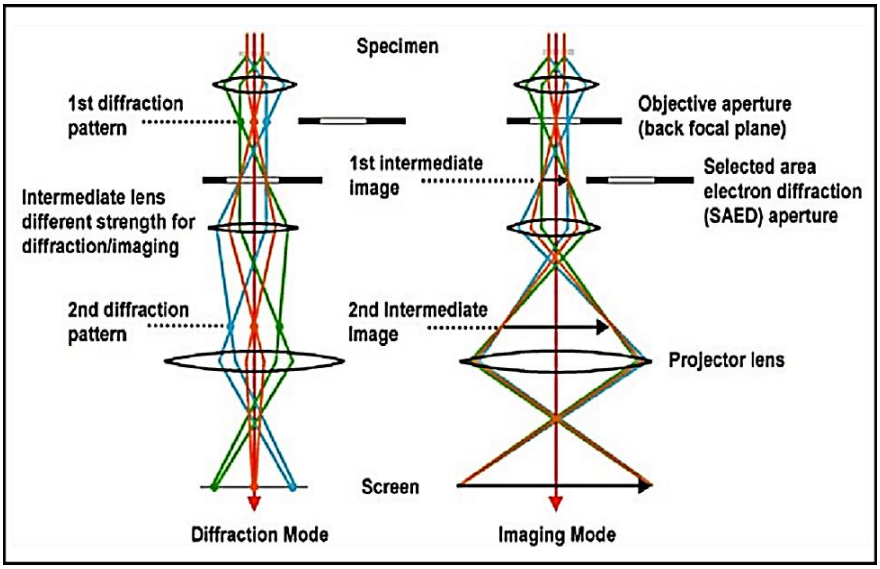

Figure 2.9: Diagram showing the principle of the formation of image and diffraction pattern in HRTEM.

The morphology and size of the synthesized CQDs were investigated using a FEI TECNAI G2-20 TWIN HR-TEM. For sample preparation, a 5 μL drop of the CQD solution, typically in water, was carefully placed on carbon-coated copper grids. These grids were then dried using a heating lamp to evaporate the excess solvent. This preparation method allowed for a detailed analysis of the CQDs at the nanoscale, providing valuable insights into their size, shape, and surface characteristics.

2.3.9 Atomic Force Microscopy (AFM):

AFM is indeed a form of scanning probe microscopy that has been shown to have an exceptional resolution on the order of fractions of a nanometer. It is fascinating to know that this resolution is more than 1000 times better than the optical diffraction limit. The atomic force microscope is widely used in materials science and has found many applications in biological sciences but has been limited in use in vision science.

AFM microscopes operate on the principle of surface sensing using an extremely sharp tip on a micromachined silicon probe. This tip is used to image a sample by raster scanning across the surface line by line, although the method varies

dramatically between distinct operating modes. AFM operation can be described in terms of three main modes: contact mode, tapping mode, and non-contact mode.

AFM operates in different modes based on the interaction between the probe tip and the sample surface. In **contact mode** (or static mode), the AFM probe tip remains in continuous contact with the sample surface while a constant force is applied. The deflection of the cantilever is monitored to generate a topographic image. This mode offers high lateral force sensitivity but may cause wear on both the tip and the surface. In **tapping mode** (also known as intermittent contact, AC mode, or vibrating mode), the AFM probe tip oscillates near its resonant frequency and intermittently touches the sample surface. The oscillation amplitude is measured to create a topographic image. Compared to contact mode, tapping mode minimizes damage to both the sample and the probe tip. In **non-contact mode** (or frequency modulation AFM), the probe tip oscillates above the sample without making direct contact. The interaction is dominated by van der Waals forces, and changes in oscillation frequency due to variations in tip-sample distance are used to construct the image. Non-contact mode is highly sensitive and preserves the sample's integrity but requires precise control for stability and accurate imaging. A constant-height image is created when the values of the frequency obtained by scanning the sample surface along the x-y direction are plotted against the x-y coordinates of each measurement point. In this type of image, the height of the sample is not regulated in the z-direction, allowing for variations in concavity and convexity to be reflected in the distance between the tip-apex and the sample. These variations cause a frequency shift, which is captured and represented in the constant-height image.

Alternatively, to maintain a constant deflection force (df), the probe can be moved up and down in the z-direction using negative feedback (z-feedback loop) while the sample surface is scanned in the x-y direction. This process allows for the creation of a topographic image, where the amounts of negative feedback (probe movement in z-direction) are plotted against the x-y coordinates of each measurement point. Essentially, the topographic image shows the path traced by the probe tip while maintaining a constant df, and can also be thought of as a plot of a constant-height surface of the df. The operation of the AFM is illustrated in Figure 2.10 [16].

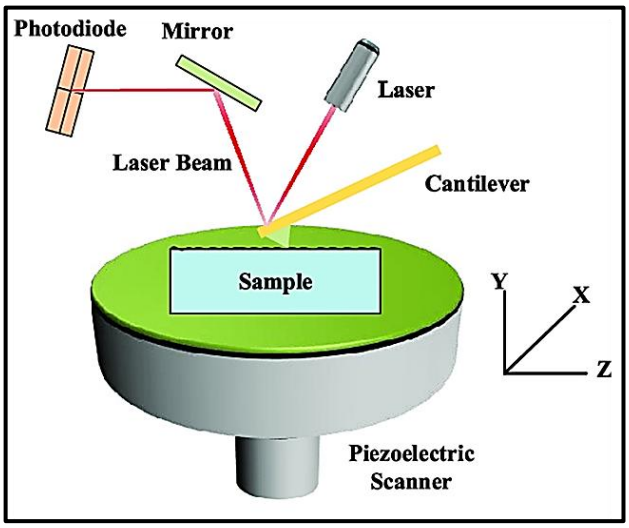

Figure 2.10: Schematic presentation of AFM.

The topographic image obtained from an AFM is influenced by the interaction between the probe and the sample, specifically the bond order. This means that the image may not perfectly represent the true surface morphology. The topographic image obtained from an AFM is generally considered to reflect the geographical shape of the surface more accurately. This is because AFM measures mechanical interactions between the probe and the sample.

The surface topography and size of the synthesized CQDs were analyzed using AFM with the Park Systems AFM-NX 10. A small drop of CQD solution, dissolved in sterile distilled water, was placed on UV-treated PLL-coated glass slides using the drop-casting technique. The slides were then allowed to air dry, resulting in a surface-functionalized CQD coating. The dried samples were evaluated in true noncontact mode at a scanning rate of 0.5 Hz, enabling detailed analysis of the CQDs surface features and size at the nanoscale.

2.3.10 Confocal Microscopy:

Confocal microscopy is an advanced optical imaging method using a pinhole to eliminate out-of-focus light, thereby enhancing micrograph contrast and resolution. Confocal microscopy covers two primary variants: Laser Scanning Confocal Microscopy (LSCM) and Spinning Disk Confocal Microscopy. Despite both systems offering optical sectioning capabilities, they rely on distinct underlying technologies.

Laser scanning confocal microscopes utilize a focused laser beam scanned across the sample to achieve imaging while spinning disk confocal microscopes employ a rapidly rotating disk with microlenses to generate multiple focused beams simultaneously. Both systems fulfill diverse experimental needs and preferences, each offering unique advantages in terms of imaging speed, resolution, and sample compatibility. The technique employs a laser to stimulate fluorescence from fluorophores marking distinct areas of a sample. By employing a pinhole or confocal aperture, light emitted from off target planes is filtered out, enabling precise visualization of the specimen's desired focal plane.

Modern confocal microscopes retain the core components of the original design, including pinholes, objective lenses, and low-noise detectors. However, they also incorporate advanced features such as fast-scanning mirrors, wavelength-selective filters, and laser illumination systems. While traditional gas lasers like argon and helium-neon remain in use, there is a growing preference for diode lasers, fiber lasers, and solid-state lasers due to their enhanced stability, uniformity, reduced heat production, and a broader range of visible wavelengths. Detectors, primarily highly sensitive photomultipliers (PMTs), continue to be crucial components owing to their ability to amplify signals over a photoelectric device, maximizing the light budget and ensuring efficient light rejection characteristics of confocal microscopy (Figure 2.11).

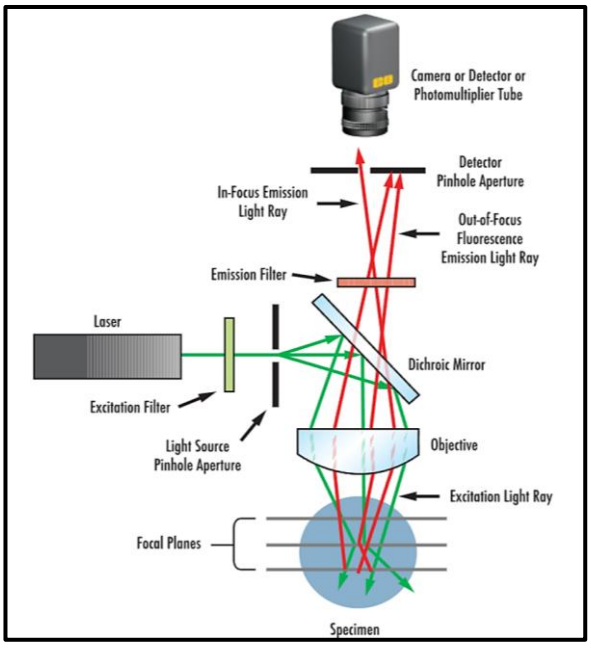

Figure 2.11: Schematic presentation of confocal microscopy.

Confocal microscopy operates on the fundamental principle of aligning both the illumination and detection optics to converge at the same diffraction-limited point. This focal point is systematically traversed across the sample to construct a comprehensive image on the detector. By precisely coordinating the optical components, the technique enables detailed imaging and analysis of the sample's microstructures with exceptional clarity and resolution. The sample is scanned by a laser beam to generate the image, which is then digitally recorded and stored as a computer file. This digital file preserves the intricate details captured during the scanning process, facilitating further analysis and manipulation of the specimen's characteristics.

Confocal microscopy offers the capability to capture high-resolution images from a thin slice of a thick sample with minimal background noise and limited out-of-focus interference. This optical sectioning technique finds widespread application in biomedical sciences and materials science alike. Practically, the process involves placing the sample on the microscope stage, capturing an image at the top focal plane, and sequentially adjusting the stage or objective to acquire images at subsequent focal planes. This iterative process results in a volumetric image or "z-stack," providing comprehensive 3D spatial information about the sample. Analysis of such data, especially when collected under sub-saturation conditions, enables quantification of parameters like volume, localization, and surface area, facilitating detailed characterization and measurement of sample structures [17].

In the subsequent chapters, confocal microscopy was employed for bioimaging studies using the Leica TCS SP5 confocal microscope. This advanced imaging technique allowed for high-resolution, three-dimensional visualization of the CQDs in biological systems. The Leica TCS SP5 instrument uses a laser scanning system to capture images by detecting fluorescence emitted from the CQDs after excitation, enabling precise imaging of cellular structures or tissue samples labeled with the CQDs. The confocal nature of the system ensures optical sectioning, providing clear images without interference from out-of-focus light, and allowing for the examination of CQDs' distribution, uptake, and behavior in complex biological environments. This technique is particularly valuable for studying the biocompatibility and potential applications of CQDs in medical or biological research.

2.4 References:

1. Ullal N., Mehta R., Sunil D., Separation and purification of fluorescent carbon dots–an unmet challenge. Analyst. 1 (1) (2024) 1680-1700, DOI-10.1039/D3AN02134C.

2. Shamsipur M., Barati A., Taherpour A. A., Jamshidi M., Resolving the multiple emission centers in carbon dots: from fluorophore molecular states to aromatic domain states and carbon-core states. Journal of Physical Chemistry Letters. 9 (15) (2018) 4189-4198, DOI-10.1021/acs.jpclett.8b02043.

3. Bartolomei B., Prato M., The Importance of the Purification Step and the Characterization of the Products in the Synthesis of Carbon Nanodots. Small. 19 (31) (2023) 2206714-22067189, DOI-10.1002/smll.202206714.

4. Zhu J., Wu C., Cui Y., Li D., Zhang Y., Xu J., Li C., Iqbal S., Cao M., Blue-emitting carbon quantum dots: Ultrafast microwave synthesis, purification and strong fluorescence in organic solvents. Colloids and Surfaces A: Physicochemical and Engineering Aspects. 623 (1) (2021) 126673-126675, DOI-10.1016/j.colsurfa.2021.126673.

5. Dsouza S. D., Buerkle M., Brunet P., Maddi C., Padmanaban D. B., Morelli A., Payam A. F., Maguire P., Mariotti D., Svrcek V., The importance of surface states in N-doped carbon quantum dots. Carbon. 183 (1) (2021) 1-11, DOI-10.1016/j.carbon.2021.06.088.

6. Xu X., Ray R., Gu Y., Ploehn H.J., Gearheart L., Raker K., Scrivens W.A., Electrophoretic analysis and purification of fluorescent single-walled carbon nanotube fragments. Journal of the American Chemical Society. 126 (40) (2004) 12736-12737, DOI-10.1021/ja040082h.

7. Baker J., Colón L.A., Influence of buffer composition on the capillary electrophoretic separation of carbon nanoparticles. Journal of Chromatography A. 1216 (52) (2009) 9048-9054, DOI-10.1016/j.chroma.2009.08.063.

8. Rizwan M, Gwenin C. Nanomaterials in renewable energy: UV-Visible spectroscopy characterization and applications. In Nano Tools and Devices for Enhanced Renewable Energy 1 (1) (2021) 103-120. Elsevier. DOI-10.1016/B978-0-12-821709-2.00017-7.

9. Gomes A. J., Lunardi C. N., Rocha F. S., Patience G.S., Experimental methods in chemical engineering: Fluorescence emission spectroscopy. The Canadian Journal of Chemical Engineering. 97 (8) (2019) 2168-2175, DOI-10.1002/cjce.23506.

10. Sigmon J., Larcom L. L., The effect of ethidium bromide on mobility of DNA fragments in agarose gel electrophoresis. Electrophoresis. 17 (10) (1996) 1524-1527, DOI-10.1002/elps.1150171003.

11. Eid M. M., Characterization of Nanoparticles by FTIR and FTIR-Microscopy. In Handbook of Consumer Nanoproducts. 1 (1) (2022) 1-30, DOI-10.1007/978-981-15-6453-6_89-1.

12. Khan H., Yerramilli A.S., D'Oliveira A., Alford T.L., Boffito D.C., Patience G.S., Experimental methods in chemical engineering: X-ray diffraction spectroscopy—XRD. The Canadian journal of chemical engineering. 98 (6) (2020) 1255-1266, DOI-10.1002/cjce.23747.

13. Chen X., Wang X., Fang D., A review on C1s XPS-spectra for some kinds of carbon materials. Fullerenes, Nanotubes and Carbon Nanostructures. 28 (12) (2020) 1048-1058, DOI-10.1080/1536383X.2020.1794851.

14. Clogston J. D., Patri A. K., Zeta potential measurement. Characterization of nanoparticles intended for drug delivery. 1 (1) (2011) 63-70, DOI-10.1007/978-1-60327-198-1_6.

15. Marczewska B., Marczewski K., First Glass Electrode and its Creators F. Haber and Z. Klemensiewicz–On 100th Anniversary. Zeitschrift für Physikalische Chemie. 224 (5) (2010) 795-799, DOI-10.1524/zpch.2010.5505.

16. Das S. K., Badal F. R., Rahman M. A., Islam M. A., Sarker S. K., Paul N., Improvement of alternative non-raster scanning methods for high-speed atomic force microscopy: A review. IEEE Access. 7 (1) (2019) 115603-115624, DOI-10.1109/ACCESS.2019.2936471.

17. Elliott A. D., Confocal microscopy: principles and modern practices. Current protocols in cytometry. 92 (1) (2020) 68-79, DOI-10.1002/cpcy.68.

CHAPTER III

SYNTHESIS AND CHARACTERIZATION OF SURFACE FUNCTIONALIZED CARBON QUANTUM DOTS

3.1 Introduction:

CQDs are an emerging class of nanomaterials characterized by their ultrafine sizes (below 10 nm) and discrete, quasi-spherical nanoparticle structures [1-3]. They were first discovered in 2004 during the purification of single-walled carbon nanotubes, where luminous carbon nanoparticles were observed. Initially referred to as "carbon nanoparticles," they were officially termed "carbon quantum dots" in 2006 when Sun et al. [4] introduced a method for synthesizing CQDs through simple surface passivation and chemical modification to enhance fluorescence emission [4].

Since then, CQDs have gained significant attention due to their unique structure and remarkable properties, making them highly versatile in various fields. As one of the newest carbon allotropes, CQDs exhibit several outstanding attributes, including low cytotoxicity [5], excellent biocompatibility [6], stable chemical inertness [7], efficient light-harvesting capabilities [7], and exceptional photo-induced electron transfer properties [8]. These features make them promising candidates for applications in biosensors [9-11], bioimaging [11-12], optoelectronic devices [13], and solar cells [14].

CQDs can be synthesized using a variety of preparatory routes, which are broadly classified into "top-down" and "bottom-up" strategies [15, 16]. Key synthesis techniques include chemical or laser ablation, electrochemical digestion, microwave-assisted synthesis, and solvothermal or hydrothermal methods. However, several challenges arise during CQD synthesis. Issues related to constrained pyrolysis, electrochemical synthesis, and post-treatment processes—such as centrifugation, gel electrophoresis, and dialysis—can be mitigated by optimizing reaction conditions. Parameters such as temperature, reaction time, and precursor selection significantly impact CQD characteristics, including size, fluorescence properties, water solubility, and cytotoxicity [17].

This chapter provides a detailed overview of the synthesis of surface-functionalized carbon quantum dots (PLLCQDs) and their characterization using various analytical techniques, including UV-Vis spectroscopy, fluorescence spectroscopy, X-ray photoelectron spectroscopy (XPS), X-ray diffraction (XRD), Fourier transform infrared spectroscopy (FTIR), transmission electron microscopy (TEM), and atomic force microscopy (AFM). Additionally, the synthesized PLLCQDs

were successfully utilized in fluorescent ink formulations, demonstrating their practical applicability.

3.2 Experimental Details

3.2.1 Materials:

Anhydrous glucose (catalog no. 50-99-7, Himedia, Mumbai, India), poly L-lysine (catalog no. P8920, Sigma-Aldrich, USA), potassium dihydrogen phosphate (KH_2PO_4, catalog no. GRM 249, Himedia, Mumbai, India), sodium hydroxide (NaOH, catalog no. PCT 1325, Himedia, Mumbai, India), potassium chloride (KCl, catalog no. GRM 698, Himedia, Mumbai, India), and hydrochloric acid (HCl, catalog no. AS004, Himedia, Mumbai, India) were purchased in analytical grade and used without further purification. Additionally, a 0.22 μm syringe filter (catalog no. SLGVR33RS, Sigma Merck, Germany) and a 3.5 kDa dialysis membrane (catalog no. D9527, Sigma Merck, Germany) were used in the experiments.

3.2.2 Optimization of parameters for synthesis of PLLCQDs:

3.3.2.1 Effect of temperature:

The optimization of PLLCQDs formation involved experimenting with different temperatures while keeping the concentrations of glucose and PLL constant, along with various response times. The fluorescent intensity changes were measured using a JASCO spectrofluorometer. Temperatures ranging from 80 to 200°C were tested to assess their effect on the fluorescence intensity of the synthesized PLLCQDs.

3.3.2.2 Effect of reaction Time:

Different time intervals were employed to observe the impact of reaction duration on the synthesis of PLLCQDs. The temperature, glucose, PLL concentrations, and other relevant variables were maintained constant throughout this investigation. PLLCQDs were synthesized at intervals of 5, 7, 10, 15, and 20 minutes, and their fluorescence intensity was subsequently measured.

3.3.2.3 Effect of PLL concentration:

In the investigation, various concentrations of PLL ranging from 0.02% to 0.1% (w/v) were used. The temperature and reaction time were kept constant throughout the

trials. The aim was to study how different PLL concentrations affected the synthesis process. Fluorescence intensities were measured and plotted against PLL quantity to establish a link between PLL concentration and fluorescence quantity

3.2.3 Synthesis of PLL functionalized CQDs:

The CQDs were prepared using the one-pot synthesis method. Firstly, 3 g of anhydrous glucose powder was added to a glass beaker, which was then placed on a hot plate for 10 minutes to reach a temperature of 100°C. As a result, the powder underwent a color change and turned into a brown residue. Subsequently, the residue was allowed to cool down to room temperature. The resultant residue was further processed by adding 5 mL of sterile distilled water and mixing it for 10 minutes at 500 rpm using a magnetic stirrer. The synthesized solution was mixed with 500 µL of 0.1 % poly L lysine to functionalize the CQDs. The beaker containing the solution was placed on a magnetic stirrer at a temperature of 27°C and a constant stirring speed of 500 rpm for 1 hour. Finally, the synthesized PLLCQDs were purified.

3.2.4 Purification of PLLCQDs:

0The prepared PLLCQDs were purified by centrifugation at 8000 rpm for 15 min. The collected supernatant was filtered with a 0.22 µM syringe filter. The obtained solution was further dialyzed with a 3.5 kDA dialysis membrane (details explained in chapter II). The formed PLLCQDs were stored at 4°C for additional use.

3.2.5 Quantum Yield Calculation:

The quantum yield (QY) of PLLCQDs was measured to calculate their fluorescence efficiency. The standard comparison approach was used in the current investigation to determine the QY [18]. As a standard reference material, the well-known, highly fluorescent quinine sulphate was employed. The absorbance was controlled below 0.10 using an aqueous solution of PLLCQDs and quinine sulphate (QS) (QY = 0.54, refractive index = 1.33) in 0.1 M H_2SO_4. The absorbance and fluorescence of the specific solutions were measured, by using the formula the QY of PLLCQDs (eq. 3.1) [18].

$$QY_{PLLCQDs} = QY_{QS} \times \left(\frac{I_{PLLCQDs}}{I_{QS}} \times \frac{A_{QS}}{A_{PLLCQDs}} \times \frac{\eta^2_{PLLCQDs}}{\eta^2_{QS}}\right) \quad \text{….. (eq. 3.1)}$$

Where, 'I' is the integrated fluorescence intensity, whereas 'A' is the maximum absorbance as well as 'η' is the refractive index of QS and PLLCQDs, respectively.

3.2.6 Characterizations:

To confirm the synthesis of PLLCQDs, spectroscopic and microscopic techniques were used. For the spectroscopic study, the equipment used are UV-Vis spectroscopy (Agilent Cary 60 UV–vis spectrophotometer Instrument Version 2.00), Fluorescence spectroscopy (FP-8300 Spectrofluorometer from JASCO), Fourier Transform Infrared Spectroscopy (Alpha (II) Bruker unit), X-ray Diffraction Spectroscopy (Rigaku 600 miniflex), and X-ray Photoelectron Spectroscopy ((K-Alpha XPS, 8025-BesTec twin anode XR3E2 X-ray source system). For microscopic characterization of PLLCQDs Transmission Electron Microscopy (FEI TECNAI G2-20 TWIN) and Atomic Force Microscopy (park systems AFMNX 10) were used.

3.2.7 Effect of pH and UV radiation on PL intensity:

To study the luminescence and chemical stability of PLLCQDs, the effects of pH and UV radiation were investigated. KH_2PO_4 and NaOH were used to make the basic pH buffer solutions, potassium chloride and hydrochloric acid were used to make the acidic pH buffer solutions. The pH stability of PLLCQDs was investigated at 2, 4, 6, 8, 10, and 12 pH values. Similarly, the PLLCQDs were subjected to UV light for baseline measurement 0–120 minutes to evaluate their effect on fluorescence intensity [19].

3.2.8 Preparation of fluorescent ink:

The prepared PLLCQDs were loaded into fountain pens and text was written on Whatman filter paper. The photographs were taken under daylight and UV light (365 nm), respectively.

3.3 Results and Discussion

3.3.1 Optimization of parameters for synthesis of PLLCQDs:

Optimization parameters were chosen for CQD synthesis to ensure the production of high-quality CQDs with consistent and application-specific properties. Optimizing parameters such as temperature, reaction time, and PLL concentration help

to achieve uniform particle size and desired morphology, which are crucial for consistent optical and electronic properties.

A specific temperature range is chosen to optimize the synthesis parameters of CQDs because temperature plays a crucial role in controlling the carbonization process, particle size, crystallinity, and functionalization. The fluorescence intensity and quantum yield of CQDs are highly time-dependent. The selected range allows the reaction to proceed to a point where the optical properties, such as photoluminescence, are maximized without degradation.

PLL contributes to the functionalization of CQD surfaces with amino groups. The chosen concentration range ensures optimal surface coverage, enhancing solubility and reactivity. The lower and upper limits for temperature (80–200 °C), time (5–20 min), and PLL concentration (0.02–0.1 % w/v) were selected to design the experiments.

The main effects of temperature, reaction time, and PLL concentration, as well as their influence on PL intensity, were graphically presented in Figure 3.1 (a–c). The major effect of each variable was determined by varying its value from the low level to the high level while keeping the other two variables at their central levels. Figure 3.1 (a) shows the variation in PL with change in temperature. It was observed that the PL gradually increases with rising temperature. At 200 °C, the PL is significantly higher compared to lower temperatures (80, 100, 120, and 150 °C).

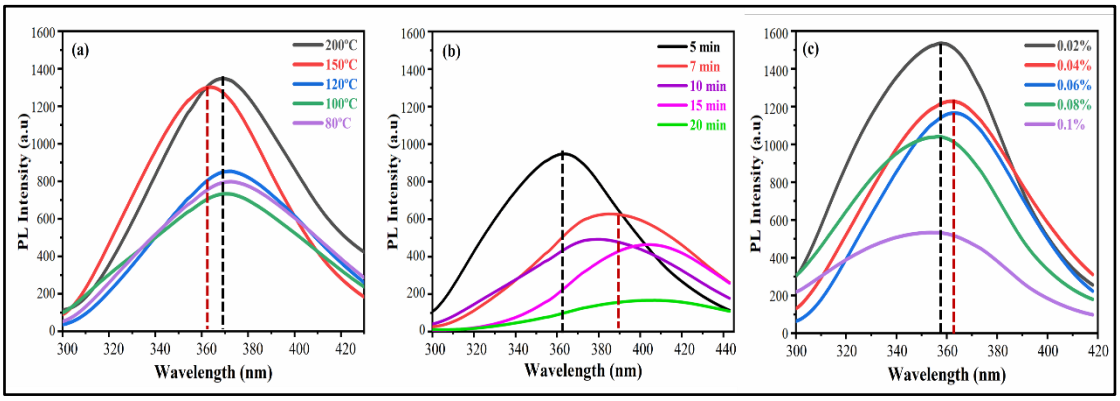

Figure 3.1: PL spectra of PLLCQDs (a) Reaction temperature, (b) Reaction time, and (c) PLL concentration.

The increase in PL with temperature is attributed to improved carbonization, the creation of emissive center, and reduced non-radiative losses. Wavelength shifts are

primarily due to quantum confinement effects, changes in the bandgap, and alterations in surface chemistry. However, prolonged reaction times can lead to over-carbonization, aggregation, or loss of surface functionality, ultimately causing a decrease in PL.

According to Figure 3.1 (b), the optimal reaction time for synthesis is 5 minutes. Along with that, PLL concentration was examined to functionalize CQDs. The various concentration of PLL was added to the CQD solution. Figure 3.1 (c) depicts the intensity of the fluorescence as it rises with falling concentration. The optimum concentration for the synthesis is 0.02% w/v PLL. The optimization of PLLCQDs synthesis was confirmed at 200°C temperature with 5 min reaction time and 0.02% PLL solution with high PL. The PL increases and the wavelength shifts at 0.02% PLL because this concentration balances surface passivation and quantum confinement effects.

Changing the synthesis parameters may lead to an increased yield of CQDs, thereby enhancing the overall PL intensity. Variations in synthesis conditions can result in the formation of different species of CQDs with distinct surface functional groups and sizes. These variations can influence the electronic structure and optical properties of CQDs, leading to changes in PL behavior.

3.3.2 Synthesis of PLLCQDs:

In the typical procedure, PLLCQDs were synthesized from glucose powder using a bottom-up approach, with PLL serving as a functionalizing agent. PLLCQDs were obtained after heating at 200 °C for 5 minutes with a PLL concentration of 0.02%. The resulting PLLCQDs exhibited good water solubility and strong luminescence properties. To confirm the successful surface functionalization of PLLCQDs, definitive physicochemical analyses, including UV-Vis spectroscopy and fluorescence spectroscopy, were conducted.

3.3.2.1 Ultraviolet-Visible spectroscopy:

UV-Visible spectroscopy was used to assess the optical properties of PLLCQDs. The absorbance was measured in the range of 200–800 nm. Under visible light, the samples appeared pale yellow, while under UV light, they emitted a blue fluorescence. Figure 3.2(a) displays the UV-Vis spectrum of PLLCQDs. Two

prominent peaks are observed in the UV-Vis absorption spectrum at approximately 226.7 nm and 281 nm, which may be attributed to the C=O and C=C transitions corresponding to n-π* and π-π* transitions, respectively [23].

3.3.2.2 Fluorescence Spectroscopy:

The PLLCQDs exhibit intense emission peaks at 471 nm when excited at 370 nm and exhibit excitation wavelength-dependent photoluminescence spectra (Figure 3.2 b). Under UV excitation, the color of the aqueous solution changes from yellow to blue as evident from naked eye observation [inset, Figure 3.2 a]. According to Figure 3.2 (c), the photoluminescence peak moves from 380 nm to 420 nm when the excitation wavelength is increased from 300 to 420 nm. The excitation-dependent behavior was found in PLLCQDs. It is attributed to multiple effects, such as the quantum confinement effect, surface traps, or reorganization of the solvent's polarization, and is therefore still under debate. According to our findings, the excitation dependence behavior is explained from a straightforward down-shifting perspective.

For broad emission spectra, color tunability is invariably achieved by down-conversion of excitations within the excitation spectrum, whether they are caused by surface traps or the quantum confinement effect of size-dispersed sp^2 regions. The size effect is a result of a quantum confinement event, whereas the surface state is comparable to a molecular state. Both of these phenomena add to the complexity of the excited states of PLLCQDs [24].

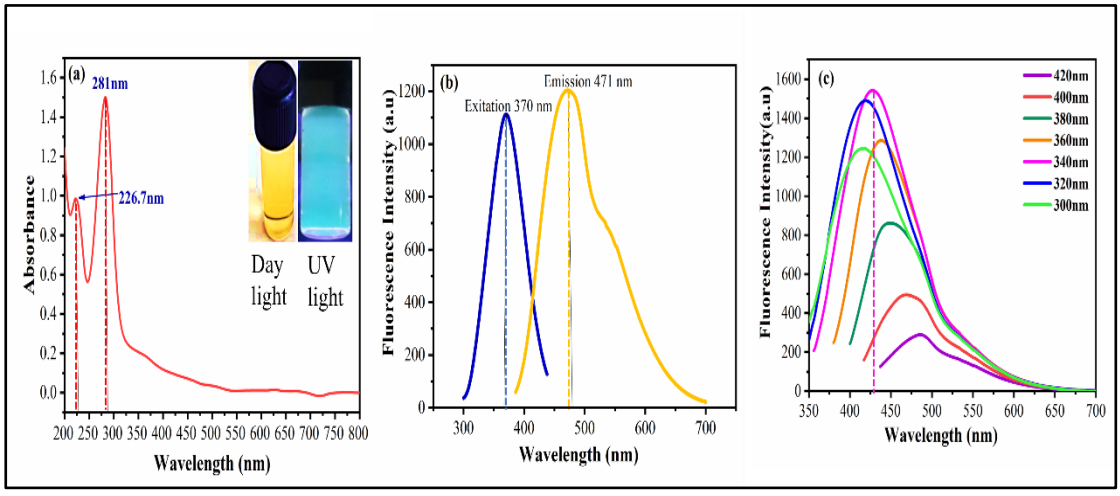

Figure 3.2: (a) UV–Vis Spectroscopy, (b) Emission and Excitation spectra, and (c) Emission spectra captured in 20 nm increment in excitation wavelength of PLLCQDs.

3.3.2.3 Quantum Yield (QY) Measurement:

QY, which measure particles ability to emit absorbed electromagnetic energy as photons, is commonly defined as the ratio of photons emitted to photons absorbed through fluorescence. Fluorescence QY is a crucial physical property of a substance under specific conditions.

Quinine sulfate produces blue fluorescence when dissolved in 0.1 M sulfuric acid, with an excitation wavelength of 360 nm and an emission wavelength of 485 nm. Therefore, quinine sulfate is commonly used as a standard reference for QY measurement. By applying the formula outlined in Equation 3.1 and using quinine sulfate in 0.1 M H_2SO_4 (QY = 0.54) as the reference solution, the QY of PLLCQDs was calculated. The fluorescence QY of PLLCQDs in an aqueous solution was determined to be 19.35% at an emission wavelength of 471 nm, as illustrated in Figure 3.2(a).

3.3.2.4 Mechanism behind PLLCQDs formation:

The mechanism of PLLCQD formation is proposed based on the precursors used and their interactions during the reaction. It is inferred that the generation of radicals and carbonization at elevated temperatures leads to the formation of PLLCQDs. The overall process can be divided into three main steps, as illustrated in Figure 3.3.

When the temperature reaches 200 °C, glucose undergoes thermal decomposition, melting and breaking its O-H, C-H, C-O, and C-C chemical bonds. This leads to the formation of reactive radicals and small carbonaceous fragments. The high temperature facilitates carbonization, which plays a crucial role in forming the carbon core of CQDs.

In the presence of PLL, the reactive species self-assemble and undergo cross-linking, forming intermediate structures. PLL actively participates in surface passivation and functionalization, introducing amino functional groups that enhance solubility and fluorescence properties. The interaction between the carbonized core and PLL results in the stabilization of the CQDs.

In the final stage, free radicals interact with PLL, leading to further polymerization and surface modification. The formation of polymer-like PLLCQDs

occurs through chemical linkages between PLL and the carbon core, ensuring enhanced optical properties and stability.

The proposed mechanism is grounded in the chemical behavior of glucose and PLL under thermal conditions, coupled with the experimental evidence of CQD formation. The generation of radicals and subsequent carbonization provide a rational explanation for the formation of PLLCQDs with desired structural and functional properties.

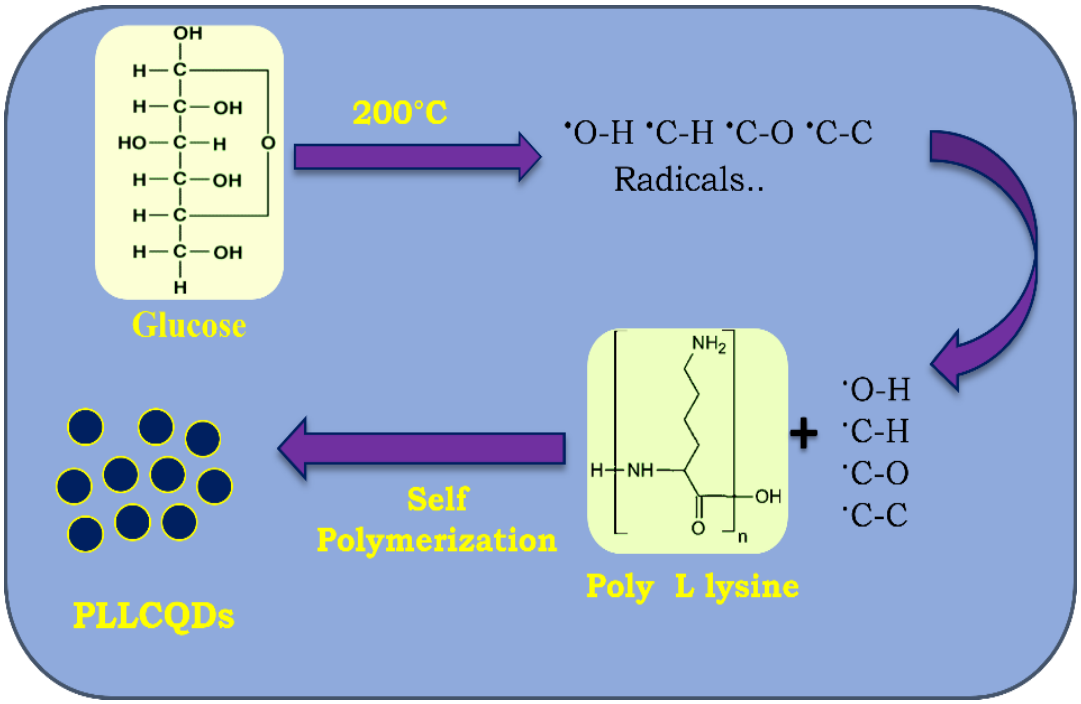

Figure 3.3: Schematic representation of mechanism for formation of PLLCQDs.

3.3.2.5 Fourier Transform Infrared Spectroscopy (FT-IR):

According to Figure 3.4, the broad transmittance at 3292 cm^{-1} is attributed to the vibrational stretching of the O-H bond. The peak at 2927 cm^{-1} corresponds to C-H stretching vibrations, typically associated with methyl groups. The characteristic transmittance at 1640 cm^{-1} is attributed to the stretching of the C=O bond. Additionally, functional amine groups exhibit strong stretching vibrations, with a transmittance peak observed at 1025 cm^{-1}. These findings indicate that numerous carbonyl and hydroxyl groups play a significant role in functionalization of574 surface of PLLCQDs [17].

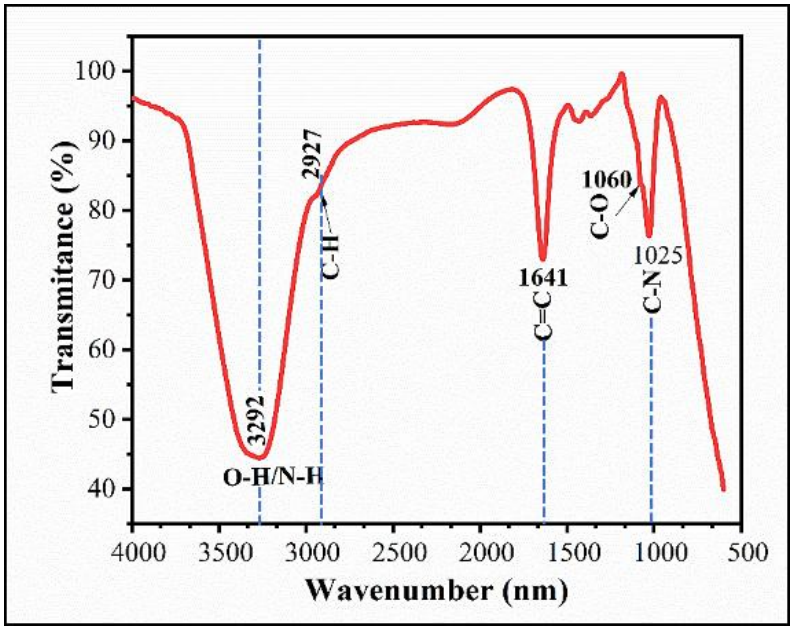

Figure 3.4: FT-IR spectrum of PLLCQDs.

3.3.2.6 X-ray Diffraction Spectroscopy (XRD):

The PLLCQDs XRD pattern displays a large peak with a central angle of 23° that is indicative of amorphous carbon distributed in an extremely chaotic manner. More oxygen-containing functional groups are present, according to the PLLCQDs weak crystalline structure [26]. In Figure 3.5, the XRD spectrum is displayed.

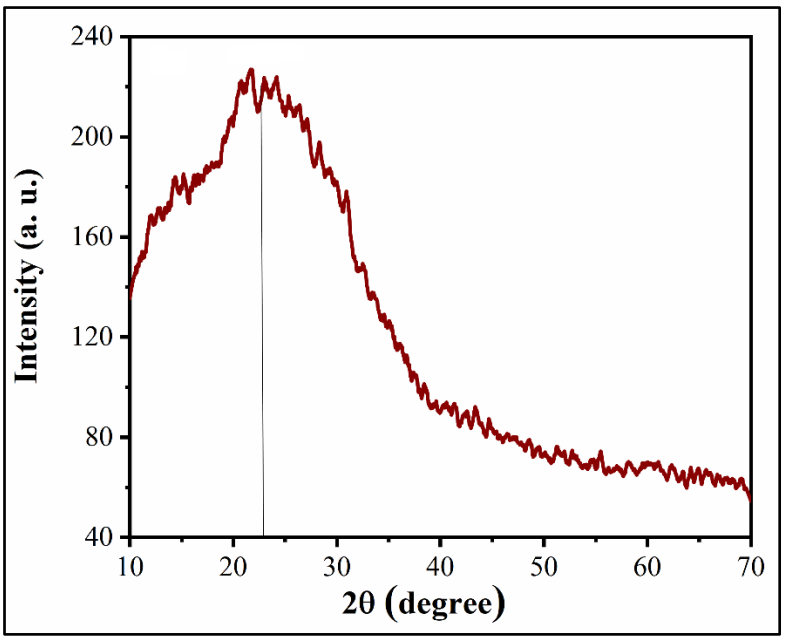

Figure 3.5: XRD Spectrum of PLLCQDs.

3.3.2.7 X-ray Photoelectron Spectroscopy (XPS):

The elemental composition and surface characteristics of the resulting PLLCQDs were further analyzed using XPS. According to the XPS spectra of PLLCQDs, three distinct peaks at 285 eV, 398 eV, and 531 eV correspond to the presence of carbon (C), nitrogen (N), and oxygen (O), respectively (Figure 3.6 a).

The high-resolution C 1s spectrum (Figure 3.6 b) reveals three deconvoluted peaks at 284.8 eV, 286.3 eV, and 287.4 eV, which correspond to C=C, C=O, and COOH functional groups, respectively [27]. The deconvolution of the O 1s spectrum yielded a peak at 531.3 eV (Figure 3.6 c), confirming the presence of oxygen-containing functional groups.

In Figure 3.6 d, the N 1s spectrum is deconvoluted into three peaks at 396.6 eV, 400.6 eV, and 401.3 eV, which correspond to pyridinic nitrogen (N), pyrrolic nitrogen (N), and amino nitrogen (N), respectively. These results confirm the successful incorporation of nitrogen and oxygen functional groups, contributing to the surface chemistry and enhanced properties of PLLCQDs.

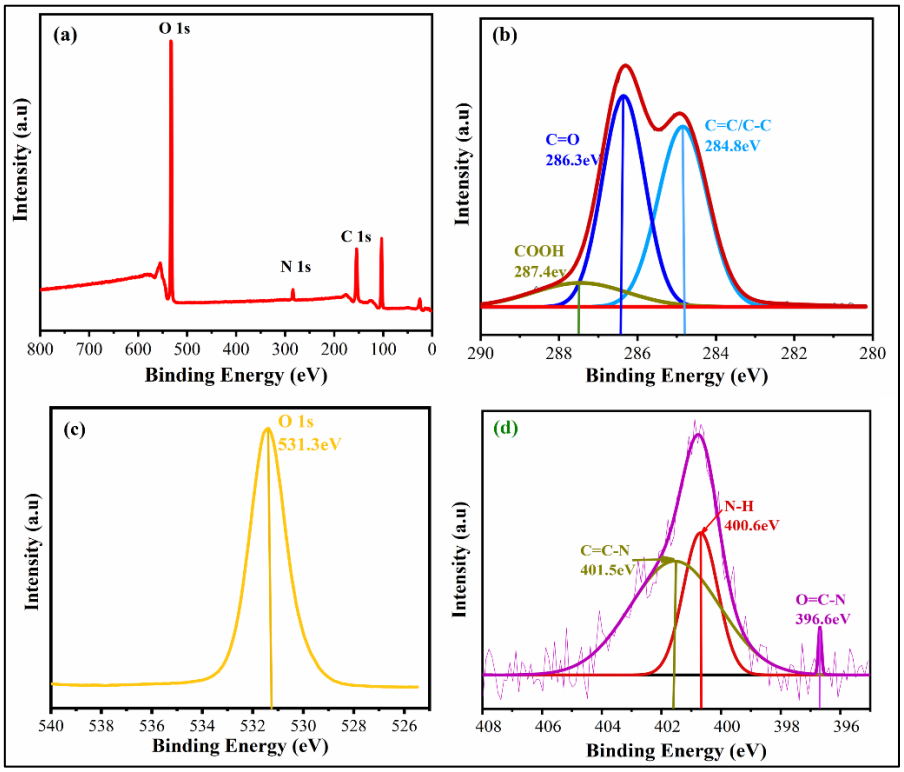

Figure 3.6: XPS spectra of PLLCQDs: (a) Survey spectrum, (b) C 1s spectrum, (c) O 1s spectrum, and (d) N 1s spectrum.

3.3.2.8 High-Resolution Transmission Electron Microscopy (HR-TEM):

The morphology of PLLCQDs was analyzed using high-resolution transmission electron microscopy (HR-TEM). The high-magnification TEM image of the synthesized PLLCQDs (Figure 3.7a) confirms the presence of well-dispersed, approximately spherical nanodots. The corresponding size distribution histogram (Figure 3.7b) indicates that the average particle size of PLLCQDs is approximately 3 nm [28].

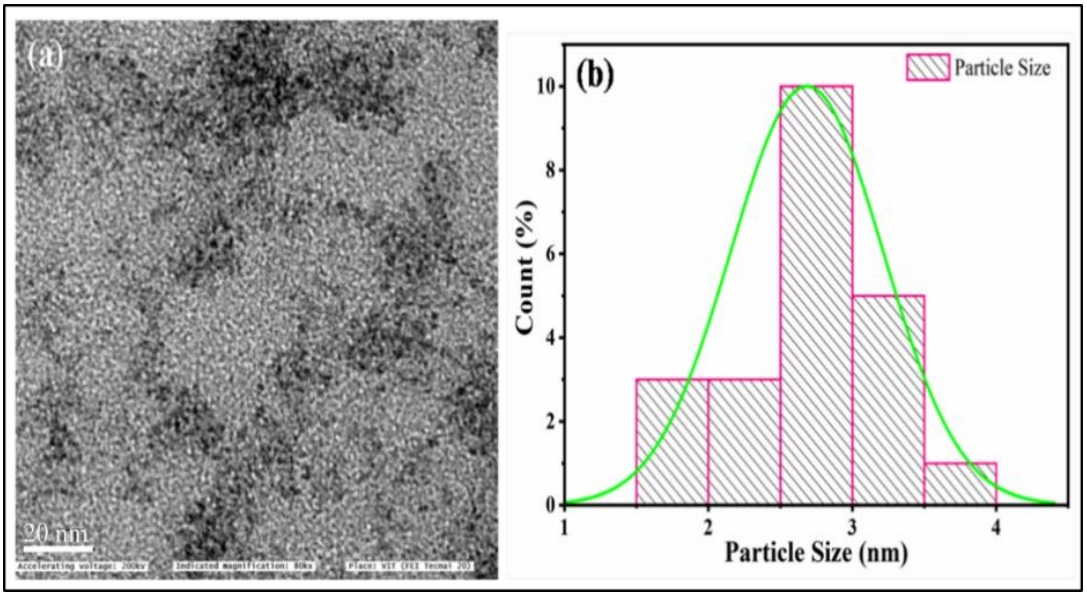

Figure 3.7: (a) HR-TEM image (magnification 80KX), and (b) Particle size histogram for PLLCQDs.

3.3.2.9 Atomic Force Microscopy:

The size and surface roughness of PLLCQDs were analyzed using atomic force microscopy (AFM). Figure 3.8 presents the AFM topographical images of PLLCQDs, providing insights into their morphological characteristics and surface texture. AFM images confirmed that PLLCQDs are small in size and oval in shape. The analysis reveals that PLLCQDs have an average diameter ranging from 2 to 4 nm, with a surface roughness of less than 2 nm. However, the roughness histogram of PLLCQDs indicates an average roughness of 4.77 nm.

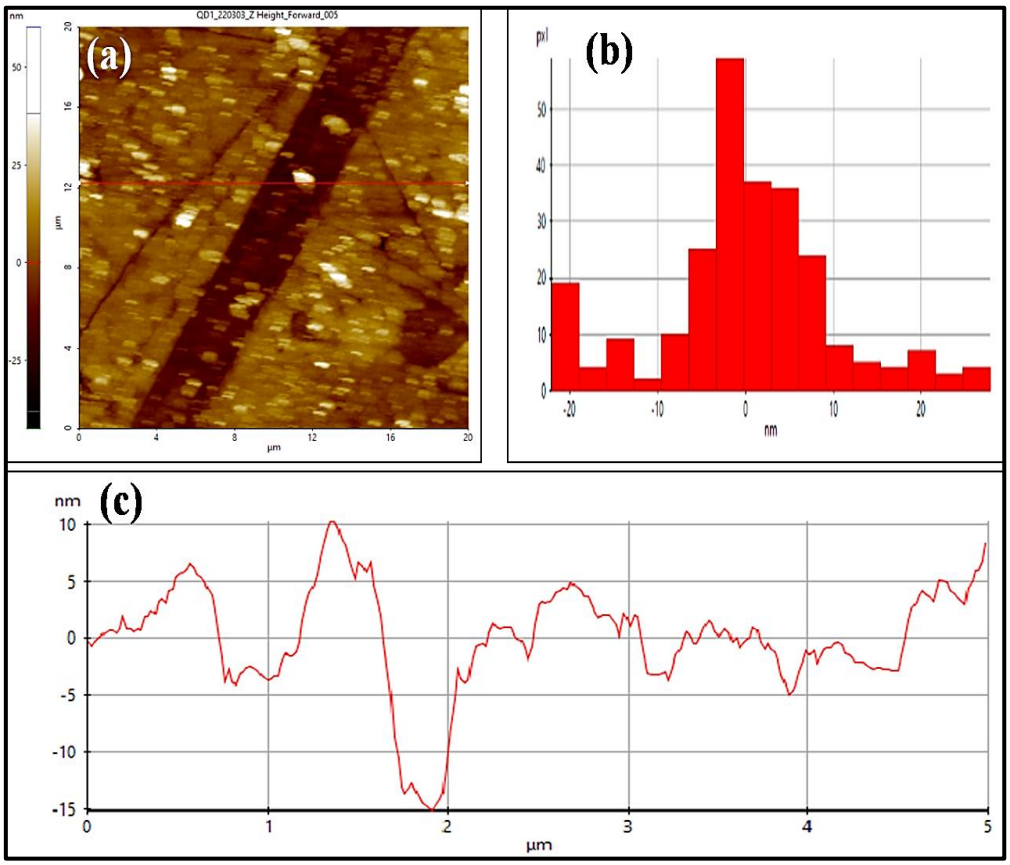

Figure 3.8: Atomic Force Microscopy (a) 2D image, (b) Line histogram of particle size, and (c) line graph for PLLCQDs.

Figure 3.8 (a) presents AFM image, while Figure 3.8 (b) displays the PLLCQD histogram, demonstrating a particle size distribution between 2 and 4 nm and a surface roughness of approximately 3 nm. Additionally, Figure 3.8 (c) shows a line profile of PLLCQDs, with the corresponding 2D AFM image depicted in Figure 3.8 (a).

3.3.3 Effect of pH and UV Radiation on PL Intensity:

The pH of the synthesized PLLCQDs caused a little difference in PL; as shown in figure 3.9 (a), the high intensity was attained at pH values of 4 and 8. No alteration in the PL intensity of PLLCQDs was seen in response to the continuous UV exposure (Figure 3.9 b). These findings imply that PLLCQD has high photo and chemical stability and is appropriate for a wide range of applications.

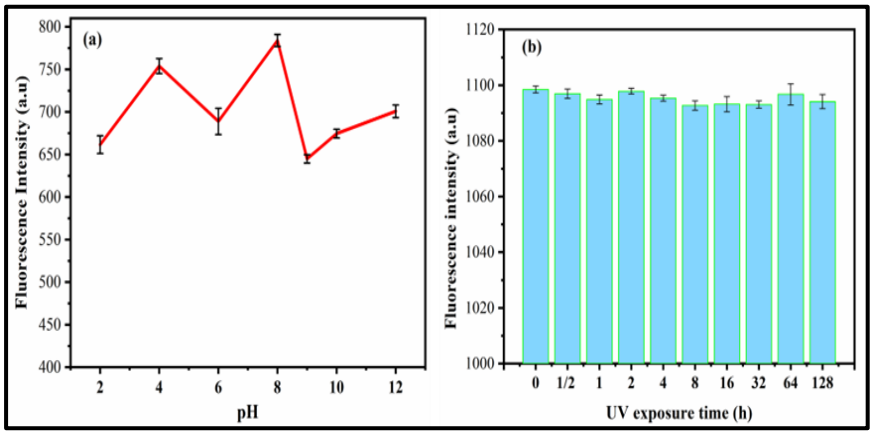

Figure 3.9: Relative PL of PLLCQD influenced by (a) pH and (b) exposure time to UV light.

3.3.4 PLLCQD as fluorescent ink application:

The PLLCQDs are suitable for use as invisible ink because of their high fluorescence intensity and photostability. The PLLCQD solution can be used as ink and placed in a regular pen. Anything written with this pen on paper is invisible under normal light but becomes visible under UV light, as demonstrated in Figure 3.10. This invisible ink is ideal for writing confidential material for confidential purposes and also holds commercial potential in printing technology. The fluorescent ink pen is user-friendly, cost-effective, and refillable for commercial applications [29].

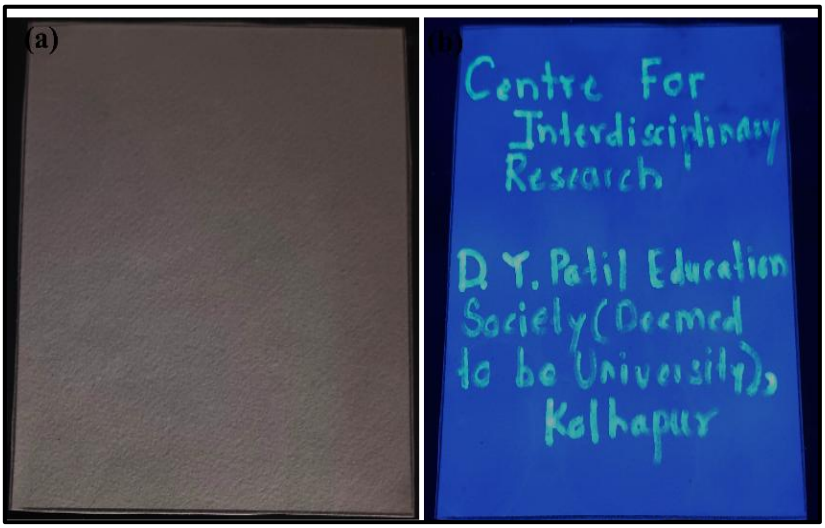

Figure 3.10: (a) Text written on a filter paper with PLLCQD ink is invisible in daylight and (b) glows under UV light (365 nm excitation).

3.5 Conclusions:

This chapter concludes that the one-step bottom-up technique successfully synthesized PLL-functionalized CQDs. The formation of PLLCQDs was confirmed through various physicochemical analyses, including UV-Vis spectroscopy, fluorescence spectroscopy, FT-IR, XRD, XPS, TEM, and AFM.

The optical properties of PLLCQDs were characterized using UV-Vis and fluorescence spectroscopy. The UV-Vis spectrum exhibited peaks at 226.7 nm and 282 nm, corresponding to n-π* and π-π* transitions, respectively. Additionally, PLLCQDs demonstrated excitation-dependent fluorescence behavior.

The FT-IR spectrum revealed characteristic peaks at 3292 cm^{-1}, 2927 cm^{-1}, 1640 cm^{-1}, and 1025 cm^{-1}, corresponding to O-H, C-H, C=O, and N-H functional groups, respectively. The quantum yield (QY) of PLLCQDs was determined to be 19.35%. XRD and XPS analyses confirmed the graphitic nature of the PLLCQDs and their elemental composition, including C, N, and O.

The size of PLLCQDs was analyzed using HR-TEM and AFM, revealing that the synthesized nanodots ranged from 2 to 3 nm in diameter. Furthermore, PLLCQDs were successfully utilized as refillable fluorescent ink for writing applications. Their high luminescence makes them suitable for use in confidential writing applications.

3.6 References:

1. Kumari M., Chaudhary G. R., Chaudhary S., Umar A., Akbar S., Baskoutas S., Bio-Derived Fluorescent Carbon Dots: Synthesis, Properties and Applications. Molecules. 27 (16) (2022) 5329-5348, DOI-10.3390/molecules27165329.
2. Zheng X. T., Ananthanarayanan A., Luo K. Q., Chen P., Glowing graphene quantum dots and carbon dots: Properties, syntheses, and biological applications. Small. 11 (14) (2015) 1620-1636, DOI-10.1002/smll.201402648.
3. Wareing T. C., Gentile P., Phan A. N., Biomass-Based Carbon Dots: Current Development and Future Perspectives. ACS Nano. 15 (10) (2021) 15471-15501, DOI-10.1021/acsnano.1c03886.
4. Sun Y. P., Zhou B., Lin Y., Wang W., Fernando K. S., Pathak P., Meziani M. J., Harruff B. A., Wang X., Wang H., Luo P.G., Quantum-sized carbon dots for bright and colorful photoluminescence. Journal of American Chemical Society. 128 (24) (2006) 7756–7757, DOI-0.1021/ja062677d.
5. Wang Y., Anilkumar P., Cao L., Liu J. H., Luo P. G., Tackett K. N., Sahu S., Wang P., Wang X., Sun Y. P., Carbon dots of different composition and surface functionalization: Cytotoxicity issues relevant to fluorescence cell imaging. Experimental Biology and Medicine. 236 (11) (2011) 1231-1238, DOI-10.1258/ebm.2011.011132.
6. Emam A. N., Loutfy S. A., Mostafa A. A., Awad H., Mohamed M. B., Cytotoxicity, biocompatibility and cellular response of carbon dots-plasmonic based nano-hybrids for bioimaging. RSC Advance, 7 (38) (2017) 23502-23514, DOI-10.1039/c7ra01423f.
7. Wang Y., Zhuang Q., Ni Y., Facile microwave-assisted solid-phase synthesis of highly fluorescent nitrogen–sulfur-codoped carbon quantum dots for cellular imaging applications. Chemistry–A European Journal. 21 (37) (2015) 13004-113011, DOI-10.1002/chem.201501723.
8. Li W., Wu S., Zhang H., Zhang X., Zhuang J., Hu C., Liu Y., Lei B., Ma L., Wang X., Enhanced biological photosynthetic efficiency using light-harvesting engineering with dual-emissive carbon dots. Advanced Functional Materials. 28 (44) (2018) 1804004-1804012, DOI-.1002/adfm.201804004.
9. Kaur P., Verma G., Converting fruit waste into carbon dots for bioimaging applications. Materials Today Sustainability.18 (1) (2022) 100137-100150, DOI-1016/j.mtsust.2022.100137.
10. Dai H., Shi Y., Wang Y., Sun Y., Hu J., Ni P., Li Z., A carbon dot based biosensor for melamine detection by fluorescence resonance energy transfer. Sensors and Actuators B: Chemical. 202 (1) (2014) 201-208, DOI-10.1016/j.snb.2014.05.058.

11. Pirsaheb M., Mohammadi S., Salimi A., Current advances of carbon dots-based biosensors for tumor marker detection, cancer cells analysis, and bioimaging. Trends in Analytical Chemistry. 115 (1) (2019) 83-99, DOI-10.1016/j.trac.2019.04.003.

12. de Oliveira B. P., de Castro Bessa N. U., do Nascimento J. F., de Paula Cavalcante C. S., dos Santos Fontenelle R. O., da Silva Abreu F. O., Synthesis of luminescent chitosan-based carbon dots for Candida albicans bioimaging. International Journal of Biological Macromolecules. 227 (1) (2023) 805-814, DOI-10.1016/j.ijbiomac.2022.12.202.

13. Pannu A. S., Sen S., Wang X. T., Jones R., Ostrikov K. K., Sonar P., Hybrid 2D perovskite and red emitting carbon dot composite for improved stability and efficiency of LEDs. Nanoscale. 15 (6) (2023) 2659-2666, DOI-10.1039/d2nr06942c.

14. Li J., Zhao H., Zhao X., Gong X., Boosting efficiency of luminescent solar concentrators using ultra-bright carbon dots with large Stokes shift. Nanoscale Horizons. 8 (1) (2023) 83-94, DOI-10.1039/d2nh00360k.

15. Pillar-Little T. J., Wanninayake N., Nease L., Heidary D. K., Glazer E. C., Kim D. Y., Superior photodynamic effect of carbon quantum dots through both type I and type II pathways: Detailed comparison study of top-down-synthesized and bottom-up-synthesized carbon quantum dots. Carbon. 140 (1) (2018) 616-623, DOI-10.1016/j.carbon.2018.09.004.

16. Sun H., Ji H., Ju E., Guan Y., Ren J., Qu X., Synthesis of fluorinated and nonfluorinated graphene quantum dots through a new top-down strategy for long-time cellular imaging. Chemistry–A European Journal. 21 (9) (2015) 3791-3797, DOI-10.1002/chem.201406345.

17. Sun B., Wu F., Zhang Q., Chu X., Wang Z., Huang X., Li J., Yao C., Zhou N., Shen J., Insight into the effect of particle size distribution differences on the antibacterial activity of carbon dots. Journal of Colloid and Interface Science. 584 (1) (2021) 505-519, DOI-10.1016/j.jcis.2020.10.015.

18. Liu Y., Chen P., Yu K., Wu Z., Wang N., Yu X., Nitrogen and sulfur co-doped carbon dots: Facile synthesis and multifunctional applications for pH sensing, temperature sensing and RNA-selective imaging. Microchemical Journal. 168 (1) (2021) 106248-106260, DOI-10.1016/j.microc.2021.106248.

19. Sharma N., Das G. S., Yun K., Green synthesis of multipurpose carbon quantum dots from red cabbage and estimation of their antioxidant potential and bio-labeling activity. Applied Microbiology and Biotechnology. 104 (1) (2020) 7187-7200, DOI-10.1007/s00253-020-10726-5.

20. Ye Z., Li G., Lei J., Liu M., Jin Y., Li B., One-step and one-precursor hydrothermal synthesis of carbon dots with superior antibacterial activity. ACS Applied Bio Materials. 3 (10) (2020) 7095-7102, DOI-10.1021/acsabm.0c00923.

21. Das P., Bose M., Ganguly S., Mondal S., Das A. K., Banerjee S., Das N. C., Green approach to photoluminescent carbon dots for imaging of gram-negative bacteria Escherichia coli. Nanotechnology. 28 (19) (2017) 195501-195515, DOI-10.1088/1361-6528/aa6714.

22. Liu M. L., Chen B. B., Li C. M., Huang C. Z., Carbon dots: synthesis, formation mechanism, fluorescence origin and sensing applications. Green chemistry. 21 (3) (2019) 449-471, DOI-10.1039/c8gc02736f.

23. Tang L., Ji R., Cao X., Lin J., Jiang H., Li X., Teng K. S., Luk C. M., Zeng S., Hao J., Lau S. P., Deep ultraviolet photoluminescence of water-soluble self-passivated graphene quantum dots. ACS Nano. 6 (6) (2012) 5102-5110, DOI-10.1021/nn300760g.

24. Zhu S., Zhang J., Qiao C., Tang S., Li Y., Yuan W., Li B., Tian L., Liu F., Hu R., Gao H., Strongly green-photoluminescent graphene quantum dots for bioimaging applications. Chemical communications. 47 (24) (2011) 6858-6860, DOI-10.1039/c1cc11122a.

25. Barati A., Shamsipur M., Arkan E., Hosseinzadeh L., Abdollahi H., Synthesis of biocompatible and highly photoluminescent nitrogen doped carbon dots from lime: analytical applications and optimization using response surface methodology. Materials Science and Engineering: C. 47 (1) (2015) 325-332, DOI-10.1016/j.msec.2014.11.035.

26. Venkateswarlu S., Viswanath B., Reddy A. S., Yoon M., Fungus-derived photoluminescent carbon nanodots for ultrasensitive detection of Hg^{2+} ions and photoinduced bactericidal activity. Sensors and Actuators B: Chemical. 258 (1) (2018) 172-183, DOI-10.1016/j.snb.2017.11.044.

27. Herbani Y., Suliyanti M. M., Concentration effect on optical properties of carbon dots at room temperature. Journal of Luminescence. 198 (1) (2018) 215-219, DOI-10.1016/j.jlumin.2018.02.012.

28. Vibhute A., Nille O., Kolekar G., Rohiwal S., Patil S., Lee S., Tiwari A. P., Fluorescent carbon quantum dots functionalized by poly L-lysine: efficient material for antibacterial, bioimaging and antiangiogenesis applications. Journal of Fluorescence. 32 (5) (2022) 1789-1800, DOI-10.1007/s10895-022-02977-4.

29. Mondal T. K., Saha S. K., Facile approach to synthesize nitrogen-and oxygen-rich carbon quantum dots for pH sensor, fluorescent indicator, and invisible ink applications. ACS sustainable chemistry & engineering. 7 (24) (2019) 19669-19678, DOI-10.1021/acssuschemeng.9b04817.

CHAPTER IV

OPTIMIZATION PARAMETERS FOR NUCLEIC ACID BINDING ON SURFACE FUNCTIONALIZED CARBON QUANTUM DOTS

4.1 Introduction:

Nucleic acids are biopolymers, macromolecules that play essential roles in all known forms of life. A major function of nucleic acids involves the storage and expression of genomic information. They are composed of nucleotides, which are the monomer components: a 5-carbon sugar, a phosphate group, and a nitrogenous base. The two main classes of nucleic acids are deoxyribonucleic acid (DNA) and ribonucleic acid (RNA). If the sugar is ribose, the polymer is RNA; if the sugar is deoxyribose, a version of ribose, the polymer is DNA.

Nucleic acid probes are more flexible and stable when employed in certain ways than other macromolecules like proteins. That is, a broad platform for the development of novel molecular recognition tools is provided by the simplicity with which DNA base alteration and DNA strands can be handled, in conjunction with varied nanomaterial modification methodologies. The widespread use of DNA and nanomaterial conjugates in spectroscopy, electrochemistry, magnetics [1], and other [2] domains serve as an example of this. The binding of DNA with different metal-ligand complexes utilizing fluorescent probes has been reported in several publications [3-5]. Huge interest has been shown in the interaction between biological molecules and carbon nanomaterials, where the former may offer a flexible nanoscale interface for biomolecular identification.

The conjugation of biological molecules with carbon nanomaterials has garnered significant interest, as the former could offer a flexible nanoscale interface for biomolecular identification. There is less information available regarding DNA interaction experiments involving carbon-based materials. Furthermore, the precise mechanism underlying this type of interaction has not been discussed. By using spectroscopic techniques, Kathiravan and his colleagues [6], reported the photoinduced interaction between colloidal TiO_2 nanoparticles and Ct-DNA and investigated the binding sites and constant. The interaction of CQDs with single-stranded DNA (ssDNA) and double-stranded DNA (dsDNA) has received sufficient attention recently. Research has demonstrated that these two interact with CQDs in different ways, resulting in remarkable fluorescence behavior [7-9]. For instance, to identify a particular DNA strand, Loo et al. [8] have developed a sensing platform that has used fluorescently labeled ssDNA probes (FAML probes) and CQDs.

Three main non-covalent interaction modes, namely electrostatic interactions, groove binding, and intercalation, are involved in the binding mode of small molecules to the DNA double helix structure. It is anticipated that positively charged CQDs will interact strongly with negatively charged nucleic acids through electrostatic interactions because of their phosphate backbone [10]. There are instances where the contact is so powerful that it may alter DNA structure.

In this chapter, the binding of Ct-DNA and PLL functionalized carbon quantum dots (PLLCQDs) have been studied and a bottom-up synthetic route was selected. The effect of Ct-DNA conjugation on the structural stability of polymer surface functionalized CQDs, as well as on the interaction between PLLCQDs and Ct-DNA was the main aim of this research. The effect of different parameters on the preparation of PLLCQD-Ct-DNA conjugate was investigated. Also, experiments were done to investigate the effect of Ct-DNA concentration, incubation time, and pH on the preparation of PLLCQD-Ct-DNA conjugate. According to the results obtained, the conjugate formed shows an increase in absorbance and fluorescence concerning only PLLCQDs and Ct-DNA. Spectral method, fluorescence analysis, and electrophoretic mobility shift assay were employed to investigate conjugation between PLLCQDs and Ct-DNA.

4.2 Experimental Details

4.2.1 Materials:

Anhydrous glucose (catalog no. 50-99-7, Himedia, Mumbai, India), PLL (catalog no. P8920, Sigma-Aldrich, USA), sodium hydroxide (NaOH, catalog no. PCT 1325, Himedia, Mumbai, India), and hydrochloric acid (HCl, catalog no. AS004, Himedia, Mumbai, India) were purchased in analytical grade and used without further purification. Calf thymus DNA freeze dried powder was purchased from Sigma-Aldrich, USA (catalog no. D8515). Phosphate-buffered saline (PBS, catalog no. 4417, Sigma-Aldrich, USA) was procured, and as per the manufacturer's instructions, dissolving one tablet in 200 mL of deionized water yields a 0.01 M phosphate buffer. Additionally, 0.0027 M potassium chloride (KCl, catalog no. GRM 698, Himedia, Mumbai, India) and 0.137 M sodium chloride (NaCl, catalog no. MB023, Himedia,

Mumbai, India) were purchased. All reagents used in this study were of analytical grade and were utilized without further purification.

4.2.2 Calf thymus DNA analysis:

Freeze dried powder of Ct-DNA was used to prepare 1 mL solution of Ct-DNA (1 mg/mL) by ethanol precipitation and 3.0 M sodium acetate (90:10, v/v), followed by cooling with dry ice.

The relative purity and precise concentration of Ct-DNA was determined using UV absorbance measurements. The absorbance was taken at 260 nm and 280 nm. The actual concentration of the Ct-DNA solution was calculated using equation 4.1.

$$C_{CtDNA} = \frac{\left(50\times\left(\frac{A260}{A280}\right)\times D_{CtDNA}\right)}{1.8} \quad \text{..... (eq. 4.1)}$$

where the absorbance at 260 nm and 280 nm, respectively, is represented by the values A_{260} and A_{280}, and Ct-DNA is the dilution factor of Ct-DNA sample. Before being used, these samples were further diluted to 20 µg/mL using 10% (w/v) phosphate buffer saline (PBS, 0.014 M NaCl, 0.001 M phosphate, pH 7.4). The concentrations recommended in the experimental protocols were used to prepare serial dilutions.

4.2.3 Preparation of PLLCQD-Ct-DNA conjugate:

The PLLCQDs were synthesized by pyrolysis method using glucose and PLL detail described in Chapter III. PLLCQD-Ct-DNA conjugate were prepared by incubating different concentrations of DNA at 27˚C for a time interval. For this study, 115 mg/ml PLLCQDs were incubated with 0.01 µM calf thymus DNA (Ct-DNA) continuously stirring for 30 min at room temperature. The conjugate formation was confirmed by a change in the UV-Vis absorption intensity. PLLCQD-Ct-DNA conjugate was successfully synthesized by varying reaction parameters including Ct-DNA concentration, pH, and incubation time in the ranges of 10 µg/mL- 1 mg/mL, pH 2-10, and 0-50 min, respectively. The prepared PLLCQD-Ct-DNA conjugate were characterized by UV-Vis absorption spectra (200-800 nm), and fluorescence spectra, zeta potential and electrophoretic mobility shift assay (EMSA). The synthesized PLLCQD-Ct-DNA conjugate was stored at 4ºC for further use.

4.2.4 Characterization of PLLCQD-Ct-DNA conjugate:

The PLLCQD-Ct-DNA conjugate optimization was evaluated by UV-Vis spectroscopy and fluorescence spectroscopy. The PLLCQD-Ct-DNA conjugate was confirmed by zeta potential and electrophoretic mobility shift assay.

4.2.4.1 Electrophoretic mobility shift assay (EMSA):

The formation of the PLLCQD-Ct-DNA conjugate was investigated by measuring the electrophoretic mobility of the complexes. PLLCQD-Ct-DNA conjugate solutions were prepared at different weight ratios (1:1, 10:1, 20:1, 40:1, and 100:1). Agarose gels (2%) were prepared in Tris-Acetate-EDTA (TAE) buffer containing 1 µg/mL ethidium bromide (EtBr). Each sample (10 µL) was mixed with 2 µL of loading buffer (0.1% sodium dodecyl sulfate, 5% glycerol, and 0.005% bromophenol blue) and loaded onto a 1% agarose gel prepared in TAE buffer (pH 8.0) containing 0.1 mg/mL EtBr. Electrophoresis was carried out at 80 V for 40 minutes. After the run, the power supply was turned off, and the gel was carefully removed from the gel box. The gel was then imaged using a UV transilluminator (Gel Doc 2000, BIO-RAD Laboratories) at a wavelength of 365 nm [33].

4.3 Results and Discussion:

4.3.1 Ct-DNA purity check:

The purity of Ct-DNA for 10-100 µg/mL concentration was checked by taking A_{260}/A_{280} ratio and observing peak at 260 nm as shown in Figure 4.1 (a) and (b). Pure DNA had maximum absorbance at 260 nm. Pure DNA has a 260/280 ratio of 1.8 whereas, good quality DNA is considered to obtain a ratio of 1.7-2.0. Figure 4.1 (a) and (b) shows that 10-100 µg/mL concentration of Ct-DNA did not show an absorbance at 260 nm whereas concentrations from 10-100 µg/mL and 1mg/mL shows a peak at 260 nm representing the purity of Ct-DNA.

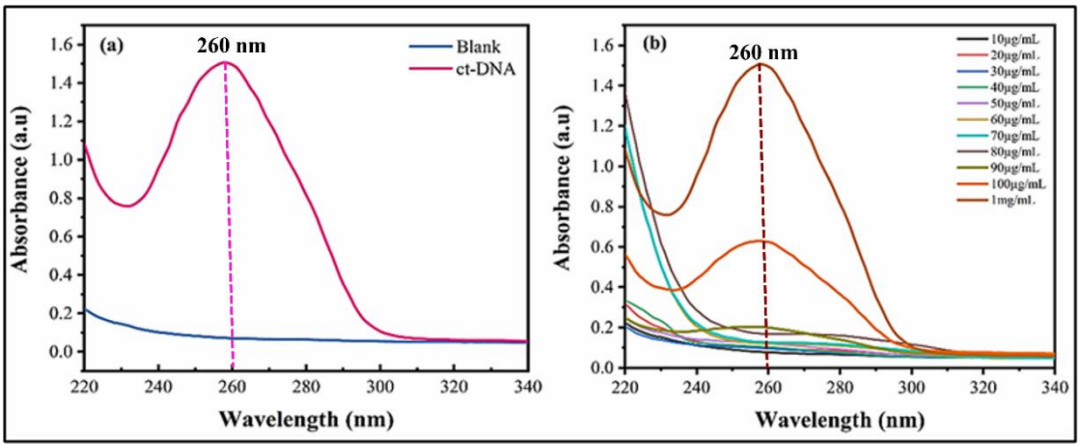

Figure 4.1: (a) Purity check of Ct-DNA comparison to blank (distilled water) and (b) purity check of various concentrations of Ct-DNA from 10-100 µg/mL and 1mg/mL by taking the absorbance spectra at 220-340 nm and observing the peak at 260 nm.

4.3.2 Optimization of synthesized PLLCQD-Ct-DNA conjugate:

The preparation of PLLCQDs via a simple pyrolysis method and their interaction with Ct-DNA were demonstrated. In this study, PLLCQDs and Ct-DNA were used for the conjugate formation. To accomplish this, the impact of Ct-DNA concentration, incubation time, and pH on the synthesis of PLLCQD-Ct-DNA conjugates was thoroughly investigated.

4.3.2.1 Effect of Ct-DNA concentration on the synthesis of PLLCQD-Ct-DNA conjugate:

The surface functionalized PLLCQDs were incubated with various concentrations of Ct-DNA and fixed concentration of PLLCQDs at 25˚C to check the effect of Ct-DNA concentration on preparation. The Ct-DNA concentrations were used as 10-100 µg/mL. Figure 4.2 (a) shows the change in absorbance at different Ct-DNA concentrations. The conjugate was formed at 20 µg/mL Ct-DNA concentration. The actual Ct-DNA concentration was confirmed by conducting the experiment in triplicate (Figure 4.2 b).

The change in absorbance shows conjugate formation compared to only Ct-DNA and PLLCQDs. The Ct-DNA and PLLCQDs show peaks at 260 and 283 nm, respectively. The conjugate formed is confirmed with redshift effect. After conjugate formation, the peak shifts and absorbance of conjugate increases. The change in

absorption indicates an increase in the size of the conjugate. The observed increase in absorption can be attributed to structural and electronic modifications linked to the growth or aggregation of PLLCQD-Ct-DNA conjugate. Larger conjugate exhibit extended π-conjugation, where electrons delocalize across the molecule. This delocalization shifts the absorption spectrum towards longer wavelengths (redshift) and increases the intensity of absorption, as evidenced by a higher molar extinction coefficient. Additionally, PLLCQD-Ct-DNA conjugate may contain more chromophores, or light-absorbing groups, which collectively enhance light absorption. In CQDs, larger particle size reduces quantum confinement effect, altering electronic energy levels and leading to broader and more intense absorption spectra. Furthermore, the growth or aggregation of PLLCQD-Ct-DNA conjugate results in electronic interactions that create new absorption features or enhance existing ones through collective electron oscillations, such as plasmonic or excitonic effects.

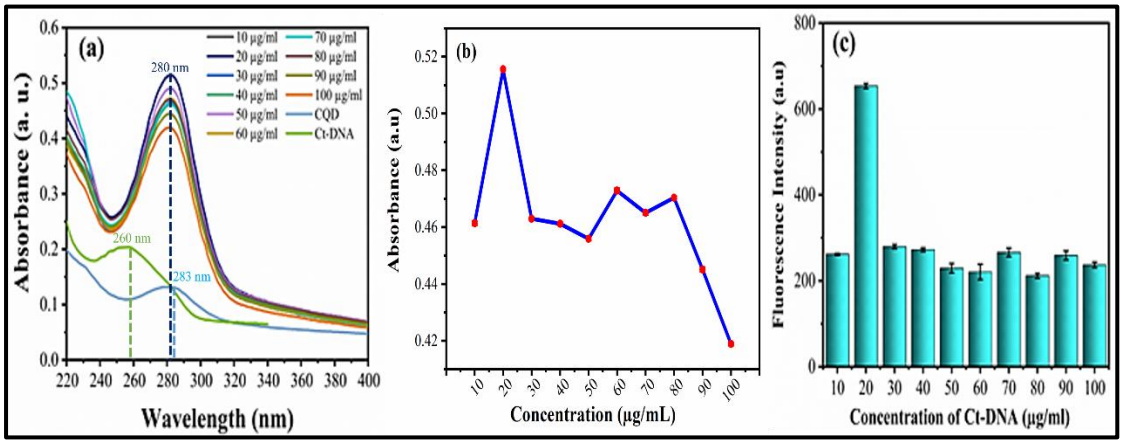

Figure 4.2: (a) UV-Vis absorbance spectra showing effect of Ct-DNA concentrations (10-100 µg/mL) on PLLCQD-Ct-DNA conjugate, (b) Change in absorbance of PLLCQD-Ct-DNA conjugate at different concentrations of Ct-DNA (10-100 µg/mL), and (c) Change in fluorescence intensity of PLLCQD-Ct-DNA conjugate at different concentrations of Ct-DNA (10-100 µg/mL).

Fluorescence intensity was checked to confirm the binding of Ct-DNA to PLLCQDs. The fluorescence intensity increases at 20 µg/mL Ct-DNA concentration (Figure 4.2 c). As per the results, 20 µg/mL Ct-DNA concentration gives a high peak of absorbance and high intensity among other Ct-DNA concentrations and is sufficient for conjugate formation.

4.3.2.2 Effect of incubation time on the synthesis of PLLCQD-Ct-DNA conjugate:

The formation of the PLLCQD-Ct-DNA conjugate depends on the interactions between Ct-DNA and CQDs, which can be influenced by incubation time. The effect of incubation time on conjugate formation is illustrated in figure 4.3. This effect was analyzed by monitoring changes in absorbance (Figure 4.3 a) and performing the measurements in triplicate (Figure 4.3 b).

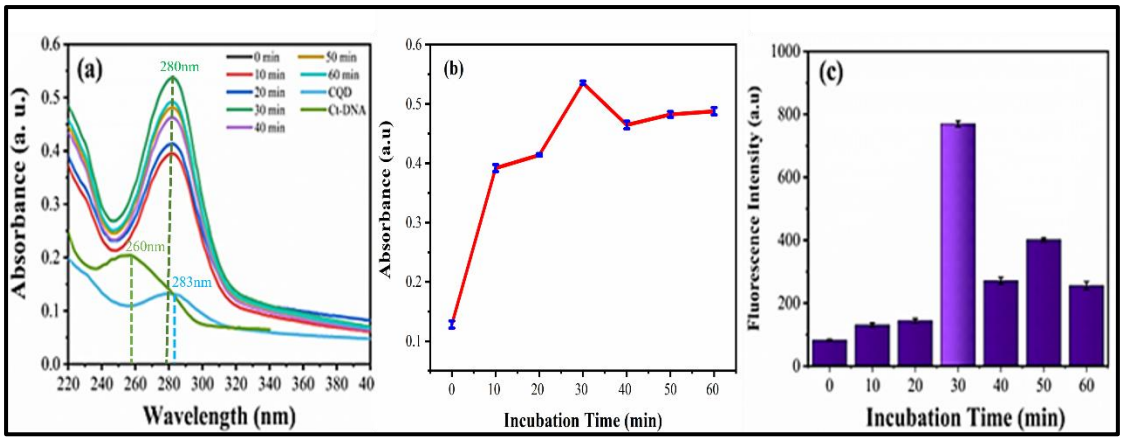

Figure 4.3: (a) UV-Vis absorbance spectra of PLLCQD-Ct-DNA conjugate at different time intervals, (b) Change in absorbance of PLLCQD-Ct-DNA conjugate at different incubation times (0-60 min), and (c) Change in fluorescence intensity of PLLCQD-Ct-DNA conjugate at different incubation time (0-60 min).

When PLLCQDs are incubated with Ct-DNA, it was observed that no conjugate formation was observed. After 10 minutes, the absorption intensity began to increases. At the 30-minute, the absorption intensity reaches its maximum, likely due to electrostatic interactions between Ct-DNA and PLLCQDs. Beyond 30 minutes, the absorption intensity declines.

To further validate conjugation, fluorescence spectra were analyzed. The fluorescence intensity of the conjugate increased at a reaction time of 30 minutes (Figure 4.3 c). These findings suggest that an incubation time of 30 minutes is optimal for PLLCQD-Ct-DNA conjugate formation.

4.3.2.3 Effect of pH on the synthesis of PLLCQD-Ct-DNA conjugate:

The synthesis of PLLCQD-Ct-DNA conjugate and its stabilization depend significantly on the reaction pH. This study investigated the effect of pH on the PLLCQD-Ct-DNA conjugate within the range of 2–10 using HCl and NaOH. As shown in figure 4.4 (a, b) no peak is observed at acidic pH. At pH 8 conjugate shows maximum absorption intensity compared to PLLCQDs and Ct-DNA. Further increase in pH results in a lower absorption intensity compared to pH 8. Likewise, the fluorescence spectra show an increase in the intensity of conjugate at pH 8 (Figure 4.4 c). Thus, from this study, it is observed that pH 8 was optimum for synthesizing PLLCQD-Ct-DNA conjugate.

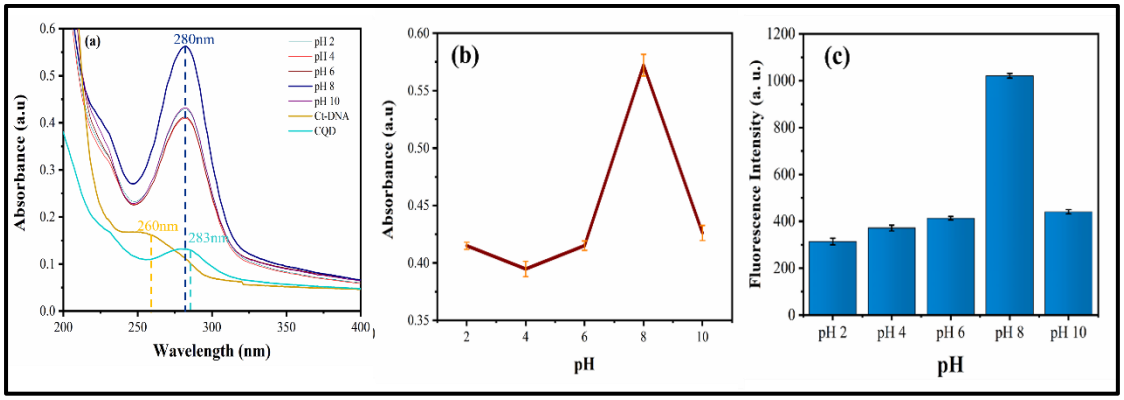

Figure 4.4: (a) UV-Vis absorbance spectra of PLLCQD-Ct-DNA conjugate at different pH (2-10), (b) Change in absorbance of PLLCQD-Ct-DNA conjugate at different pH (2-10), and (c) Change in fluorescence intensity of PLLCQD-Ct-DNA conjugate at different pH (2-10).

4.3.3 Characterization of PLLCQD-Ct-DNA conjugate:

4.3.3.1 UV-Vis Spectroscopy:

The formation of the PLLCQD-Ct-DNA conjugate was confirmed by observing changes in the absorption peak. The hyperchromic and hypochromic effects, primarily caused by alterations in the double-helical structure of DNA, play a key role in conjugate formation. Hyperchromism occurs due to the disruption of the DNA duplex secondary structure, while hypochromism results from the stabilization of the DNA duplex through electrostatic interactions with small molecules or intercalation binding mechanisms [11].

The conjugate is formed through electrostatic interactions between negatively charged Ct-DNA and positively charged PLLCQDs. In this study, a fixed concentration of PLLCQDs was used, with varying concentrations of Ct-DNA. Changes in the UV-Vis absorption spectra were recorded. A rise in the absorption spectra indicates an increase in the size of the PLLCQD-Ct-DNA conjugate.

Figure 4.5 presents the UV-Vis spectra, demonstrating the successful formation of the PLLCQD-Ct-DNA conjugate under optimized conditions: a Ct-DNA concentration of 20 µg/mL, an incubation time of 30 minutes, and a pH of 8.

Based on the absorbance spectra shown in Figure 4.5, the observed red shift (shift toward longer wavelengths) when comparing PLLCQD, PLLCQD-Ct-DNA conjugate, and Ct-DNA samples can be explained by several factors.

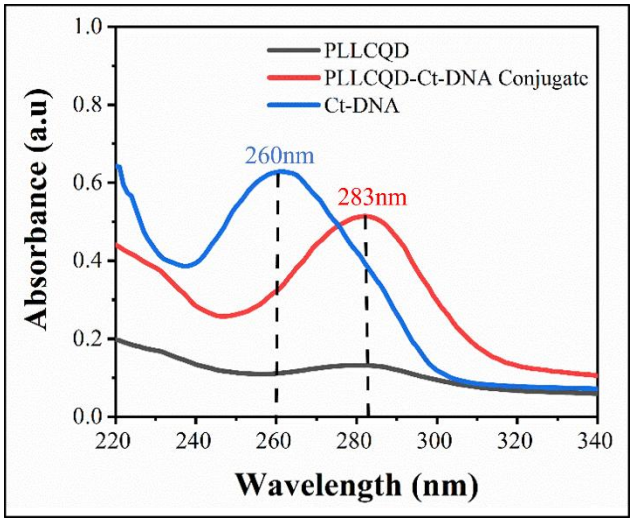

Figure 4.5: UV-Vis absorption spectra of PLLCQD-Ct-DNA conjugate showing a red shift in comparison to PLLCQD and Ct-DNA absorption peak.

Firstly, the PLLCQD-Ct-DNA conjugate exhibits a red shift compared to Ct-DNA alone due to increased conjugation upon PLLCQD binding to Ct-DNA. This interaction lowers the energy gap between electronic states, leading to absorption at longer wavelengths. Secondly, the interaction between PLLCQD and Ct-DNA may alter solvent interactions, stabilizing either the ground or excited states differently, which contributes to the red shift. Thirdly, the presence of PLLCQD may influence electron distribution in Ct-DNA. Specific substituents in PLLCQD can donate or withdraw electrons, modifying the energy levels of Ct-DNA and resulting in a red shift.

Lastly, the binding of PLLCQD to Ct-DNA can induce structural changes, such as alterations in planarity or bond lengths, further contributing to the red shift in the absorption spectra. In summary, the red shift observed in the PLLCQD-Ct-DNA conjugate, compared to Ct-DNA alone, is likely due to increased conjugation, solvent effects, electronic interactions, and structural modifications induced by PLLCQD binding.

4.3.3.2 Fluorescence Spectroscopy:

Fluorescence spectroscopy is a widely used method for examining the interaction between nanoparticles and Ct-DNA. A gradual increase in fluorescence intensity is observed with the increasing Ct-DNA concentration while maintaining a constant PLLCQD concentration. A detailed analysis of Figure 4.6 suggests that at excitation wavelength of 375 nm, a characteristic fluorescence signal of the PLLCQD-Ct-DNA conjugate appears at 463 nm. The addition of Ct-DNA to the PLLCQD-Ct-DNA conjugate further enhanced its fluorescence intensity [12].

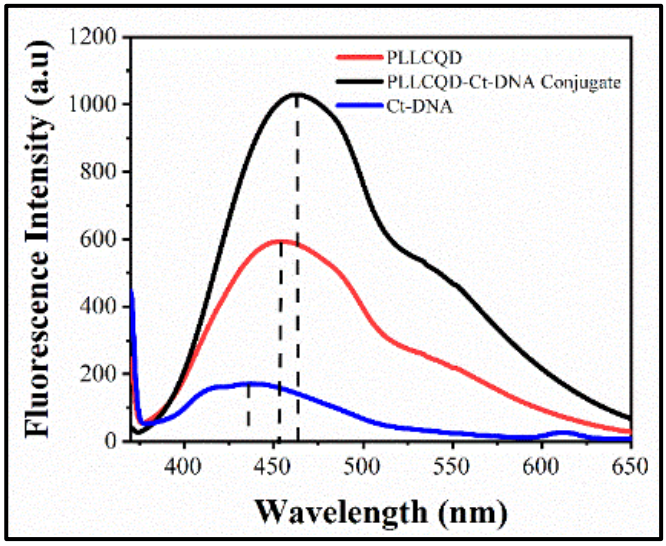

Figure 4.6: Fluorescence spectra of PLLCQD-Ct-DNA conjugate in comparison to PLLCQD and Ct-DNA at 375 nm excitation wavelength.

4.3.3.3 Zeta Potential:

Zeta potential analysis is used to evaluate the surface charge of nanoparticles, which indicates their stability. The PLLCQD-Ct-DNA conjugate was characterized

using zeta potential measurements, as shown in Figure 4.7, which presents the zeta potential values of PLLCQD, Ct-DNA, and the PLLCQD-Ct-DNA conjugate.

The formation of the PLLCQD-Ct-DNA conjugate was confirmed by comparing its zeta potential to that of PLLCQD and Ct-DNA alone. Ct-DNA exhibits a negative charge with a zeta potential of -23.16 mV, while PLLCQD shows a positive charge with a zeta potential of +18.03 mV. The PLLCQD-Ct-DNA conjugate displays a zeta potential of +8.27 mV, indicating successful binding via electrostatic interactions as shown in figure 4.7.

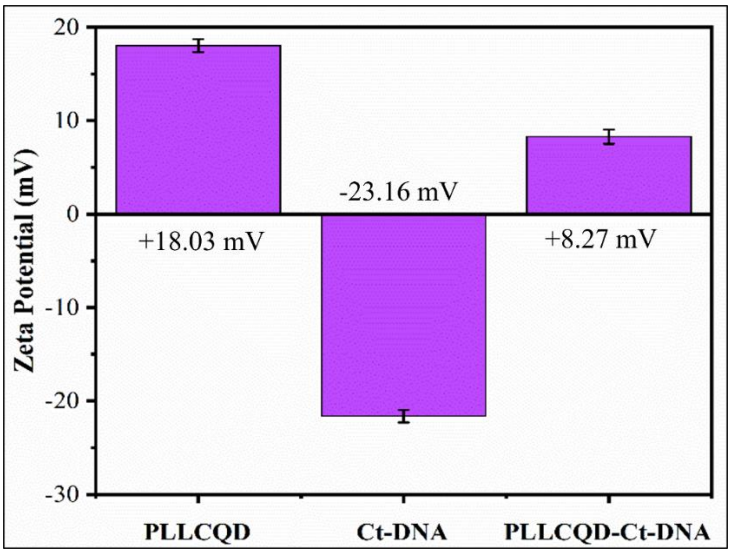

Figure 4.7: Zeta potentials (a) PLLCQD, (b) Ct-DNA, and (c) PLLCQD-Ct-DNA conjugate.

4.3.3.4 Electrophoretic mobility shift assay (EMSA):

To investigate the potential of PLLCQD and PLLCQD-Ct-DNA conjugate as an efficient transfection carrier by confirming the formation of PLLCQD-Ct-DNA conjugate which is a precondition for efficient cellular uptake, electrophoretic mobility shift assay was conducted. Electrophoretic mobility shift assay is referred to as band shift assay, gel shift assay, or gel mobility shift assay. This study was conducted by varying weight ratios of CQDs. The Ct-DNA migration gradually decreases with an increase in weight ratios (PLLCQDs: Ct-DNA), and at ratio equal to or greater than 40:1 (lane 6 and 7), there no DNA migration is observed (Figure. 4.8). A bright band that indicates the location of the DNA. The pure PLLCQDs shows a reversed

electrophoretic mobility (lane 8), which verifies the positive surface charge on the CQDs.

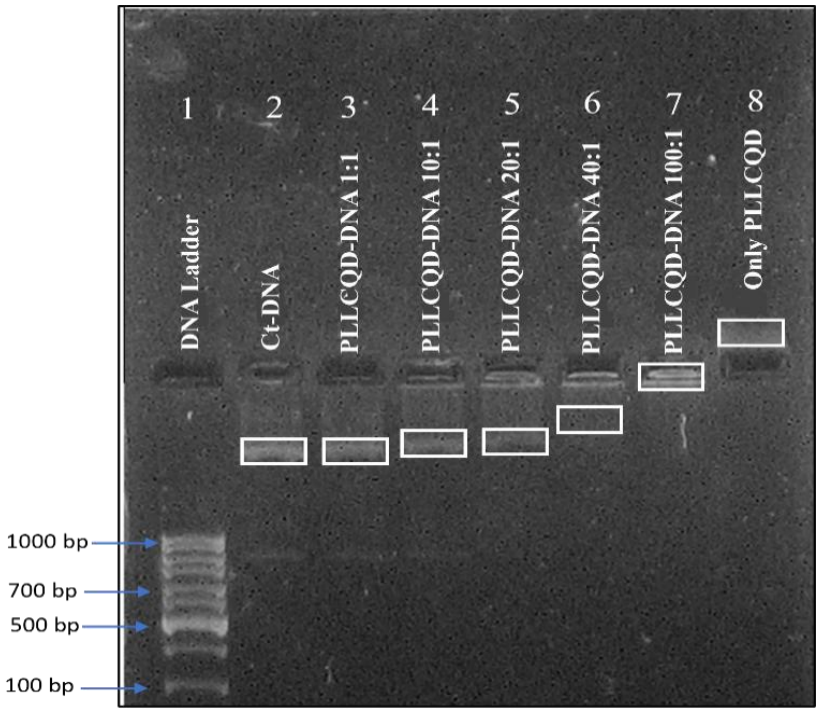

Figure 4.8: Electrophoretic mobility shift assay of conjugate. DNA ladder (lane 1), 20 µg/ml Ct-DNA (lane 2), Ct-DNA was kept constant in lanes 3-7=20 µg/ml at different PLLCQD 1, 10, 20, 40, 100 weight ratio. Lane 8 is only PLLCQDs.

The point of electroneutrality shows complete condensation of Ct-DNA by PLLCQDs resulting in the electroneutral complex. The Ct-DNA compaction by the PLLCQDs has a strong influence on electrophoretic mobility within the gel. As shown in Figure 4.8, PLLCQD-Ct-DNA conjugate band has been completely retarded and 100% binding at the lowest ratio (lane 6).

4.4 Conclusions:

This chapter concludes with the successful synthesis of the PLLCQD-Ct-DNA conjugate through parameter optimization. Standard Ct-DNA was used for conjugate preparation, with key optimization factors including Ct-DNA concentration, incubation time, and pH. The optimal conditions for conjugate formation were determined to be 20 µg/mL Ct-DNA concentration, 30 minutes of incubation, and pH 8. The change in absorbance confirmed the successful formation of the PLLCQD-Ct-DNA conjugate,

which was driven by electrostatic interactions between the negatively charged Ct-DNA and positively charged PLLCQDs.

The PLLCQD-Ct-DNA conjugate was further characterized using UV-Vis spectroscopy, fluorescence spectroscopy, and zeta potential analysis. The fluorescence intensity of the conjugate was significantly enhanced compared to bare PLLCQDs and Ct-DNA, confirming conjugate formation. A change in zeta potential also validated the successful conjugation, with the final conjugate exhibiting a zeta potential of +8.27 mV. Additionally, an electrophoretic mobility shift assay was conducted to assess the electroneutrality of the PLLCQD-Ct-DNA conjugate. The conjugate displayed reduced mobility during electrophoresis at a 100:1 PLLCQD:Ct-DNA ratio, likely due to the interaction between PLLCQDs and Ct-DNA.

In conclusion, the study demonstrates that negatively charged Ct-DNA and positively charged PLLCQDs successfully form a conjugate through electrostatic interactions. This PLLCQD-Ct-DNA conjugate was subsequently utilized for transfection studies.

4.5 References:

1. Josephson L., Perez J. M., Weissleder R., Magnetic nanosensors for the detection of oligonucleotide sequences. Angewandte Chemie. 113 (17) (2001) 3304-3306, DOI-0044-8249/01/11317-3304.

2. Rosi N. L., Mirkin C. A., Nanostructures in biodiagnostics. Chemical reviews. 105 (4) (2005) 1547-1562, DOI-10.1021/cr030067f.

3. Kumar P., Gorai S., Santra M. K., Mondal B., Manna D., DNA binding, nuclease activity and cytotoxicity studies of Cu (II) complexes of tridentate ligands. Dalton Transactions. 41 (25) (2012) 7573-7581, DOI-10.1039/C2DT30232B.

4. Arjmand F., Parveen S., Afzal M., Shahid M., Synthesis, characterization, biological studies (DNA binding, cleavage, antibacterial and topoisomerase I) and molecular docking of copper (II) benzimidazole complexes. Journal of Photochemistry and Photobiology B: Biology. 114 (1) (2012) 15-26, DOI-10.1016/j.jphotobiol.2012.05.003.

5. Sathyadevi P., Krishnamoorthy P., Jayanthi E., Butorac R. R., Cowley A. H., Dharmaraj N., Studies on the effect of metal ions of hydrazone complexes on interaction with nucleic acids, bovine serum albumin and antioxidant properties. Inorganica Chimica Acta. 384 (1) (2012) 83-96, DOI-10.1016/j.ica.2011.11.033.

6. Kathiravan A., Renganathan R., Photoinduced interactions between colloidal TiO_2 nanoparticles and calf thymus-DNA. Polyhedron. 28 (7) (2009) 1374-1378, DOI-10.1016/j.poly.2009.02.040.

7. Ouyang X., Liu J., Li J., Yang R., A carbon nanoparticle-based low-background biosensing platform for sensitive and label-free fluorescent assay of DNA methylation. Chemical Communications. 48 (1) (2012) 88-90, DOI-10.1039/C1CC15511C.

8. Loo A. H., Sofer Z., Bouša D., Ulbrich P., Bonanni A., Pumera M., Carboxylic carbon quantum dots as a fluorescent sensing platform for DNA detection. ACS applied materials & interfaces. 8 (3) (2016) 1951-1957, DOI-10.1021/acsami.5b10160.

9. Milosavljevic V., Nguyen H. V., Michalek P., Moulick A., Kopel P., Kizek R., Adam V., Synthesis of carbon quantum dots for DNA labeling and its electrochemical, fluorescent and electrophoretic characterization. Chemical Papers. 69 (1) (2015) 192-201, DOI-10.2478/s11696-014-0590-2.

10. Sun H., Ren J., Qu X., Carbon nanomaterials and DNA: From molecular recognition to applications. Accounts of Chemical Research. 49 (3) (2016) 461-470, DOI-10.1021/acs.accounts.5b00515.

11. Liang C. Y., Xia W., Yang C. Z., Liu Y. C., Bai A. M., Hu Y. J., Exploring the binding of carbon dots to calf thymus DNA: from green synthesis to fluorescent molecular probe. Carbon. 130 (1) (2018) 257-266, DOI-10.1016/j.carbon.2018.01.009.

12. Hu Z., Tong C., Synchronous fluorescence determination of DNA based on the interaction between methylene blue and DNA. Analytica chimica acta. 587 (2) (2007) 187-193, DOI-10.1016/j.aca.2007.01.050.

CHAPTER V

SURFACE FUNCTIONALIZED CARBON QUANTUM DOT-NUCLEIC ACID CONJUGATE FOR *IN-VITRO* BIOIMAGING APPLICATIONS

5.1 Introduction:

CQDs offer several advantages over other semiconductor nanoparticles and organic dyes, including exceptional optical stability, minimal cytotoxicity, strong chemical inertness, high fluorescence, and excellent biocompatibility [1-6]. In particular, CQDs are of great interest in optical imaging, a routine method for investigating complex structures in organisms in real time, due to their unique biocompatibility, excellent resolution, and long-term detection capabilities [7-9].

Cell imaging plays a crucial role in drug development and discovery processes. Live-cell fluorescence imaging enables selective staining of various cell types and cells at different stages of differentiation, revealing intricate details about cellular mechanisms and functions [10].

Intracellular imaging involves introducing external materials into living cells to visualize intracellular processes. This technique allows researchers to image and detect molecules within cells, including RNA, DNA, metal ions, metabolites, proteins, and nanoparticles. Intracellular imaging is valuable for advancing bioimaging, detecting intracellular biomolecules, and monitoring cellular levels, locations, and cell-to-cell variations [11].

Several chemical families fall under the category of non-protein organic fluorophores, including cyanine derivatives, squaraine derivatives, and xanthene derivatives (such as fluorescein and rhodamine). Most organic fluorophores, including fluorescein, Alexa Fluor, and BODIPYs, are commercially available and have found extensive applications in various fields of life sciences. Due to their low molecular weight and compact size, organic fluorophores are easily absorbed into cells, making them a popular choice for a wide range of *in vitro* and *in vivo* cell research [12].

However, these small organic compounds have inherent disadvantages that severely restrict their applications in situations requiring exceptional PL properties. Most organic fluorophores have a narrow absorption spectrum, limiting their use to a specific range of light types. Additionally, their lack of a clear, symmetric emission peak can lead to signal overlaps, restricting their effectiveness in multicolor imaging.

Furthermore, the inherently modest Stokes shift of organic fluorophores can result in scattered light interference and unwanted excitation, significantly reducing sensitivity. Long-term imaging studies are also challenging because most organic fluorophores suffer from photobleaching and unstable PL behavior due to environmental changes. In addition to these PL-related limitations, organic fluorophores often exhibit poor solubility in biological media, further hindering their applications [13].

To address emerging imaging challenges, there is a continuous need to develop novel imaging methodologies and enhance the performance of existing diagnostic assays. The use of nanoparticles has the potential to elevate *in vitro* diagnostics to a new level of performance.

5.2 Experimental details:

5.2.1 Materials:

Dulbecco's Modified Eagle's Medium (DMEM; catalog no. A294A, Himedia, Mumbai, India), fetal bovine serum (FBS; catalog no. A5669401, ThermoFisher Scientific, USA), and 0.25% trypsin-EDTA (catalog no. TCL006, Himedia, Mumbai, India) were purchased. The human embryonic kidney cell line (HEK-293) was obtained from the National Centre for Cell Science (NCCS), India. The HEK-293 cells were cultured in DMEM supplemented with 10% FBS, 100 µg/mL penicillin, and 100 µg/mL streptomycin in a humidified incubator at 37°C with 5% CO_2.

5.2.2 Characterization of PLLCQD-Ct-DNA conjugate:

Fluorescent measurements were performed with FP-8300 Spectrofluorometer. UV-Vis spectroscopy was carried out with Agilent Cary 60 UV–Vis spectrophotometer. Surface morphology analyses were carried out using FEI TECNAI G2-20 TWIN transmission electron microscopy.

5.2.3 Measurement of quantum yield (QY):

The QY is calculated using the slope of the line determined from the plot of the absorbance against the integrated fluorescence intensity as a comparative method. The QY can be calculated using the following equation 3.1 (refer chapter 3).

5.2.4 Cell culture:

The HEK-293 cells were cultured in DMEM supplemented with 10% FBS and 100 µg/mL penicillin-streptomycin. The cells were maintained at 37ºC in a humidified incubator with 5% CO_2 to provide optimal conditions for growth and proliferation. FBS supplies essential growth factors, while penicillin-streptomycin prevents bacterial contamination during cell culture. The humidified atmosphere maintains proper moisture levels, supporting cellular health.

5.2.5 Cell viability assay:

The MTT [3-(4,5-Dimethylthiazol-2-yl)-2,5-Diphenyltetrazolium Bromide] cytotoxicity assay was performed on HEK-293 cells. The HEK-293 cells were cultured on 8-well Nunc Lab-Tek Chambered cover glass in DMEM medium at a density of 4×10^5 cells per well. The cells were allowed to adhere overnight before the medium was replaced with 200 µl of PLLCQDs and PLLCQD-Ct-DNA conjugate. After incubation for 48 hours, the absorbance of the samples was measured at 450 nm using a nanodrop microplate reader. The data obtained from the assays were expressed as the mean percentage ± standard error of measurement and were compared to the optical density values of untreated cells. The experiments were performed in triplicate [14].

5.2.6 *In-vitro* Ct-DNA uptake study:

The DNA uptake by cells can be determined by calculating the binding constants and binding efficiency. Binding constants quantify the strength of the interaction between two molecules, such as a DNA-binding agent (i.e., PLLCQDs) and DNA. These constants are typically derived from spectroscopic or titration data by analyzing changes in measurable properties such as absorbance, fluorescence, or circular dichroism. A higher binding constant often indicates stronger interactions, which can enhance the ability of the binding agent to facilitate DNA uptake into cells.

The absorption spectra of the PLLCQD-Ct-DNA conjugate were recorded at different time intervals. Ct-DNA internalization and the corresponding binding constants were calculated to study Ct-DNA uptake using a molar extinction coefficient of 66,000 M^{-1} at A_{260} nm, and the DNA concentration was determined. Aliquots of the DNA solution were internalized into the cells, and the corresponding absorption spectra

were recorded at various time intervals (0, 12, 24, and 48 hours). The intrinsic binding constant was calculated using equation 5.1 [15].

$$\frac{[DNA]}{(\varepsilon_a - \varepsilon_b)} = \frac{[DNA]}{(\varepsilon_{b-} \varepsilon_{f)}} + \frac{1}{K_b\ (\varepsilon_b - \varepsilon_a)} \quad \ldots\ldots \quad \text{(eq. 5.1)}$$

where, [DNA] = concentration of Ct-DNA,

ε_a = Apparent molar extinction coefficient of the cells

ε_b = the molar extinction coefficient of the cells + internalized Ct-DNA

ε_f = the molar extinction coefficient of the internalized Ct-DNA

5.3 Results and Discussion:

5.3.1 Transmission Electron Microscopy (TEM):

Figure 5.1(a) illustrates the TEM of PLLCQD-Ct-DNA conjugate structure, while the particle size distribution histogram in Figure 5.1(b) indicates that PLLCQD-Ct-DNA conjugates range in size from 7-8 nm.

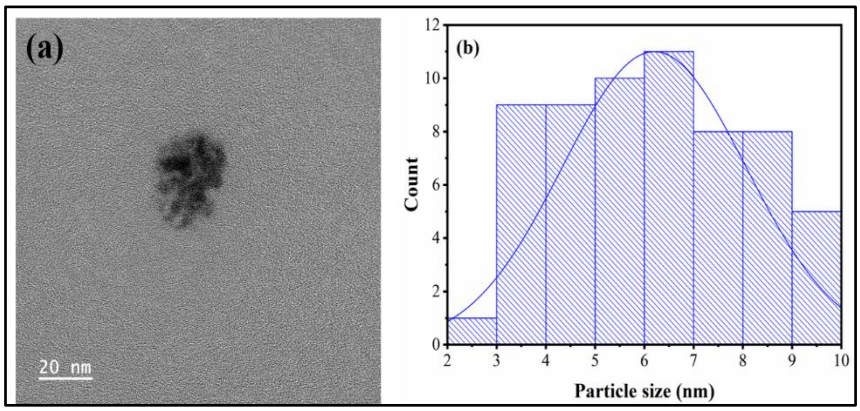

Figure 5.1: (a) TEM characterization and (b) particle size histogram of PLLCQD-Ct-DNA conjugate.

5.3.2 Cell viability assay:

Figure 5.2 (a) illustrates the relationship between cell viability and the concentration of compounds (PLLCQD-Ct-DNA and PLLCQD) used in the study. It shows the viability of HEK-293 cells treated with PLLCQDs and the PLLCQD-Ct-DNA conjugate. PLLCQD-treated cells exhibited notable cell viability compared to the control group. Cell viability is observed for 100–600 µg/mL concentration range. On

the other hand, the PLLCQD-Ct-DNA conjugate shows cell viability up to concentration of 600 µg/mL, as shown in Figure 5.2 (a). Based on these findings, a concentration of 600 µg/mL of PLLCQD-Ct-DNA conjugate has been selected for further experimentation.

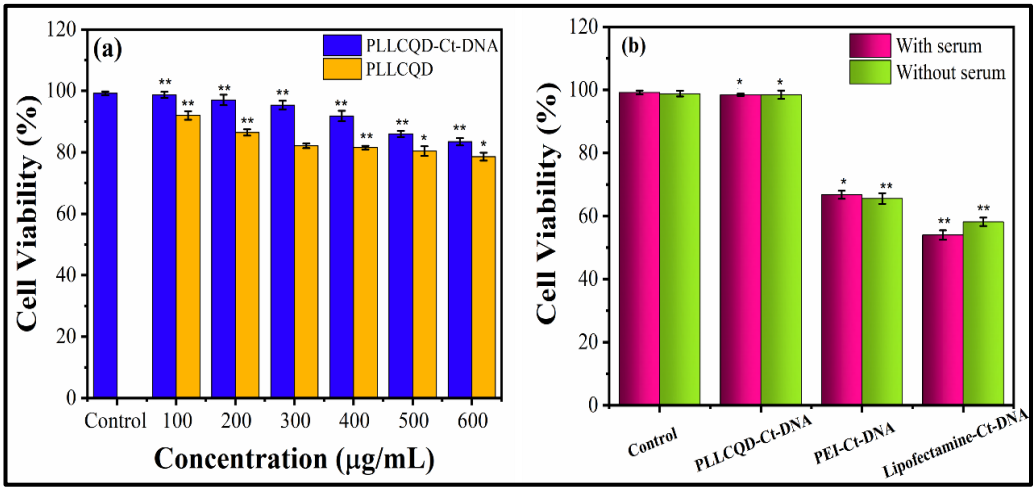

Figure 5.2: (a) Cytotoxicity of PLLCQD and PLLCQD-Ct-DNA conjugate, and (b) Percentage of viable cells after treated with PEI and Lipofectamine 2000 after transfection. The significance levels are indicated by asterisks: *p < 0.01 and **p < 0.05.

For comparison, other groups, including polyethyleneimine (25 kDa PEI) and Lipofectamine 2000, were also evaluated for cell viability after transfection with the same Ct-DNA concentration (Figure 5.2 b). A higher amine content enhances buffering capacity, facilitating DNA release from endosomes into the cytoplasm [16]. Notably, the study revealed that the PLLCQD-Ct-DNA conjugate successfully delivered genes to cells in both serum-free and serum-containing media. In contrast, Lipofectamine 2000 demonstrated significantly reduced delivery efficiency in the presence of serum. This reduction was anticipated due to the formation of a protein corona on the surface of PLLCQDs, leading to receptor-mediated endocytosis of PLLCQD-Ct-DNA conjugate [17].

In this study, PEI-25 kDa was recognized as a highly effective gene transfection agent, albeit with cytotoxic effects. Conversely, PLL is known for its superior biocompatibility. The cytotoxicity of the PLLCQD-Ct-DNA conjugate was assessed using an MTT cell viability assay following transfection. The data in figure 5.2(b)

indicate that the PLLCQD-Ct-DNA conjugate exhibits significantly lower cytotoxicity compared to the control groups, highlighting its enhanced biocompatibility. Consequently, the study observes a marked downregulation of Lipofectamine 2000, likely due to its toxicity.

A two-sample t-test was performed to compare the mean cell viability between the PLLCQD-Ct-DNA, PLLCQD treatment, and control groups. The results indicated a significant difference in cell viability between the groups ($p < 0.05$ and $p < 0.01$), suggesting that the treatment had a notable effect.

5.3.3 Intracellular Ct-DNA uptake:

The binding constants are related to DNA uptake by analyzing the absorption spectra over time. The intrinsic binding constant (K_b) provides valuable information about the affinity between PLLCQD and Ct-DNA, helping to quantify the efficiency of DNA uptake by the cells.

The absorption spectra of the PLLCQD-Ct-DNA conjugate were measured at different time intervals: 0, 12, 24, and 48 hours and the results were analyzed. Using the molar extinction coefficient of Ct-DNA (66,000 M^{-1} cm^{-1} at A_{260} nm), the concentration of Ct-DNA ([DNA]) in each sample was calculated at these time points.

The apparent molar extinction coefficient of the cells (ε_a) was calculated at each time point using equation 5.1. Subsequently, the molar extinction coefficient of the cells with internalized Ct-DNA (ε_b) was determined for each time point. The known molar extinction coefficient of the internalized Ct-DNA (ε_f), was constant throughout the experiment. For each time interval, the values of $[DNA]/(\varepsilon_a - \varepsilon_b)$ were calculated. Additionally, the values of $[DNA]/(\varepsilon_b - \varepsilon_f)$ were determined for each time interval. These calculations were performed to facilitate plotting and analysis.

Table 5.1 presents data related to the absorption spectra and the calculated values for the PLLCQD-Ct-DNA conjugate at different time intervals. The analysis of the absorption spectra over time for the PLLCQD-Ct-DNA conjugate demonstrates a linear relationship between the calculated values based on the provided equation. Table 5.2 summarizes the calculated values of $[DNA]/(\varepsilon_b - \varepsilon_f)$ and $[DNA]/(\varepsilon_a - \varepsilon_b)$.

Table 5.1: Calculated values for PLLCQD-Ct-DNA conjugate at different time intervals.

Time (h)	[DNA] (M)	ε_a M^{-1} cm^{-1}	ε_b M^{-1} cm^{-1}	ε_f M^{-1} cm^{-1}
0	1.08×10^{-5}	62000	64000	66000
12	0.93×10^{-5}	62200	64200	66000
24	0.56×10^{-5}	62400	64400	66000
48	0.19×10^{-5}	62600	64600	66000

The required values for plotting were calculated for each time interval. First, the values of [DNA]/($\varepsilon_a-\varepsilon_b$) were computed, followed by the calculation of [DNA]/($\varepsilon_b-\varepsilon_f$). These calculations allowed for the creation of a plot where the X-axis represented [DNA]/($\varepsilon_b-\varepsilon_f$) and the Y-axis represented [DNA]/($\varepsilon_a-\varepsilon_b$). The data were then plotted to visualize the relationship between these parameters over the different time intervals (Figure 5.3).

Table 5.2: Calculated values [DNA]/($\varepsilon_b-\varepsilon_f$) and [DNA]/($\varepsilon_a-\varepsilon_b$) for binding constant analysis.

Time (h)	[DNA]/($\varepsilon_b-\varepsilon_f$)	[DNA]/($\varepsilon_a-\varepsilon_b$)
0	-5.4×10^{-9}	-5.4×10^{-9}
12	-5.16×10^{-9}	-4.6×10^{-9}
24	-3.5×10^{-9}	$-2.8\times10_{-9}$
48	-1.35×10^{-9}	-9.5×10^{-10}

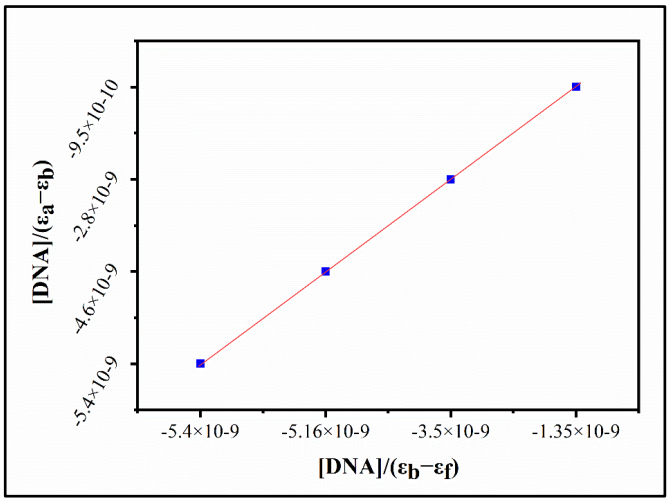

Figure 5.3: Time-dependent absorption spectra analysis of PLLCQD-Ct-DNA conjugate: Relationship between [DNA]/($\varepsilon_a-\varepsilon_b$) and [DNA]/($\varepsilon_b$ - ε_f).

The interpretation of figure 5.3 and the corresponding calculations demonstrate that the binding constant can be accurately determined using the provided equation and data. The observed linear relationship confirms that the binding interactions between PLLCQD and Ct-DNA remain consistent over time, allowing for an efficient analysis of Ct-DNA uptake and binding properties.

Cellular uptake assays are essential for quantifying the entry of labeled substances into cells or assessing the efficacy of unlabeled compounds in inhibiting this process. These assays provide crucial insights into the transport and internalization of compounds and are instrumental in evaluating the potential of test compounds. Labeled substances can include neurotransmitters, metabolites, drugs, or proteins.

Absorption spectral analysis was performed to quantify the internalization of Ct-DNA into HEK-293 cells. The uptake of the PLLCQD-Ct-DNA conjugate into cells was observed through incremental absorption by the cells at a fixed Ct-DNA concentration. The internalization of Ct-DNA was verified by calculating the absorption ratio at A_{260}/A_{280} nm (Figure 5.4 a).

Figure 5.4 (a) presents the fluorescence intensity for three different samples: PLLCQD-Ct-DNA (blue), PEI-Ct-DNA (orange), and Lipofectamine-Ct-DNA (green). Fluorescence intensity was measured at three different time intervals: 12, 24, and 48 hours. Relative fluorescence spectral analysis indicates that the CQD-Ct-DNA conjugate exhibited greater uptake efficiency than PEI and Lipofectamine. After 12 hours, the fluorescence intensity increases compared to the positive controls, including PEI (25 kDa) and Lipofectamine 2000. The findings demonstrate that CQDs exhibits significantly greater uptake efficiency than standard transfection agents PEI-25K and Lipofectamine 2000.

Figure 5.4 (b) illustrates the absorbance under two different conditions: PLLCQD-Ct-DNA concentration (green) and cell DNA concentration (purple). Absorbance was measured at three time intervals: 12, 24, and 48 hours. The results indicate that Ct-DNA was transfected into cells with an efficiency of up to 90%. This novel finding suggests that PLLCQDs can serve as an alternative to conventional transfection agents while maintaining biocompatibility. The remarkable transfection efficiency of PLLCQDs is likely attributed to their strong Ct-DNA condensation ability,

which protects them from enzymatic degradation during transfection. Additionally, their small size and positive surface charge contribute to their high transfection efficiency [17, 18].

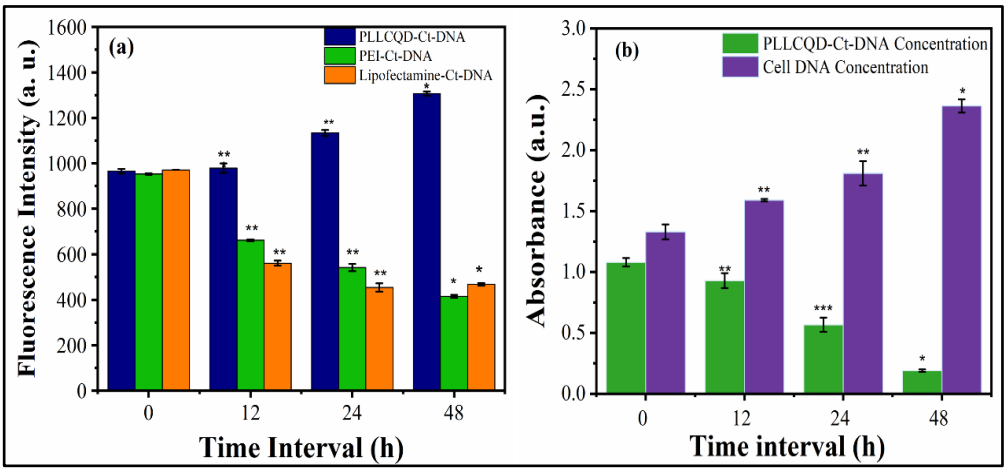

Figure 5.4: Time dependent analysis of PLLCQD-Ct-DNA (a) Fluorescence intensity for PLLCQD-Ct-DNA, PEI-Ct-DNA, and Lipofectamine-Ct-DNA over 0, 12, 24, and 48 hours, and (b) Absorbance of PLLCQD-Ct-DNA and Cell DNA concentration at the same intervals. The significance levels are indicated by asterisks: *p < 0.01 and **p < 0.05.

A series of ANOVA tests were conducted to assess DNA internalization efficiency in cells using fluorescence intensity and absorbance measurements across different methods and concentrations. For fluorescence intensity, results shows a significant difference between methods (PLLCQD-DNA, PEI-CQD-DNA, Lipofectamine-DNA) over time intervals ($p < 0.05$), indicating method-dependent variation in internalization efficiency. For absorbance, results indicates a significant difference between groups (CQD-Ct-DNA Concentration, Cell DNA Concentration) over time ($p < 0.05$), suggesting concentration-dependent differences. These findings underscore the critical roles of both method and concentration in optimizing DNA internalization, as reflected by significant variations in both fluorescence intensity and absorbance metrics.

5.3.4 Intracellular bioimaging:

The fluorescence enhancement of the PLLCQD-Ct-DNA conjugate is governed by the extent of complex formation and its subsequent dissociation within the

intracellular environment. To explore its potential applicability in intracellular trafficking, cellular imaging experiments were conducted using three types of conjugates: PLLCQD-Ct-DNA, PEI-Ct-DNA, and Lipofectamine-Ct-DNA, on HEK-293 cells. The cellular uptake and localization of Ct-DNA were further analyzed using confocal microscopy.

The study reveal that cells treated with the PLLCQD-Ct-DNA conjugate exhibits significantly stronger fluorescence signal and higher fluorescence efficiency compared to cells treated with PEI-Ct-DNA and Lipofectamine-Ct-DNA conjugates. Notably, the PLLCQD conjugates demonstrate minimal background interference, with negligible autofluorescence post-transfection into HEK-293 cells. This highlights the superiority of PLLCQDs in enhancing fluorescence signals while minimizing nonspecific noise, making them excellent candidates for bioimaging applications.

Furthermore, the multicolor emission capability of the PLLCQD-Ct-DNA conjugate was demonstrated under various excitation conditions. Confocal imaging captured its fluorescence emission under bright-field illumination as well as laser excitations at 405 nm (blue), 473 nm (red), and 559 nm (green), as depicted in Figure 5.5. These findings underscore the utility of PLLCQDs as a promising tool for precise and efficient intracellular trafficking and imaging applications.

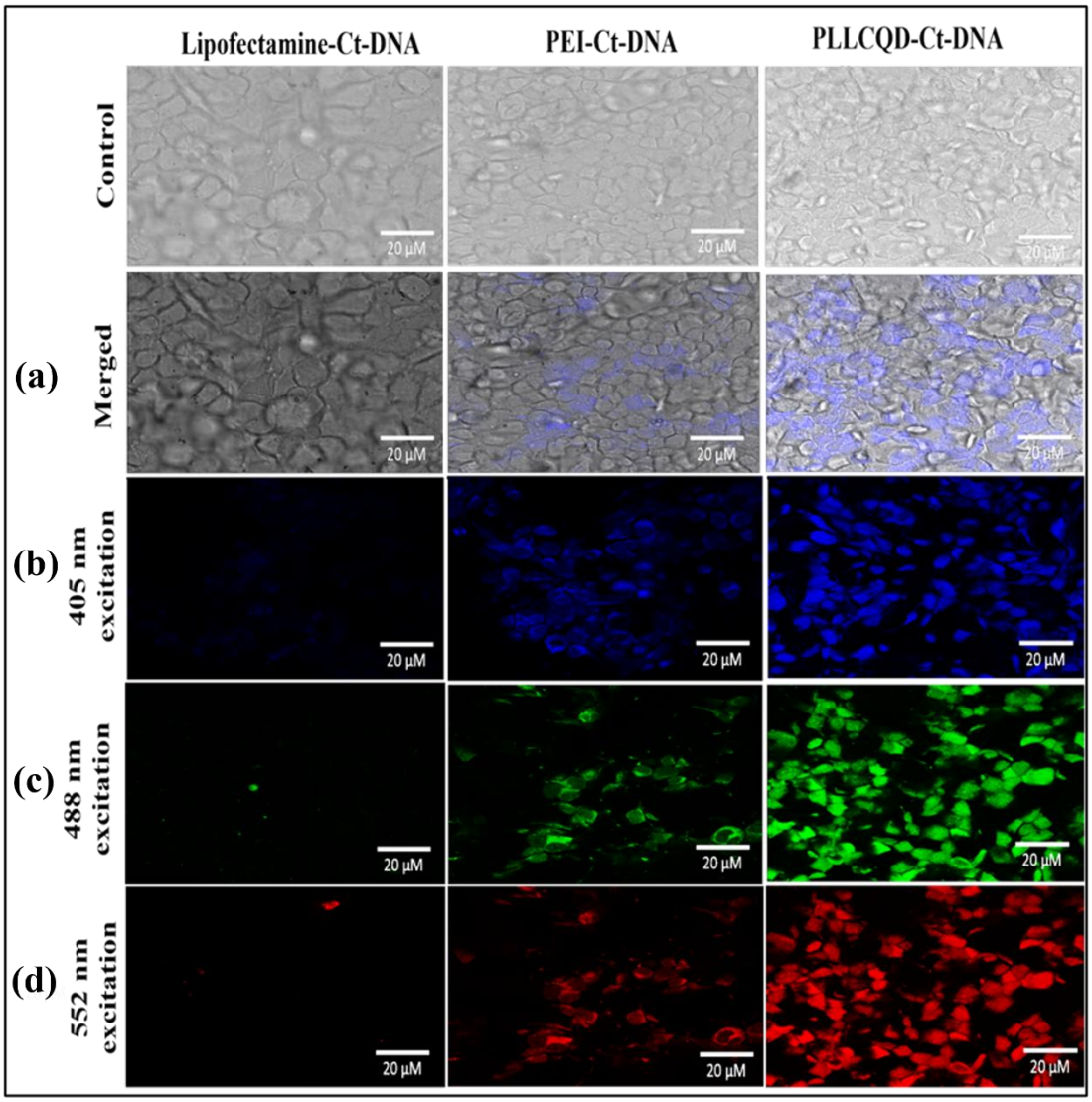

Figure 5.5: Confocal fluorescence microscopy images illustrating the intracellular transport of Lipofectamine-Ct-DNA, PEI-Ct-DNA, and PLLCQD-Ct-DNA conjugates in HEK-293 cells after 48 hours of treatment with a 600 µg/mL concentration. The PLLCQD-Ct-DNA conjugate exhibited distinct fluorescence signals under various excitation conditions: (a) bright-field image merged with fluorescence, (b) blue fluorescence at 405 nm excitation, (c) green fluorescence at 488 nm excitation, and (d) red fluorescence at 552 nm excitation.

5.4 Conclusions:

This chapter concludes the study on the internalization of the PLLCQD-Ct-DNA conjugate into human endothelial kidney (HEK-293) cells. The binding constant was determined, demonstrating the relationship between the binding interactions of

PLLCQDs and Ct-DNA, allowing for an efficient analysis of DNA uptake and binding properties.

The PLLCQD-Ct-DNA conjugate exhibited particle size of 7–8 nm. It also demonstrated good biocompatibility and showed potential functionality in HEK-293 cells. The cell viability results indicated that the PLLCQD-Ct-DNA conjugate maintained 100% cell viability up to a concentration of 600 µg/mL. Intracellular imaging results further confirmed that the PLLCQD-Ct-DNA conjugate achieved higher cellular uptake compared to PEI and Lipofectamine in HEK-293 cells. Notably, up to 90% of Ct-DNA internalization was achieved in HEK-293 cells after 48 hours of incubation with the PLLCQD-Ct-DNA conjugate.

Although the precise mechanism of CQD cellular uptake remains unclear, it is widely accepted that endocytosis is the primary route for CQD internalization in cells. In summary, the localization of the PLLCQD-Ct-DNA conjugate enables targeted intracellular delivery, making it a promising candidate for fluorescence imaging-based studies and diagnostic applications.

5.5 References:

1. Feng X., Zhao Y., Yan L., Zhang Y., He Y., Yang Y., Liu X., Low-temperature hydrothermal synthesis of green luminescent carbon quantum dots (CQD), and optical properties of blends of the CQD with poly (3-hexylthiophene). Journal of Electronic Materials. 44 (1) (2015) 3436-3443, DOI-10.1007/s11664-015-3893-3z.
2. Yuan T., Meng T., He P., Shi Y., Li Y., Li X., Fan L., Yang S., Carbon quantum dots: an emerging material for optoelectronic applications. Journal of Materials Chemistry C. 7 (23) (2019) 6820-6835, DOI-10.1039/C9TC01730E.
3. Molaei M. J., A review on nanostructured carbon quantum dots and their applications in biotechnology, sensors, and chemiluminescence. Talanta. 196 (1) (2019) 456-478, DOI-10.1016/j.talanta.2018.12.042.
4. Dimos K., Carbon quantum dots: surface passivation and functionalization. Current Organic Chemistry. 20 (6) (2016) 682-695, DOI-1875-5348/16.58.
5. Tungare K., Bhori M., Racherla K. S., Sawant S., Synthesis, characterization and biocompatibility studies of carbon quantum dots from Phoenix dactylifera. 3 Biotech. 10 (12) (2020) 540-553, DOI-10.1007/s13205-020-02518-5.
6. Khan A., Ezati P., Kim J. T., Rhim J. W., Biocompatible carbon quantum dots for intelligent sensing in food safety applications: Opportunities and sustainability. Materials Today Sustainability. 29 (1) (2022)100306-100315, DOI-10.1016/j.mtsust.2022.100306.
7. Montalti M., Cantelli A., Battistelli G., Nanodiamonds and silicon quantum dots: ultrastable and biocompatible luminescent nanoprobes for long-term bioimaging. Chemical Society Reviews. 44 (14) (2015) 4853-4921, DOI- 10.1039/C4CS00486H.
8. Molaei M. J., Carbon quantum dots and their biomedical and therapeutic applications: a review. RSC advances. 9 (12) (2019) 6460-6481, DOI-10.1039/C8RA08088G.
9. Whitlow J., Pacelli S., Paul A., Multifunctional nanodiamonds in regenerative medicine: Recent advances and future directions. Journal of Controlled Release. 261 (1) (2017) 62-86, DOI-10.1016/j.jconrel.2017.05.033.
10. Seynhaeve A. L., Ten Hagen T. L., Using in vitro live-cell imaging to explore chemotherapeutics delivered by lipid-based nanoparticles. Journal of Visualized Experiments. 1 (129) (2017) 55405-55409, DOI-10.3791/55405.

11. Sun Z., Nguyen T., McAuliffe K., You M., Intracellular imaging with genetically encoded RNA-based molecular sensors. Nanomaterials. 9 (2) (2019) 233-252, DOI-10.3390/nano9020233.

12. Gonçalves M. S., Fluorescent labeling of biomolecules with organic probes. Chemical reviews. 109 (1) (2009) 190-212, DOI-10.1021/cr0783840.

13. Alford R., Simpson H. M., Duberman J., Hill G. C., Ogawa M., Regino C., Kobayashi H., Choyke P. L., Toxicity of organic fluorophores used in molecular imaging: literature review. Molecular imaging. 8 (6) (2009) 7290-2009, DOI-10.2310/7290.2009.00031.

14. Goswami J., Barman H., Hazarika P., Manna P., Devi A., Saikia L., Biomass-derived phosphorous-doped carbon quantum dots (P-CQD): An excellent biocompatible material for in-vitro cell imaging. Inorganic Chemistry Communications. 162 (1) (2024) 112276-112291, DOI-10.1016/j.inoche.2024.112276.

15. John V. L., Joy F., Kollannoor A. J., Joseph K., Nair Y., Vinod T. P., Amine functionalized carbon quantum dots from paper precursors for selective binding and fluorescent labeling applications. Journal of Colloid and Interface Science. 617 (1) (2022) 730-744, DOI-10.1016/j.jcis.2022.03.070.

16. Hwang H. S., Hu J., Na K., Bae Y. H., Role of polymeric endosomolytic agents in gene transfection: A comparative study of poly (L-lysine) grafted with monomeric L-histidine analogue and poly (L-histidine). Biomacromolecules. 15 (10) (2014) 3577-86, DOI-10.1021/bm500843r.

17. Wang L., Wang X., Bhirde A., Cao J., Zeng Y., Huang X., Sun Y., Liu G., Chen X., Carbon dots based two-photon visible nanocarriers for safe and highly efficient delivery of siRNA and DNA. Advanced healthcare materials. 3 (8) (2014) 1203-1218, DOI-10.1002/adhm.201300611.

18. Biswal M. R., Bhatia S., Carbon dot nanoparticles: exploring the potential use for gene delivery in ophthalmic diseases. Nanomaterials. 11 (4) (2021) 935-949, DOI-10.3390/nano11040935.

CHAPTER VI

SUMMARY AND CONCLUSIONS

6.1 Summary:

This thesis explores the synthesis, functionalization, and application of CQDs conjugated with nucleic acids for advanced bioimaging applications. CQDs, known for their excellent photostability, biocompatibility, and tunable optical properties, were surface-functionalized to enhance their interactions with nucleic acids, enabling precise control over their biofunctional properties.

Objectives of the study included:

1. **Synthesis of Functionalized CQDs:**

   Stable and photoluminescent poly L lysine functionalized carbon quantum dots (PLLCQDs) were successfully synthesized, displaying blue fluorescence with a quantum yield of 19.35%. These PLLCQDs demonstrated stability for up to 128 hours. Spectroscopic and microscopic characterizations confirmed the synthesis, revealing the formation of 2-3 nm sized PLLCQDs.

2. **PLLCQD-Nucleic Acid (Ct-DNA) Conjugation:**

   The PLLCQD-Ct-DNA conjugate was successfully formed by optimizing conditions of 20 µg/ml Ct-DNA concentration, 30-minute time interval, and pH of 8. This conjugate was formed through electrostatic interactions. Characterization was carried out using UV-Vis spectroscopy, fluorescence spectroscopy, and zeta potential measurements. The fluorescence intensity of the conjugate increased when compared to bare PLLCQDs and Ct-DNA. The stability range of the PLLCQD-Ct-DNA conjugate was +8.27 mV. An increase in the size of the conjugate was observed compared to PLLCQDs. Furthermore, the electrophoretic mobility shift assay confirmed the electroneutrality of the PLLCQD-Ct-DNA conjugate.

3. **Bioimaging Applications:**

   The performance of PLLCQD-Ct-DNA conjugates in bioimaging was thoroughly evaluated using HEK-293 cells. This evaluation involved assessing the ability of the PLLCQD-Ct-DNA conjugates to effectively enter the cells and exhibit fluorescence for imaging application. The binding interaction between the PLLCQDs and the Ct-DNA was carefully analyzed, with a particular focus on

determining the binding constant, which provided insights into the strength and stability of the conjugation. This was done by conducting absorbance experiments, where the fluorescence of the conjugates was measured before and after their interaction with Ct-DNA, and the results were used to calculate the binding constant. The strong binding affinity between the PLLCQDs and Ct-DNA, as indicated by the binding constant, suggested a stable and efficient conjugation, ensuring that the conjugates remained intact during cellular uptake. Fluorescent imaging was performed on HEK-293 cells, demonstrating the successful internalization of the PLLCQD-Ct-DNA conjugate and their potential as effective bioimaging tools. These findings confirmed the conjugates capacity for precise cellular localization and visualization, supporting their application in advanced bioimaging and diagnostics.

6. Major conclusions:

- ✓ Surface functionalized carbon quantum dots (PLLCQDs) with an average size of 2-3 nm have been synthesized.
- ✓ These PLLCQDs are fluorescent in nature. Upon exposure to UV light, CQDs glow blue colour fluorescence.
- ✓ These PLLCQDs were conjugated to calf thymus DNA at 20 µg/ml Ct-DNA concentration, 30 min reaction time, and at 8 pH.
- ✓ PLLCQD-Ct-DNA conjugate possesses good biocompatibility and exhibited a potential function in HEK-293 cells.
- ✓ PLLCQD-Ct-DNA conjugate exhibited greater cellular uptake in HEK-293 cells compared to PEI and lipofectamine.
- ✓ Up to 90 % of Ct-DNA internalization in HEK-293 cells was done at 48 hours of incubation with PLLCQD-Ct-DNA conjugate.
- ✓ The PLLCQD-Ct-DNA conjugate was used for bioimaging of HEK-293 cells.

6.3 Future scope of work:

Future research faces an exciting challenge in further understanding the basic mechanisms and forces involved in PLLCQD-DNA conjugates. Gaining insights into these conjugates will be instrumental in creating diverse nano-biomaterial systems for advanced biomedical applications. The extra benefit of tenability that surface

functionalized CQD offer to CQD-DNA systems is something that can be further investigated in gene delivery applications. following are mentioned some of the future scope for this study.

The potential of surface-functionalized CQD-nucleic acid conjugates extends beyond basic bioimaging, offering opportunities for advanced imaging techniques such as super-resolution microscopy and *in vivo* imaging, enabling higher resolution and deeper tissue penetration. These conjugates can also be explored for targeted drug delivery, where nucleic acids facilitate the precise delivery of therapeutic agents to cancer cells or other diseased tissues, enhancing treatment efficacy while minimizing side effects. Comprehensive biocompatibility and toxicity studies are crucial to ensuring their safety for clinical applications, providing essential data for regulatory approvals. Additionally, multiplexed imaging platforms can be developed to simultaneously detect multiple targets using different nucleic acid sequences conjugated to CQDs, offering more comprehensive diagnostic capabilities. The integration of these conjugates into theranostic applications, which combine therapeutic and diagnostic functions in a single platform, can revolutionize personalized medicine by enabling real-time monitoring of treatment responses. Efforts toward commercialization and clinical trials are essential to translating these innovations into practical medical diagnostics and treatment tools, ultimately benefiting healthcare. Furthermore, research can be extended to explore their potential in environmental and industrial applications, where CQD-nucleic acid conjugates could be utilized for pollutant detection or chemical process monitoring, demonstrating their versatility beyond biomedical applications.

STUDY OF SURFACE FUNCTIONALIZED CARBON QUANTUM DOT - NUCLEIC ACID CONJUGATE FOR BIOIMAGING APPLICATIONS

A thesis submitted to

D. Y. PATIL EDUCATION SOCIETY,

(DEEMED TO BE UNIVERSITY), KOLHAPUR

FOR THE DEGREE OF

DOCTOR OF PHILOSOPHY

IN

STEM CELL AND REGENERATIVE MEDICINE

UNDER THE FACULTY OF

INTERDISCIPLINARY STUDIES

BY

Ms. ANUJA ARVIND VIBHUTE

M.Sc.

UNDER THE GUIDANCE OF

Dr. ARPITA PANDEY-TIWARI

M.Sc., Ph.D.

DEPARTMENT OF MEDICAL BIOTECHNOLOGY AND

STEM CELL AND REGENERATIVE MEDICINE

CENTRE FOR INTERDISCIPLINARY RESEARCH,

D. Y. PATIL EDUCATION SOCIETY,

(DEEMED TO BE UNIVERSITY), KOLHAPUR- 416 006.

(2024)

RECOMMENDATIONS

Recommendations

7.1 Recommendations

In this presented research work, PLLCQDs are synthesized by one-pot pyrolysis method. The synthesized PLLCQDs have a surface positive charge due to cationic polymer poly L lysine. Interaction of PLL to CQDs enhances electrostatic interaction between the cell membrane and positively charged ions of attachment factors. Excellent intrinsic properties of PLL-based polymers include biodegradability, biocompatibility, and the capacity to change configuration in response to stimuli. A flexible base for the synthesis of copolymers and complexes with a variety of uses is provided by the side amine groups on PLL, which are also readily changed with a broad range of bioactive compounds. Therefore, more cationic polymers can be explored as surface modifier of CQD for nucleic acid conjugation.

The cationic PLLCQDs are conjugated with calf thymus DNA through electrostatic interactions. The PLLCQD-Ct-DNA conjugate was confirmed using UV-Vis, fluorescence spectroscopy, zeta, TEM, and electrophoretic mobility shift assay. The calf thymus DNA is incubated with PLLCQDs at room temperature, at pH 9 for 30 min, and 20 µg/ml Ct-DNA concentration required to form a PLLCQD-Ct-DNA conjugate. The PLLCQD-Ct-DNA conjugate is used for cell cytotoxicity and intracellular imaging in HEK-293 cells. The PLLCQD-Ct-DNA conjugate shows good biocompatibility and exhibit potential applicability in cellular imaging in HEK-293 cells. Potential of PLLCQD-Ct-DNA conjugate can be explored for targeted intracellular imaging.

The present research work deals with the synthesis of surface functionalized PLLCQDs by simple, single step or one pot synthesis method using PLL as cationic polymer. To produce nano-sized, cationic PLLCQDs, a variety of synthesis parameters, including temperature, PLL concentration, pH, and reaction duration were optimized. By fine-tuning variables including reaction time, DNA concentration, and pH, the conjugation of DNA on PLLCQDs was accomplished.

To demonstrate its potential applicability in the intracellular trafficking exploiting cellular imaging was conducted by using PLLCQD, PLLCQD-Ct-DNA conjugate with HEK-293 cells. The role of PLLCQDs was further determined on cellular uptake by confocal microscopy. Intracellular uptake and monitoring of fluorescence at different time interval intracellular imaging results demonstrate that

PLLCQD-Ct-DNA conjugate had a higher cellular uptake and no autofluorescence as compare to PEI and lipofectamine in HEK-293 cells. The PLLCQD is cost cost-effective, easy, and less time-consuming synthesis procedure that can be a replacement of contrast agents/ organic dyes i. e Alexa Fluor, fluorescein, coumarin, cyanine, or rhodamine. The PLLCQDs can be used as transfection agents by attaching respective gene sequences for the transport of therapeutic genes into specific cells for applications like gene delivery, and cancer. The detail *in vitro* and *in vivo* studies can be carried out for finding out more insights on use of PLLCQD as bioimaging agent. However, further research is needed to explore strategies for enhancing their quantum yield.

In conclusion, the PLLCQD-DNA conjugates were found to be easy to prepare, exhibiting promising fluorescence characteristics while maintaining excellent biocompatibility. These conjugates demonstrated significant potential for applications in *in vivo* bioimaging, where their biocompatibility and fluorescence properties could enable precise cellular and tissue-level imaging. Furthermore, the PLLCQD effectively interact with nucleic acids and hence, can be used as bioimaging agent in targeted gene delivery applications.

ANNEXURE

D. Y. PATIL MEDICAL COLLEGE KOLHAPUR

Constiuent Unit of D. Y. Patil Education Society (Deemed to be University),Kolhapur.
Re-accredited by NAAC with 'A' Grade

Dr. Rakesh Kumar Sharma
Dean & Professor (Obst. & Gyn)

Padmashree Dr. D. Y. Patil
Founder president

Dr. Sanjay D. Patil
President

No. DYPMCK/...429.../2021/IEC

Date: 24 MAR 2021

INSTITUTIONAL ETHICS COMMITTEE, D. Y. PATIL MEDICAL COLLEGE, KOLHAPUR.

This is to certify that the research project titled,

"Study of Surface Functionalized Carbon Quantum DOT - Nucleic Acid Conjugates for Bioimaging Applications."

Submitted by : **Ms. Anuja Arvind Vibhute**

Under the supervision of appointed Guide (if any): **Dr. Arpita Pandey Tiwari**

Has been studied by the Institutional Ethics Committee (IEC) at its meeting held on **24/03/2021** and granted approval for the study with due effect with the following caveats:

1. If you desire any change in the protocol or standard recording document at any time, please submit the same to the IEC for information and approval before the change is implemented.
2. As per recommendations of ICMR, you must register your study with the Central Trials Registry- India (CTRI), hosted at the ICMR's National Institute of Medical Statistics (http://icmr-nims.nic.in). The registration details as provided by the website are to be submitted to the Institutional Ethics Committee within a period of 3 months from issue of this letter.
3. All serious and/or unexpected adverse events due to the drug/procedures tested in the study must be informed to the IEC within 24 hours and steps for appropriate treatment must be immediately instituted.
4. In case of injury/disability/death of any participant attributable to the drug/procedure under study, all compensation is to be made by the sponsor of the study.
5. The Chief investigator/Researcher must inform the IEC immediately if the study is terminated earlier than planned with the reasons for the same.
6. The final results of the study must be communicated to the IEC within 3 months of the completion of data collection.
7. The researcher must take all precautions to safeguard the rights, safety, dignity and wellbeing of the participants in the study.
8. The researcher must be up to date about all information regarding the risk/benefit ratio of any drug/procedure being used and any new information must be conveyed to the IEC immediately. The IEC reserves the right to change a decision on the project in the light of any new knowledge.
9. Before publishing the results of the study, the researcher must take permission from the Dean of the Institution.
10. Annual progress report should be submitted for all sponsored projects to the committee.
11. Unethical conduct of research in non-sponsored projects will result in withdrawal of the ethics approval and negation of all data collected till that date.

Prof. C. D. Lokhande
(Act. Member Secretary, IEC)

INTELLECTUAL PROPERTY INDIA
PATENTS | DESIGNS | TRADE MARKS
GEOGRAPHICAL INDICATIONS

सत्यमेव जयते

क्रम सं/SL No :022144612

पेटेंट कार्यालय,भारत सरकार | The Patent Office, Government Of India

पेटेंट प्रमाण पत्र | Patent Certificate

(पेटेंट नियमावली का नियम 74) | (Rule 74 of The Patents Rules)

पेटेंट सं. / Patent No.	:	538842
आवेदन सं. / Application No.	:	202321020467
फाइल करने की तारीख / Date of Filing	:	23/03/2023
पेटेंटी / Patentee	:	D.Y.PATIL EDUCATION SOCIETY (DEEMED TO BE UNIVERSITY)
आविष्कारकों का नाम /Name of Inventor(s)	:	1.DR.ARPITA PANDEY TIWARI 2.MS.ANUJA ARVIND VIBHUTE 3.PROF.CHANDRAKANT DNYANDEV LOKHANDE

प्रमाणित किया जाता है कि पेटेंटी को, उपरोक्त आवेदन में यथाप्रकटित *"A METHOD FOR DETECTION OF FOLIC ACID FROM HUMAN SERUM/URINE SAMPLES USING SURFACE FUNCTIONALIZED CARBON QUANTUM DOTS"* नामक आविष्कार के लिए, पेटेंट अधिनियम, 1970 के उपबंधों के अनुसार आज तारीख मार्च 2023 के तेइसवें दिन से बीस वर्ष की अवधि के लिए पेटेंट अनुदत्त किया गया है।

It is hereby certified that a patent has been granted to the patentee for an invention entitled *"A METHOD FOR DETECTION OF FOLIC ACID FROM HUMAN SERUM/URINE SAMPLES USING SURFACE FUNCTIONALIZED CARBON QUANTUM DOTS"* as disclosed in the above mentioned application for the term of 20 years from the 23rd day of March 2023 in accordance with the provisions of the Patents Act,1970.

अनुदान की तारीख : 21/05/2024
Date of Grant :

पेटेंट नियंत्रक
Controller of Patents

टिप्पणी - इस पेटेंट के नवीकरण के लिए फीस, यदि इसे बनाए रखा जाना है, मार्च 2025 के तेइसवें दिन को और उसके पश्चात प्रत्येक वर्ष मे उसी दिन देय होगी।

Note. - The fees for renewal of this patent, if it is to be maintained, will fall / has fallen due on 23rd day of March 2025 and on the same day in every year thereafter.

INTELLECTUAL PROPERTY INDIA
PATENTS | DESIGNS | TRADE MARKS | GEOGRAPHICAL INDICATIONS

सत्यमेव जयते

Extracts from the Register of Copyrights

प्रतिलिप्यधिकार कार्यालय, भारत सरकार | Copyright Office, Government Of India

दिनांक/Dated:26/09/2023

1.	पंजीकरण संख्या/Registration Number	:	**L-133612/2023**
2.	आवेदक का नाम, पता तथा राष्ट्रीयता Name, address and nationality of the applicant	:	THE REGISTRAR , D. Y. PATIL EDUCATION SOCIETY, DEEMED TO BE UNIVERSITY, KASABA BAWADA, KOLHAPUR-416006 INDIAN
3.	कृति के प्रतिलिप्यधिकार में आवेदक के हित की प्रकृति Nature of the applicant's interest in the copyright of the work	:	PUBLISHER
4.	कृति का वर्ग और वर्णन Class and description of the work	:	LITERARY/ DRAMATIC WORK
5.	कृति का शीर्षक Title of the work	:	PRACTICAL HANDBOOK OF IMMUNOLOGY
6.	कृति की भाषा Language of the work	:	ENGLISH
7.	रचयिता का नाम, पता और राष्ट्रीयता तथा यदि रचयिता की मृत्यु हो गई है, तो मृत्यु की तिथि Name, address and nationality of the author and if the author is deceased, date of his decease	:	DR. ARPITA PANDEY TIWARI, ASSOCIATE PROFESSOR , DEPARTMENT OF STEM CELL AND REGENERATIVE MEDICINE, CENTRE FOR INTERDISCIPLINARY RESEARCH, D. Y. PATIL EDUCATION SOCIETY, DEEMED TO BE UNIVERSITY, KASABA BAWADA, KOLHAPUR-416006 INDIAN MS. ANUJA A. VIBHUTE, PH. D. SCHOLAR , DEPARTMENT OF STEM CELL AND REGENERATIVE MEDICINE, CENTRE FOR INTERDISCIPLINARY RESEARCH, D. Y. PATIL EDUCATION SOCIETY, DEEMED TO BE UNIVERSITY, KASABA BAWADA, KOLHAPUR-416006 INDIAN
8.	कृति प्रकाशित है या अप्रकाशित Whether the work is published or unpublished	:	PUBLISHED
9.	प्रथम प्रकाशन का वर्ष और देश तथा प्रकाशक का नाम, पता और राष्ट्रीयता Year and country of first publication and name, address and nationality of the publisher	:	2023 INDIA THE REGISTRAR , D. Y. PATIL EDUCATION SOCIETY, DEEMED TO BE UNIVERSITY, KASABA BAWADA, KOLHAPUR-416006 INDIAN
10.	बाद के प्रकाशनों के वर्ष और देश, यदि कोई हों, और प्रकाशकों के नाम, पते और राष्ट्रीयताएँ Years and countries of subsequent publications, if any, and names, addresses and nationalities of the publishers	:	N.A.
11.	कृति में प्रतिलिप्यधिकार सहित विभिन्न अधिकारों के स्वामियों के नाम, पते और राष्ट्रीयताएं और समनुदेशन और अनुज्ञप्तियों के विवरण के साथ प्रत्येक के अधिकार का विस्तार, यदि कोई हो। Names, addresses and nationalities of the owners of various rights comprising the copyright in the work and the extent of rights held by each, together with particulars of assignments and licences, if any	:	THE REGISTRAR , D. Y. PATIL EDUCATION SOCIETY, DEEMED TO BE UNIVERSITY, KASABA BAWADA, KOLHAPUR-416006 INDIAN
12.	अन्य व्यक्तियों के नाम, पते और राष्ट्रीयताएं, यदि कोई हों, जो प्रतिलिप्यधिकार वाले अधिकारों को समनुदेशित करने या अनुज्ञप्ति देने के लिए अधिकृत हों Names, addresses and nationalities of other persons, if any, authorised to assign or licence of rights comprising the copyright	:	N.A.
13.	यदि कृति एक 'कलात्मक कृति' है, तो कृति पर अधिकार रखने वाले व्यक्ति का नाम, पता और राष्ट्रीयता सहित मूल कृति का स्थान। (एक वास्तुशिल्प कृति के मामले में कृति पूरी होने का वर्ष भी दिखाया जाना चाहिए) If the work is an 'Artistic work', the location of the original work, including name, address and nationality of the person in possession of the work. (In the case of an architectural work, the year of completion of the work should also be shown).	:	N.A.
14.	यदि कृति एक 'कलात्मक कृति' है जो किसी भी माल या सेवाओं के संबंध में उपयोग की जाती है या उपयोग किए जाने में सक्षम है, तो आवेदन में प्रतिलिप्यधिकार अधिनियम, 1957 की धारा 45 की उप–धारा (i) के प्रावधान के अनुसार व्यापार चिह्न रजिस्ट्रार से प्रमाणन शामिल होना चाहिए। If the work is an 'Artistic work' which is used or capable of being used in relation to any goods or services, the application should include a certification from the Registrar of Trade Marks in terms of the provision to Sub-Section (i) of Section 45 of the Copyright Act, 1957.	:	N.A.
15.	यदि कृति एक 'कलात्मक कृति' है, तो क्या यह डिजाइन अधिनियम 2000 के अंतर्गत पंजीकृत है? यदि हां, तो विवरण दें। If the work is an 'Artistic work', whether it is registered under the Designs Act 2000, if yes give details.	:	N.A.
16.	यदि कृति एक 'कलात्मक कृति' है, जो डिजाइन अधिनियम 2000 के तहत एक डिजाइन के रूप में पंजीकृत होने में सक्षम है, तो क्या यह औद्योगिक प्रक्रिया के माध्यम से किसी वस्तु पर प्रयुक्त की गई है और यदि हाँ, तो कितनी बार पुनरुत्पादित किया गया है? If the work is an 'Artistic work', capable of being registered as design under the Designs Act 2000.whether it has been applied article though an industrial process and ,if yes ,the number of t it is reproduced.	:	N.A.
17.	टिप्पणी, यदि कोई हो/Remarks, if any	:	

डायरी संख्या/Diary Number: 21025/2023-CO/L

Registrar of Copyrights

Journal of Fluorescence (2022) 32:1789–1800
https://doi.org/10.1007/s10895-022-02977-4

RESEARCH

Fluorescent Carbon Quantum Dots Functionalized by Poly L-Lysine: Efficient Material for Antibacterial, Bioimaging and Antiangiogenesis Applications

Anuja Vibhute[1] · Omkar Nille[2] · Govind Kolekar[2] · Sonali Rohiwal[3] · Shubham Patil[4] · Seunghyun Lee[4] · Arpita Pandey Tiwari[1]

Received: 6 April 2022 / Accepted: 27 May 2022 / Published online: 11 June 2022

Abstract

This study illustrates the synthesis of functionalized carbon quantum dots (CQDs) by the one-pot pyrolysis method. The functionalization agent used in CQD synthesis was poly l- lysine (PLL). Various physicochemical techniques were employed to confirm the successful formation of PLLCQD including High resolution transmission electron microscopy (HR-TEM), UV-Vis spectroscopy, fluorescence spectroscopy; Atomic force microscopy (AFM), X-ray Photoelectron Spectroscopy (XPS) and X-ray diffraction (XRD) and Fourier transform infrared (FTIR) spectroscopy. The size of PLLCQD was confirmed by HRTEM and AFM. The synthesized PLLCQD shows bright blue fluorescence and has a quantum yield of 19.35%. The highest emission band was observed at 471nm when excited to 370nm. The prepared PLLCQD exhibited excellent antibacterial activity against Escherichia coli and Staphylococcus aureus with inhibition zone 7-20 mm. The concentrations of 0.9 to 0.1gmL-1 were studied to determine minimum inhibitory concentration (MIC) by the agar well diffusion assay method. MIC of 0.2gml -1 concentration of PLLCQD is achieved. The anti-angiogenic activity of PLLCQD was determined using (Chick Chorioallantoic Membrane) CAM assay. CAM assay is a reliable in -vivo model to study angiogenesis also; many stimulators and inhibitors have been examined by this method. This study proves higher antibacterial efficiency of PLLCQD over non functionalized CQD. PLLCQD was successfully employed in bio-imaging of the bacterial cell through fluorescence microscopy. Further, PLLCQD displayed cytotoxic effect on endothelial cells and inhibited blood vessel formation in the CAM model.

Keywords Carbon quantum dots · Poly l lysine · Antibacterial activity · Antiangiogenesis · Bioimaging

✉ Arpita Pandey Tiwari
arpitaptiwari@gmail.com

Anuja Vibhute
anujavibhute06@gmail.com

Omkar Nille
omkarnille@gmail.com

Govind Kolekar
gbkolekar@gmail.com

Sonali Rohiwal
rohiwalsonali@gmail.com

Shubham Patil
shubham.nanotechnology@gmail.com

Seunghyun Lee
seansl@khu.ac.kr

[1] Department of Stem Cell and Regenerative Medicine and Medical Biotechnology, D. Y. Patil Education Society(Deemed to Be University), Kolhapur 416 006, Maharashtra, India

[2] Fluorescence Spectroscopy Research Laboratory, Department of Chemistry, Shivaji University, Kolhapur, Maharashtra, India

[3] Laboratory of Cell Regeneration and Plasticity, Institute of Animal Physiology and Genetics AS CR, v.v.i. Rumburska 89, Libechov 277 21, Czech Republic

[4] Department of Electronics and Information Convergence Engineering, Kyung Hee University (Global Campus), 1732, Deogyoung Road, Giheung, Gyeonggi, Yongin 17104, South Korea

Journal of Fluorescence
https://doi.org/10.1007/s10895-024-04103-y

RESEARCH

Bio-Conjugated Carbon Quantum Dots for Intracellular Uptake and Bioimaging Applications

Anuja Vibhute[1] · Tejaswini Patil[1] · Arpita Pandey-Tiwari[1]

Received: 15 September 2024 / Accepted: 27 December 2024

Abstract

Carbon quantum dots (CQDs) demonstrate outstanding biocompatibility and optical properties, making them ideal for monitoring cellular uptake. Due to their ultra-small size (typically < 10 nm) and fluorescent nature, CQDs hold significant potential as nanoparticles for bioimaging and tracking intracellular processes. The study examined the optimization parameters for conjugating calf thymus DNA (Ct-DNA) to CQDs to facilitate Ct-DNA internalization in mouse fibroblast cells (L929) and human breast cancer cells (MCF-7). The formation of the CQD-Ct-DNA complex was confirmed by various characterization techniques such as, UV-Vis spectroscopy, fluorescence spectroscopy, transmission electron microscopy, and zeta potential analysis. The CQD-Ct-DNA complex, at a 600 µg/mL concentration, demonstrated up to 83.7% cell viability for the L929 cell line and 75.6% for the MCF7 cell lines. The research also compared the transfection ability of CQD with commonly used transfection agents lipofectamine and Polyethyleneimine (PEI) for Ct-DNA internalization. The results demonstrated that CQD could efficiently internalize Ct-DNA compared to the other agents. Thus, the CQD-Ct-DNA complex shows promising potential in bioimaging applications as an effective non-viral vector.

Keywords Bioimaging · Carbon quantum dots · Cellular uptake · Ct-DNA

ORCID ID: 0000-0002-2692-0011.

Introduction

Carbon-based nanomaterials have emerged as novel materials with diverse applications, including bioimaging, biosensing, drug delivery, and antimicrobial fields [1–4]. These materials exhibit unique properties including straightforward and cost-effective synthesis, high water solubility, biocompatibility, high fluorescence quantum yield, excitation-dependent/independent emission characteristics, surface defects facilitating interaction with other molecules, and surface passivation. Carbon-based nanomaterials are synthesized using various methods, including top-down approaches such as laser ablation and chemical vapor deposition, as well as bottom-up methods like hydrothermal and solvothermal techniques. These methods utilize a wide range of chemical precursors and environmentally friendly resources for synthesis [5, 6].

CQDs are particularly valuable for optical imaging because of their exceptional resolution, unique biocompatibility, and long-term detection [7–9]. Optical imaging is a common technique for examining complicated structures in living things. It is anticipated that positively charged CQDs will interact strongly with negatively charged nucleic acids through electrostatic interactions because of their phosphate backbone [10]. Using spectroscopic techniques, Kathiravan [9] and his colleague reported the photoinduced interaction between colloidal TiO_2 nanoparticles and calf thymus DNA and investigated the binding sites and constant. The interaction of CQDs with single-stranded DNA (ssDNA) and double-stranded DNA (dsDNA) has received sufficient attention recently. Research has demonstrated that these

✉ Arpita Pandey-Tiwari
arpitaptiwari@gmail.com

Anuja Vibhute
anujavibhute06@gmail.com

Tejaswini Patil
patiltejaswini1010@gmail.com

[1] Department of Medical Biotechnology and Stem Cell and Regenerative Medicine, Centre for Interdisciplinary Research, D. Y. Patil Education Society (Deemed to be University), Kolhapur, Maharashtra 416 006, India

Published online: 09 January 2025

Journal of Fluorescence
https://doi.org/10.1007/s10895-023-03159-6

RESEARCH

Green Synthesis of Fluorescent Carbon Dots from *Annona squamosa* Leaves: Optical and Structural Properties with Bactericidal, Anti-inflammatory, Anti-angiogenesis Applications

Anuja Vibhute[1] · Tejaswini Patil[1] · Dhanaji Malavekar[2] · Shubham Patil[3] · Seunghyun Lee[3,4] · Arpita Pandey Tiwari[1]

Received: 14 December 2022 / Accepted: 25 January 2023

Abstract
A hydrothermal method was employed for green synthesis of fluorescent carbon dots (GCDs) from *Annona squamosa* leaves. The synthesized GCDs were confirmed by microscopic and spectroscopic techniques such as: High Resolution Transmission Electron Microscopy (HR-TEM), Atomic Force Microscopy (AFM), UV–Vis spectrometry, Fluorescence spectrometry, X-Photoelectron Spectroscopy (XPS), X-ray Diffraction spectroscopy (XRD), and Fourier Transform Infrared Spectroscopy (FTIR). The produced GCDs had shown multiple properties, including massive antibacterial activity at concentration 200 µg/ml. The stabilization of human red blood cells served as a method to assess the anti-inflammatory activity. We also looked at how GCDs affected the angiogenesis process. The density of blood vessels was significantly decreased after treatment with GCDs, according to the results of the Chorio-Allantoic Membrane assay ($p < 0.05$). As per the study prepared GCDs from fallen leaves of *Annona squamosa* have multifunctional applications.

Keywords Green synthesis · *Annona squamosa* · Carbon Quantum Dots · Antibacterial · Bioimaging · Anti-angiogenesis

Introduction

Carbon dots (CDs) have steadily emerged as superior substitutes for heavy metal-based quantum dots, which are semiconductive in nature for similar applications, in the quest to build ecologically safe and environmentally friendly fluorescent nanomaterials [1]. Due to their distinctive, appealing qualities, including photostability, wavelength-tunable emission, solubility in water, low toxicity, and ease of functionalization, carbon dots have attracted a lot of attention. CDs have been used for potential applications in the fields of cell imaging [2, 3], drug transport, sensing [4–6], catalysis, and anti-cancer therapy [7] due to their unique features. The synthesis of CDs is multistep and tedious procedure, which is often costly. To obtain intrinsic fluorescence properties, surface functionalization with other ligands is

✉ Arpita Pandey Tiwari
arpitaptiwari@gmail.com

Anuja Vibhute
anujavibhute06@gmail.com

Tejaswini Patil
patiltejaswini1010@gmail.com

Dhanaji Malavekar
dhanajimalavekar@gmail.com

Shubham Patil
shubham.nanotechnology@gmail.com

Seunghyun Lee
seansl@khu.ac.kr

[1] Department of Medical Biotechnology and Stem Cell and Regenerative Medicine, D. Y. Patil Education Society (Deemed to Be University), Kolhapur 416 006, Maharashtra, India

[2] Optoelectronic Convergence Research Center, Department of Materials Science and Engineering, Chonnam National University, Gwangju 61186, South Korea

[3] Department of Electronics and Information Convergence Engineering, Kyung Hee University (Global Campus), 1732, Deogyoung Road, Giheung, Yongin, Gyeonggi 17104, South Korea

[4] Integrated Nano Electronics Laboratory, Department of Electrical Engineering, Kyung Hee University, 1732, Deogyoung Road, Giheung, Yongin, Gyeonggi 17104, South Korea

Published online: 17 February 2023

Applied Surface Science Advances 11 (2022) 100311

Contents lists available at ScienceDirect

Applied Surface Science Advances

journal homepage: www.sciencedirect.com/journal/applied-surface-science-advances

Fluorescent carbon quantum dots: Synthesis methods, functionalization and biomedical applications

Anuja Vibhute, Tejaswini Patil, Rutuja Gambhir, Arpita Pandey Tiwari *

Department of Stem cell and Regenerative medicine and Medical Biotechnology, D. Y. Patil Education Society (Deemed to be University), Kolhapur, Maharashtra 416006, India

ARTICLE INFO

Keywords:
Carbon quantum dots
Fluorescence
Bioimaging
Biomedical applications

ABSTRACT

Carbon Quantum Dots (CQDs), a type of carbon material having size less than 10 nm and strong fluorescence is creating a new paradigm in the field of bioimaging and other biomedical applications. Owing to simple and low cost of synthesis, tunable and precise optical properties, high photostability and ease of surface functionalization with biological entities there is a huge potential in the field of CQDs based cell imaging applications. A thorough knowledge and understanding of synthesis methods and optical properties are crucial in translation of CQDs based bioimaging research from research lab to commercial purposes for societal benefit. Different methods of synthesis like electrochemical, laser ablation, microwave radiation, and hydrothermal and optical properties like photoluminescent (PL) property, quantum confinement effect, doping influence on optical properties of CQDs are covered in this review. Surface functionalization agents employed for different bio applications have been reviewed along with the current challenges. The applications of CQDs in bioimaging, biosensing and drug delivery along with the existing challenges and future prospects are discussed.

1. Introduction

The nanocomposites have been interests for molecular imaging, biosensors, and other biological applications. In 2013, a new trend arrived in the emerging carbon nanomaterials family; fluorescent carbon quantum dots CQDs have considerable attention due to their tunable size and unique optical properties [1]. CQDs are contemplating a type of zero-dimensional carbonic nanomaterial, compared to spherical, tubular, and are in graphene family nanomaterials [2]. Carbon dots (C-dot), also known as carbon quantum dots or graphene quantum dots possess chemical structure and physical properties similar to those of graphene oxide. They differ from graphene oxide in terms of size, being quasi spherical nanoparticles with diameter below 10 nm [3]. The origin of CQDs was accidental during single-walled carbon nanotubes synthesis which is further named carbon nanoparticles (CNPs). CQDs have outstanding physical properties including tunable photoluminescence, up-conversation fluorescence, improved surface Raman spectroscopy, and fluorescent resonance energy transfer (FRET) which is based on quantum effect and surface state [4]. Fig. 1 represents an overview of CQD advantages.

The small-sized CQDs have been achieved by carbonization, microwave oven irradiation synthesis methods by using renewable resources and tiny molecules. Depending on fluorescence intensity and variations in synthesis methods abundance of sensing protocols can be achieved. [5]. CQDs have been reported for a variety of biomedical applications [6], such as in food safety [7], bioimaging [8], biosensing [9], drug delivery [10], wound healing [11]. CQDs have other important applications too, such as photocatalysis [12], chemical sensing [13], gas sensing [14], energy storage [15], solar cells [16] and photodynamic therapy [17].

This review gives an outline of the fundamental properties of CQDs along with their top-down, and bottom-up approaches to synthesis. In addition *in-vivo*, invitro bioimaging followed by biosensing and drug delivery applications is mentioned. This review would offer valuable insights into the topic and explore more about CQDs.

2. History and structure of CQD

The fluorescent CQD was discovered accidentally, during the purification of single-walled carbon nanotubes by Yan et al. in 2004 [18]. Another group of scientist's Sun et al. found the carbon nanoparticles from graphite powder using the laser ablation technique and named

* Corresponding author.
E-mail address: arpitaptiwari@gmail.com (A.P. Tiwari).

https://doi.org/10.1016/j.apsadv.2022.100311
Received 30 June 2022; Received in revised form 28 September 2022; Accepted 28 September 2022
Available online 7 October 2022

International Journal of Biological Macromolecules 257 (2024) 128126

Contents lists available at ScienceDirect

International Journal of Biological Macromolecules

journal homepage: www.elsevier.com/locate/ijbiomac

Route-dependent tailoring of carbon dot release in alginate hydrogel beads (HB-Alg@WTR-CDs): A versatile platform for biomedical applications

Omkar S. Nille [a], Akshay S. Patil [b], Anuja A. Vibhute [c], Shital S. Shendage [a], Arpita P. Tiwari [c], Prashant V. Anbhule [a], Daewon Sohn [b], Anil H. Gore [d,*], Govind B. Kolekar [a,**]

[a] Fluorescence Spectroscopy Research Laboratory, Department of Chemistry, Shivaji University, Kolhapur, Maharashtra, India
[b] Department of Chemistry and Research Institute for Convergence of Basic Science, Hanyang University, Seoul Campus, Seoul, South Korea
[c] Department of Medical Biotechnology, D.Y. Patil Education Society, (Deemed to be University), Kolhapur, Maharashtra. India
[d] Tarsadia Institute of Chemical Science, Uka Tarsadia University, Maliba Campus, Bardoli, Tarsadi, Surat, Gujarat, India

ARTICLE INFO

Keywords:
Waste tea residue carbon dots (WTR-CDs)
Sustainable
Biocompatible
Hydrogel beads
Smart releasing probe
Angiogenesis

ABSTRACT

The present investigation explores the different pathways for development of waste tea residue carbon dots (WTR-CDs) loading into hydrogel matrix for WTR-CDs releasing probe. Fluorescent WTR-CDs incorporated into hydrogel matrix were synthesized by valorisation of kitchen waste tea by simple carbonization method (λ_{em} = 450 nm, $\Phi_{WTR-CDs}$ =18.45 %). Biopolymeric alginate-based hydrogel beads (HB-Alg) were prepared by simple extrusion method. Three routes (ex-situ/in-situ) were employed for loading of WTR-CDs into hydrogel matrix. Successful synthesis of WTR-CDs and its loading into hydrogel matrix was confirmed via various characterization techniques. Developed protocol was employed for stimuli-responsive cumulative release of WTR-CDs study (pH = 3.0, 7.4, 9.0) was monitored over 7 days. Results suggests that, the HB-Alg@WTR-CDs-A system with in-situ loaded WTR-CDs have sustained release due to ionic interaction of WTR-CDs with crosslinked polymer network, whereas in HB-Alg@WTR-CDs-B, WTR-CDs loaded in wet-beads having burst release in which loosely bound WTR-CDs into hydrogel cavities releases rapidly. While, in case of HB-Alg@WTR-CDs-C, lowest release was observed due to weakly surface bound WTR-CDs, low loading and shrinkage of pores into dry-beads. Radical scavenging activity was studied and shown antioxidant properties of WTR-Powder, WTR-CDs and HB-Alg@WTR-CDs-A,B,C. Cytotoxicity of all systems was checked via CAM assay and significant growth in blood vascularization with no loss of chick embryo confirming the released WTR-CDs are biocompatible. Successful investigation and summarization of results ensure that, waste-valorisation, simple, sustainable, and smart hydrogel systems with different routes of WTR-CDs loading have opened a window to understand the mechanistic pathways in release behaviour. This robust approach for improvement of smarter and biocompatible materials can be fruitfully applicable in advanced, controlled and stimuli responsive delivery probes.

1. Introduction

The recent scientific evolution has been focused on developing a new class of environmentally friendly, sustainable as well as waste-to-wealth-based nanocomposites having simple, safer, and smarter multi-disciplinary applicability. In last few decades, numerous health-related problems have aroused of which drug delivery probes are of great interest to the scientific society. The biopolymeric (sodium alginate, gelatin, chitosan, starch, etc.), physically or chemically crosslinked and three-dimensionally (3D) networked hydrogels have been highly recognized in pharmaceutical and biomedical applications [1]. Interestingly, biopolymeric hydrogels possess good mechanical strength, hydrophilicity, swellability, water/ analyte/ drug holding capacity, large porosity, biocompatibility, biodegradability, non-cytotoxicity, and stimuli responsivity (temperature and pH-sensitive) making it perfect candidate for drug delivery probes [2,3].

In the last few years, nanomaterials and their composite hydrogels have drawn the attention of researchers and biomedical applications due to their fascinating drug delivery performance. Since, the structure of nanocomposite hydrogels resembles with macromolecular components

* Corresponding author at: Tarsadia Institute of Chemical Science, UKA Tarsadia University, Bardoli 394350, Gujrat, India.
** Corresponding author at: Department of Chemistry, Shivaji University, Kolhapur 416004, MS, India.
E-mail addresses: anilanachem@gmail.com (A.H. Gore), gbk_chem@unishivaji.ac.in (G.B. Kolekar).

https://doi.org/10.1016/j.ijbiomac.2023.128126
Received 28 July 2023; Received in revised form 6 October 2023; Accepted 3 November 2023
Available online 18 November 2023

Applied Surface Science Advances 13 (2023) 100372

Contents lists available at ScienceDirect

Applied Surface Science Advances

journal homepage: www.sciencedirect.com/journal/applied-surface-science-advances

Green synthesis of gold nanoparticles via *Capsicum annum* fruit extract: Characterization, antiangiogenic, antioxidant and anti-inflammatory activities

Tejaswini P. Patil [a], Anuja A. Vibhute [a], Snehal L. Patil [b], Tukaram D. Dongale [b], Arpita P. Tiwari [a,*]

[a] *Department of Medical Biotechnology and Stem Cell & Regenerative Medicine, D.Y. Patil Education Society (Institution Deemed to be University), Kolhapur, Maharashtra 416006, India*

[b] *Computational Electronics and Nanoscience Research Laboratory, Shivaji University, Kolhapur, Maharashtra 416004, India*

ARTICLE INFO

Keywords:
Anti-inflammatory
Biosynthesis
Capsicum annum
CAM assay
Gold nanoparticles
Scavenging activity

ABSTRACT

Biological synthesis of gold nanoparticles (AuNPs) is gaining attention of researchers because of their varieties of biomedical applications. This study reported the novel, eco-friendly synthesis of AuNPs using dried fruit extract of *Capsicum annum* (*C. annum*). Biosynthesized gold nanoparticles (Ca-AuNPs) showed UV absorption peak at 540 nm and were found to be stable for up to three months. The nanoparticles were further characterized by Transmission Electron Microscopy (TEM), Fourier Transform Infrared (FT-IR), Energy Dispersive X-ray Analysis (EDAX) and X-ray diffraction (XRD) analysis. The nanoparticles were spherical in shape with size range of 20–30 nm and zeta potential study confirmed the surface charge of -26.5 mV. The Ca-AuNPs were tested for anti-angiogenic activity using Chorioallantoic membrane (CAM) assay that implied a significant anti-angiogenic efficiency of Ca-AuNPs at 100 μg/mL concentration. The antioxidant activity of Ca-AuNPs studied by 2,2- diphenyl-1-picrylhydrazyl (DPPH) assay was found to be significant with 86.0% radical scavenging activity. These nanoparticles also revealed anti-inflammatory activity at concentration range 100–1200 μg/mL with IC-50 value619.4 μg/mL. The present study includes synthesis of Ca-AuNPs by using phytoconstituents of plant material as reducing agents to efficiently exploit the biomedical applications of the nanoparticles.

1. Introduction

Nanoparticles have wide applicability in the field of biomedicine, drug delivery, material chemistry and pollution control [1,2]. The capping agents of nanoparticles such as, PEG, PVA, BSA and different plant extract also play important role in various biological applications [3]. Biosynthesized nanoparticles have reported to shown effective antibacterial and photocatalytic activity [4,5]. It has been reported that metal nanoparticles, such as iron oxide, zinc oxide, Cu_2Sn_3 (CTS), gold nanoparticles, and quantum dots, have been employed in a variety of applications, including optics, biosensing, catalysis, antibacterial activity, and therapy [6–9]. In recent years, gold nanoparticles (AuNPs) are gaining attention in research area due to their unique intrinsic features such as, size tunability, large surface to volume ratio, optical properties, excellent biocompatibility, low toxicity and easy surface modification [10,11]. Thus, they are widely used in medical research for diagnosis [12] and therapies [13,14]. Gold nanoparticles are synthesized by various techniques like, chemical reduction method, lithography and physical methods [15]. Each method successfully synthesizes the metallic nanoparticles but has several disadvantages such as, requirement of toxic chemicals in synthesis method, high pressure and high processing cost, and may be toxic to environment [16]. Hence, it is necessary to develop novel, eco-friendly process for AuNPs synthesis. The biological synthesis of AuNPs using plants, algae, fungi and microorganisms minimizes the disadvantages of above methods as they are simple in nature, reduces the need of toxic chemicals, and are based on green chemistry approach [17]. Biosynthesis of AuNPs using plant is gaining interest of researchers as the phytoconstituents of plant extract are acting as both reducing and stabilizing agent which results in effective and rapid synthesis. Different plant extracts are reported to be rich in active phytoconstituents that promoted stable AuNPs synthesis methods for various applications like, drug delivery, antibacterial,

* Corresponding author.
E-mail address: arpitaptiwari@gmail.com (A.P. Tiwari).

https://doi.org/10.1016/j.apsadv.2023.100372
Received 15 October 2022; Received in revised form 9 January 2023; Accepted 9 January 2023
Available online 18 January 2023

Journal of Cluster Science
https://doi.org/10.1007/s10876-022-02287-6

REVIEW PAPER

Gold Nanoparticles: Synthesis Methods, Functionalization and Biological Applications

Tejaswini Patil[1] · Rutuja Gambhir[1] · Anuja Vibhute[1] · Arpita Pandey Tiwari[1]

Received: 29 March 2022 / Accepted: 17 May 2022

Abstract

Nanotechnology has vast applications in medicine and biomedical engineering like tissue engineering, diagnosis, and therapy. Nowadays incorporation of functionalized nanostructures in various biomedical applications has generated considerable research interest. Gold nanoparticles (AuNPs) are one of the most stable metal nanoparticles with unique physicochemical properties and are reflected as a promising candidate for widespread biological applications. Among different synthesis methods, biological synthesis methods are advantageous as it reduces the need for toxic chemicals for reduction purpose. Surface functionalization provides colloidal stability to gold nanoparticles which are achieved by using various materials. This review mainly focuses on the biological applications of AuNPs such as bioimaging, biosensing, anticancer therapy, drug delivery, hyperthermia, and antimicrobial activity. The surface plasmon resonance (SPR) related optical properties are used for biosensing and bioimaging applications for diagnosis to detect pathogens as well as biomarkers. Biomolecules and drug functionalized AuNPs are effectively used to treat various cancer and other diseases. Thus, the study of gold nanoparticles opens a new percept in the biological field for varieties of applications.

Keywords Gold nanoparticles · Synthesis · Biological applications · Bioimaging · Anticancer · Antibacterial

Introduction

Nanoscale materials have begun to pervade the areas of biomedical applications. The large matter is reduced to get nanoscale size material with unique physicochemical properties which differ from the actual bulk component. The size, shape, and surrounding environment of nanoparticles influence the physical properties that govern the alteration for a range of applications in different fields [1]. In recent years, conventional biomedical methods have been successfully replaced with modern nanotechnology methods for considerable accuracy, sensitivity, efficiency, and high-speed measurement. Among different nanoparticles, the gold nanoparticles (AuNPs) are one of the most explored nanoparticles for biological applications due to their desirable physicochemical properties like easy synthesis, easy surface modification, biocompatibility, non-toxicity, and large surface to volume ratio, and size tunability as shown in Fig. 1. The physical properties and color diversity of AuNPs depend on the size and shape whereas the bulk gold exhibit different properties as compared to nanoscale particles [2].

The colloidal gold suspension has a particle size in the range of 1–100 nm and its color change from wine red to purple depending on the particle size. The nanometer-sized gold exhibit different properties from bulk gold. Gold nanoparticles have optical and electrochemical properties which strongly depend on their size, shape, interparticle distance, and surface chemistry. Different synthesis methods were developed for various sized AuNPs preparation. The variation in particle size depends on the synthesis parameters like reaction temperature, pH, precursor concentration as well as the ratio of precursor to reducing agent. The various sizes of AuNPs influence the Surface Plasmon Resonance (SPR) frequency [3]. The AuNPs tend to precipitate in fluids due to the high surface energy of gold. This self-assembly is prevented by surface modification of AuNPs with the help of various functionalizing molecules such as polymers that decrease the surface energy of gold and stabilize the AuNPs. Surface chemistry of gold nanoparticles is crucial for their

✉ Arpita Pandey Tiwari
arpitaptiwari@gmail.com

[1] Department of Stem Cell and Regenerative Medicine and Medical Biotechnology, Center for Interdisciplinary Research, D.Y. Patil Education Society, Institution Deemed to be University, Kolhapur, Maharashtra, India

Published online: 04 June 2022

Surface-Functionalized Iron Oxide (Fe_3O_4) Nanoparticles for Biomedical Applications

Rutuja P. Gambhir, Anuja A. Vibhute, Tejaswini P. Patil, and Arpita P. Tiwari

Abbreviation

ab@IONP	Antibody functionalized IONP
AC	Alternating current
APTES	3-aminopropyltriethyloxysilane
AuNPs	Gold nanoparticles
BBB	Blood-brain barrier
BSA	Bovine serum albumin
CEA	Carcinoembryonic antigen
CMC	Carboxymethylcellulose
CNT	Carbon nanotube
CT	Computed tomography
DNA	Deoxyribonucleic acid
GET	Glycosaminoglycan binding-enhanced transduction
GFP	Green fluorescent protein
HA	Hyaluronic acid
HEK	Human embryonic kidney cell
IgG	Immunoglobulin G
IONP	Iron oxide nanoparticle
LDH	Layered double hydroxide
MNP	Magnetic nanoparticle
MPA	Mercaptopropionic acid
MPTES	Mercaptopropyltriethoxysilane
MR	Magnetic resonance

R. P. Gambhir · A. A. Vibhute · T. P. Patil · A. P. Tiwari (✉)
Department of Medical Biotechnology, D Y Patil Education Society, (Deemed to be University), Kolhapur, Maharashtra, India

F. I. Ezema et al. (eds.), *Chemically Deposited Metal Chalcogenide-based Carbon Composites for Versatile Applications*, https://doi.org/10.1007/978-3-031-23401-9_15

AMITY UNIVERSITY
MUMBAI

INTERNATIONAL WORKSHOP on

RECENT TRENDS IN FUNCTIONAL NANOMATERIALS FOR TECHNOLOGICAL APPLICATIONS

August 2-3, 2022 (Virtual Mode)

CERTIFICATE OF APPRECIATION

This is to certify that Mr. / Ms. Anuja Arvind Vibhute has Presented Poster in International Workshop on Recent Trends in Functional Nanomaterials for Technological Applications which was held on the 2 & 3 rd of August 2022 organized by Center for Nanoscience and Nanotechnology, Amity University, Mumbai and ICON Labs, Navi Mumbai, India.

Dattatray J Late
Convenor

Co-convenor

Savitribai Phule Pune University

Department of Biotechnology

75th Anniversary Celebration
सावित्रीबाई फुले पुणे विद्यापीठ

International Conference on

Biology Beyond Boundaries

29th to 31st January 2024

Certificate of Presentation

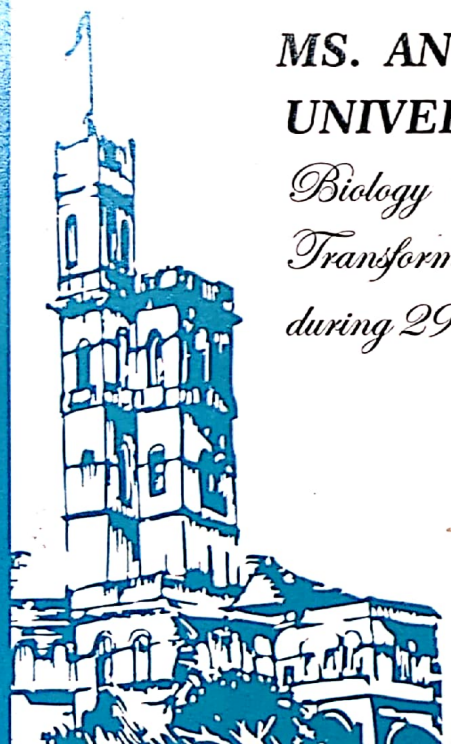

***MS. ANUJA VIBHUTE** from **D. Y. PATIL EDUCATION SOCIETY,(DEEMED TO BE UNIVERSITY), KOLHAPUR** has presented a paper (~~Oral~~ / Poster) in International Conference on Biology Beyond Boundaries: Mitochondrial Insights, Computational Breakthroughs, and Clinical Transformations organized by the Department of Biotechnology, Savitribai Phule Pune University, Pune during 29-31 January 2024.*

Prof. Rajesh N. Gacche
Convener

SAVITRIBAI PHULE PUNE UNIVERSITY

Prof. Dhyan Chandra
Convener

ROSWELL PARK COMPREHENSIVE CANCER CENTER

Prof. Raymond B. Birge
Convener

RUTGERS, USA

Dnyansadhana Shikshan Prasarak Mandal, Nivade Sanchalit,

M. H. Shinde Mahavidyalaya,Tisangi

Tal. Gaganbavda, Dist. Kolhapur 416206

(Affiliated to Shivaji University, Kolhapur)

"One Day International Conference On Advanced Materials and Applications" (ICAMA-2023) (Online)

Certificate

This is to Certify that Prof./Dr./Mr./Mrs. Vibhute Anuja Arvind of D.Y.Patil Education Society Kolhapur has *participated* in the "One Day International Conference On Advanced Materials and Applications (ICAMA-2023)" Jointly Organized by Department of Chemistry and IQAC of M. H. Shinde Mahavidyalaya Tisangi, Tal-Gaganbavda, Dist-Kolhapur (MS) held on Saturday, 1st July 2023.

Dr. R. P. Patil
Convenor

Dr. B. S. Padval
I/C Principal

GBR Foundation

CERTIFICATE OF APPRECIATION

KAIROS KINETIC

THIS CERTIFICATE PROUDLY PRESENTED TO

Anuja Arvind Vibhute

for participating in the hands on workshop entitled
"MOLECULAR DOCKING"
conducted jointly by Global Biomedical Research Foundation, Chennai
and Kairos Kinetic (OPC) Private Limited, Chennai on 9th September 2023.

Dr. Sree T. Sucharitha MD
Founder and CEO
Kairos Kinetic (OPC) Pvt. Ltd.

Dr. I. Kannan Ph.D.
Founder and Director
Global Biomedical Research Foundation

D. Y. PATIL EDUCATION SOCIETY,
INSTITUTION DEEMED TO BE UNIVERSITY,
KOLHAPUR

D.Y.PATIL MEDICAL COLLEGE, KOLHAPUR

DEPARTMENT OF MICROBIOLOGY

INTERNATIONAL CONFERENCE ON EMERGING AND RE-EMERGING INFECTIONS

ICERI - 2022 | *Certificate*

NO:MMC/Accre.Cert/MED-0207/2013/
CME CODE NO: MMC/WEB/2022/C-015391

This is to certify that

Mr/Ms./Dr. **Anuja Arvind Vibhute**

has participated as Delegate / PG Student in the International Conference on

"EMERGING AND RE-EMERGING INFECTIONS (ICERI) – 2022" held on 8th April, 2022.

The Maharashtra Medical Council (MMC) has granted 2 (TWO) Credit points for the delegates.

Dr. Mrs. R. A. Chougale
Convener
ICERI-2022

Dr. Mrs. V. S. Vatkar
Organising Secretary
ICERI-2022

Dr. R. K. Sharma
DEAN,
D. Y. Patil Medical College, Kolhapur

Rayat Shikshan Sanstha's

Yashavantrao Chavan Institute of Science,

(Karmaveer Bhaurao Patil University , Satara, Maharashtra, India)

NAAC Reaccredited at A+ grade with CGPA:3.57

RUSA Sponsored

International Conference on Emerging Trends in Applied Microbiology and Food Sciences (ETAMFS)

(2nd and 3rd December 2022)

CERTIFICATE

This is to certify that Prof./Dr./Mr./Ms./Mrs. Anuja Arvind Vibhute

of D.Y. Patil, Kolhapur has participated / presented paper (Oral / Poster) entitled Fluorescent CQD for antibacterial Bioimaging & Anti-angiogenesis App

in the **International Conference on Emerging Trends in Applied Microbiology and Food Sciences (ETAMFS2022)** organized by Department of Microbiology and Food Processing and Packaging.

Mrs. G.V. Utekar	Mr. P.R. Dure	Dr. V. M.Ghorpade	Mrs. V. S. Patil	Prin. Dr. B.T. Jadhav
Organizing Secretary	Coordinator	Convener	Chairman	President

D. Y. PATIL EDUCATION SOCIETY

(Deemed to be University), KOLHAPUR

NAAC 'A+' Grade in 3rd Cycle

Certificate

This is to certify that Ms. Vibhute Anuja Arvind of Department of Stem Cell and Regenerative Medicine, Kolhapur has delivered the invited talk/ chaired the session/ presented oral/ presented poster/ participated in the International Conference on Nanotechnology Addressing the Convergence of Materials Science, Biotechnology and Medical Science (IC-NACMBM-2024) held at the Centre for Interdisciplinary Research, D. Y. Patil Education Society (Deemed to be University), Kolhapur, Maharashtra, India from 12th to 14th February 2024. Her contribution to the conference is highly appreciated.

Dr. Jayavant L. Gunjakar	Prof. Meghnad G. Joshi	Prof. Chandrakant D. Lokhande
Convener	Convener	Chairman